

# Physical and Molecular Pathways Involved in Cellular Sensing of Mechanical Signals

Submitted in partial fulfillment of the requirements for  
the degree of

Doctor of Philosophy  
in  
Biomedical Engineering

Stephanie A. Wong

B.S., Biological Engineering, Cornell University

Carnegie Mellon University  
Pittsburgh, PA

August, 2016

# Acknowledgements

To my advisor Yu-li Wang: Thank you for constantly challenging me to be my best and grow as a researcher and writer. For teaching me to think outside the established norms and view things in new and interesting ways. I appreciate the all the time and energy you put in to mentoring me and helping me complete my research.

I would also like to acknowledge funding from the Department of Biomedical Engineering and from NIH grant GM-32476 to YLW and NIH Pre-Doctoral BiRM Training Grant T32EB003392 to SW.

To my thesis committee, Professor Christopher Bettinger, Professor Ge Yang, and Professor Lance Davidson: Thank you for your support and valuable insight as I pursued my dissertation research. I appreciate the time you have committed to helping me.

To the other members of the Wang Lab: Thank you for creating a collaborative and welcoming lab environment, for being my sounding board for experimental plans, my presentation proof readers, and for teaching me essential lab techniques I was unfamiliar with.

To the ladies of PTC: Thank you for listening to me when I needed someone to talk to about research or life, for helping me believe in myself and my abilities, for being my best friends these past five years, and especially to Rachelle and Rebecca for keeping me sane through the move to Scott Hall and the writing of this dissertation.

To my family: Thank you for encouraging me throughout this entire process, for letting me know that all people who pursue a PhD go through similar experiences, and for counselling me when I needed direction. Your love and support means the world to me.

To my husband Kevin: Thank you for being such a wonderful partner throughout this journey, for understanding when I had to go into lab late nights or weekends, for accepting my tiny kitten habit, for supporting me in whatever path I chose, and for pushing me to set goals for myself and see things through to the end.

# Abstract

Mechanical properties of the extracellular environment provide important cues that regulate cell behavior. Particularly, the cellular response to substrate rigidity has become an important parameter to consider in disease treatment as well as tissue engineering. The goal of this thesis is to understand how adherent cells sense and respond to external rigidity cues. It has been challenging to study the mechanism that drives the preferential migration of cells towards stiffer substrates at a rigidity border due to difficulties in capturing cells as they transiently encounter a rigidity interface. Using a model system developed for testing cellular responses at a simulated rigidity border, I find that NIH 3T3 cells preferentially localize to the rigid portion of the model system. Cells use filopodia extensions to probe substrate rigidity in front of the leading edge and use substrate strain to determine whether the filopodia protrusions retract or expand to occupy the area. Myosin II mediated contractility is necessary to generate forces for both probing the substrate and retraction in response to substrate strain. Focal adhesion kinase null (FAK  $-/-$ ) cells, known to be defective in durotaxis, are able to readily cross the rigidity border, while re-expression of focal adhesion kinase (FAK) rescues rigidity sensing. The model experimental system allows efficient analyses of conditions affecting rigidity sensing of cells. The results suggest that enhanced Rho activity, likely through Rho downstream effector mDia1, may underlie many rigidity sensing defects including those caused by FAK deficiency and microtubule disassembly. Additionally, I show that probing mechanisms at the front of a cell are used not only for probing rigidity but for sensing the state of migration. Design of a new checkerboard micropattern with alternating adhesive and non-adhesive areas revealed that the appearance of new traction forces and focal adhesions at the leading edge promotes the down-regulation of pre-existing traction forces and focal adhesions that lag behind. These results suggest that in migrating cells continuous protrusion and mechanical probing directly in front of existing adhesions modulates traction force build up and serves as a key mechanism for regulating mechanical output in response to physical cues.

# Contents

Acknowledgements	ii
Abstract	iii
Contents	iv
List of Tables and Figures	vii
<b>1 Introduction</b>	<b>1</b>
1.1 External Cues Guide Cell Behavior	2
1.1.1 Cell behavior is regulated by biophysical cues from the extracellular environment	2
1.1.2 Cells respond to dynamic changes in the extracellular environment	5
1.2 The Influence of Substrate Rigidity	8
1.2.1 Substrate rigidity affects cellular physiology and behavior	8
1.2.2 The influence of matrix rigidity on disease progression	11
1.3 How Cells Interact with the Extracellular Environment	14
1.3.1 Cells “feel” the extracellular environment through the generation of traction forces	14
1.3.2 How rigidity mediates intracellular signaling	16
1.4 Organization of the Thesis	20
1.5 References	22
<b>2 Preparation of a Micropatterned Rigid-Soft Composite Substrate for Probing Cellular Rigidity Sensing</b>	<b>31</b>
2.1 Introduction	32
2.2 Experimental Methods	34
2.2.1 Cell culture	34
2.2.2 Microscopy and image analysis	34
2.2.3 Characterization of composite substrates	35
2.3 Creation of a Model Experimental System	36
2.3.1 Design of a durotaxis pattern	36
2.3.2 Preparation of the polyacrylamide gel base	38

2.3.3	Micropatterning the polyacrylamide surface with SU-8 photoresist .....	41
2.3.4	Surface coating with ECM proteins and cell seeding .....	43
2.3.5	Troubleshooting .....	44
2.4	Testing and Characterization of the Micropatterned Rigidity Border .....	48
2.4.1	Validating robust grafting of SU-8 islands to the underlying polyacrylamide gel.....	48
2.4.2	Response of NIH 3T3 cells to a micropatterned rigidity border.....	48
2.4.3	Additional considerations when fabricating patterns.....	50
2.5	Discussion .....	52
2.6	References.....	55
<b>3</b>	<b>Fibroblasts Probe Substrate Rigidity with Filopodia Extensions before Occupying an Area</b>	<b>57</b>
3.1	Introduction.....	58
3.2	Experimental Methods.....	60
3.2.1	Preparation of composite substrates.....	60
3.2.2	Cell culture and pharmacological treatments.....	61
3.2.3	Fixation and fluorescent labeling.....	61
3.2.4	Microscopy and image analysis .....	62
3.2.5	Scanning electron microscopy .....	63
3.3	Results.....	64
3.3.1	NIH 3T3 cells modulate the size of focal adhesions based on the rigidity of the underlying substrate .....	64
3.3.2	NIH 3T3 cells are able to detect substrate rigidity outside the cell border.....	65
3.3.3	Filopodia are involved in probing substrate rigidity.....	68
3.3.4	Nascent protrusions detect substrate rigidity outside the cell border based on substrate strain .....	70
3.3.5	Myosin II is required for both the probing forces and the subsequent retraction from soft substrates.....	71
3.4	Discussion .....	74
3.5	References.....	78
<b>4</b>	<b>FAK Plays an Essential Role in Rigidity Sensing through its Regulation of Rho Activities</b>	<b>81</b>
4.1	Introduction.....	82
4.2	Experimental Methods.....	84
4.2.1	Preparation of substrates .....	84
4.2.2	Cell culture and pharmacological treatments.....	85
4.2.3	Traction force microscopy .....	86
4.2.4	Microscopy and image analysis .....	87
4.3	Results.....	88
4.3.1	Defect of FAK -/- cells in durotaxis as measured with a cell-on-a-chip composite substrate.....	88
4.3.2	Impaired response of FAK -/- cells to substrate strain .....	89
4.3.3	Involvement of Rho activity in rigidity sensing defect.....	91
4.3.4	Role of contractility in the defect of rigidity sensing of FAK -/- cells.....	93

4.3.5	A role for Rho effector mDia1 in rigidity sensing.....	95
4.4	Discussion.....	97
4.5	References.....	100
<b>6</b>	<b>Migration State Regulates Traction Force through Mechanical Crosstalk between Newly Formed and Existing Adhesions</b>	<b>103</b>
5.1	Introduction.....	104
5.2	Experimental Methods.....	106
5.2.1	Substrate preparation.....	106
5.2.2	Cell culture.....	107
5.2.3	Traction force microscopy.....	107
5.3	Results.....	109
5.3.1	The difference in traction force between stationary and migrating cells cannot be explained by cell spreading area or aspect ratio.....	109
5.3.2	Mechanical output at existing focal adhesions is regulated by the formation of new focal adhesions.....	110
5.4	Discussion.....	114
5.5	References.....	116
<b>6</b>	<b>Conclusions and Future Directions</b>	<b>118</b>
6.1	Conclusions.....	119
6.1.1	Creation and testing of a model system for studying durotaxis.....	119
6.1.2	Cells use filopodia protrusions to test substrate rigidity in front of the leading edge.....	119
6.1.3	FAK $-/-$ cells show impaired probing of substrate rigidity due to elevated Rho activity.....	120
6.1.4	Traction force generation involves mechanical crosstalk between newly formed and existing adhesions.....	121
6.1.5	Significance and biological importance.....	122
6.2	Future Directions.....	123
6.2.1	The effect of strain rate on protrusion stability and rigidity sensing.....	123
6.2.2	The involvement of Rho effector mDia1 in rigidity sensing.....	123
6.2.3	Biological significance of traction force difference between migrating and stationary cells.....	124
6.3	References.....	126

# List of Figures and Tables

## Figures

1.1	Biomimetic substrates are designed to recapitulate biophysical cues of the <i>in vivo</i> environment .....	3
1.2	Schematic showing the timescale of responses to substrate rigidity .....	9
1.3	Schematic showing force transmission at adhesions .....	18
2.1	Durotaxis pattern design .....	36
2.2	Steps in composite substrate fabrication.....	37
2.3	ECM coating of SU-8 layer .....	43
2.4	Examples of micropatterning defects.....	45
2.5	Example of cell adhesion off the micropattern .....	46
2.6	Cracking of the polyacrylamide layer can disrupt pattern quality .....	47
2.7	Elastic recovery of the hydrogel upon the application of forces to small islands.....	48
2.8	Response of NIH 3T3 cells to a micropatterned rigidity border.....	49
2.9	Comparison of cell spreading on composite substrates and micropatterned gels of homogenous rigidity .....	50
2.10	Difficulties with using other cell types on the designed durotaxis pattern .....	51
3.1	Focal adhesions respond to rigidity on composite substrates .....	65
3.2	NIH 3T3 cells can detect substrate rigidity beyond the cell border.....	66
3.3	Arp2/3 and Rac1 are involved in cell spreading on control substrates.....	68
3.4	Visualizing actin-containing filopodia extensions between the cell body and adjacent small islands .....	69
3.5	Interfering with filopodia formation can disrupt rigidity sensing.....	70
3.6	Mechanosensitivity of nascent and mature protrusions .....	71
3.7	Myosin II is required for the response to substrate rigidity .....	72
3.8	Schematic of rigidity sensing in front of the leading edge .....	77
4.1	Durotaxis defect captured on the composite substrate.....	89
4.2	FAK $-/-$ cells are more successful at occupying adjacent small islands than FAK rescued cells .....	90
4.3	Protrusions of FAK $-/-$ cells have an impaired response to substrate strain .....	91
4.4	Increased Rho activity can impair rigidity sensing.....	92
4.5	Inhibiting Rho can rescue rigidity sensing in FAK $-/-$ cells .....	93
4.6	Traction stress regulation cannot fully assess impaired rigidity sensing .....	94
4.7	Inhibition of mDia1 reduces spreading of FAK $-/-$ cells on soft substrates.....	96
5.1	Spread area and aspect ratio of migrating and stationary cells .....	109
5.2	Strain energy generation of migrating and stationary cells .....	110
5.3	Traction force and cell speed on designed checkerboard adhesive pattern .....	111
5.4	High resolution substrate strain dynamics of cells migrating on checkerboard patterns or continuous lines .....	112

## Tables

2.1	Thickness of micropatterned SU-8 layer .....	44
-----	--	----

# Chapter 1

## Introduction

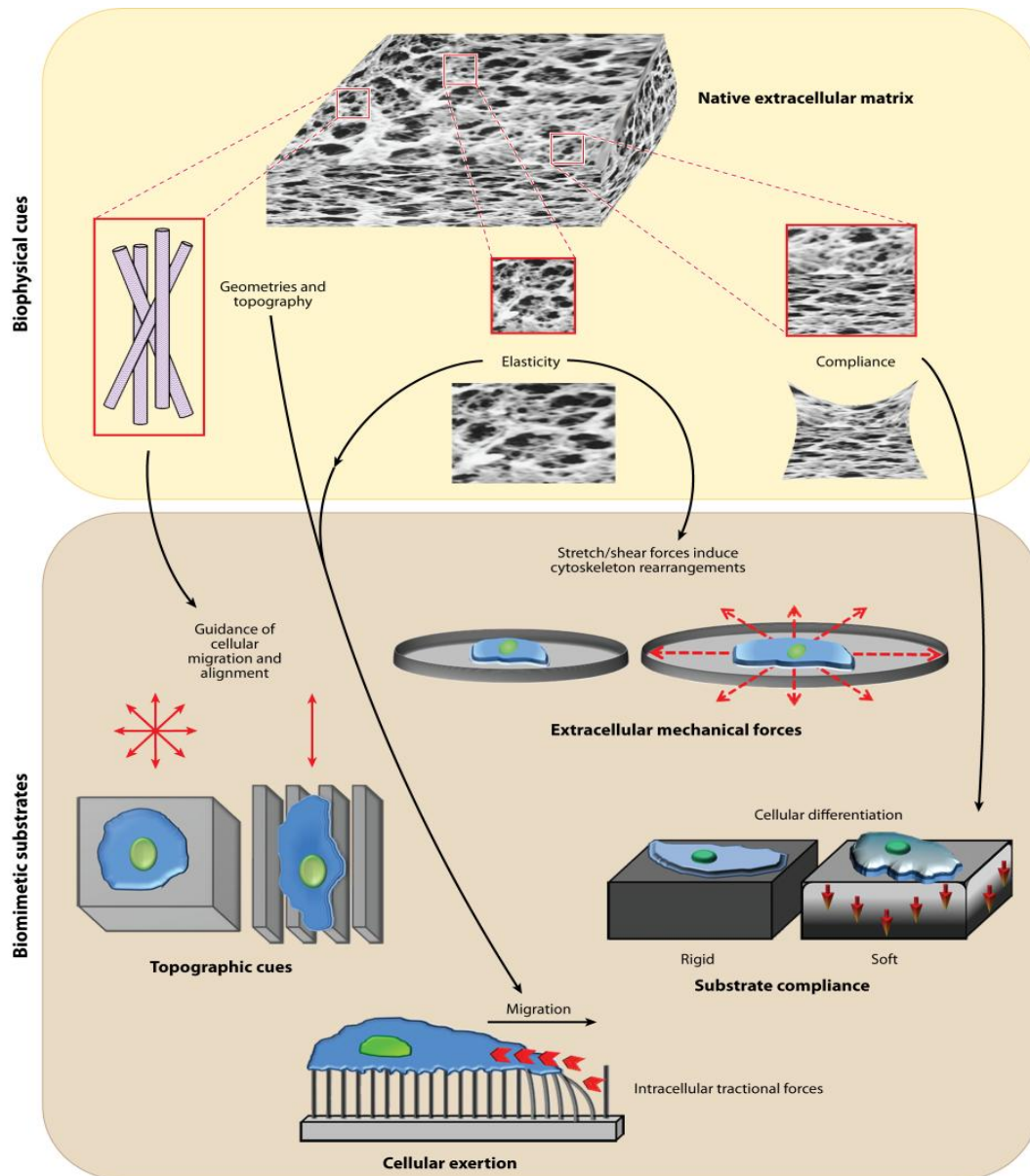
## 1.1 External Cues Guide Cell Behavior

### 1.1.1 Cell behavior is regulated by biophysical cues from the extracellular environment

Cells are highly responsive to a wide variety of signals from the extracellular environment. Well studied are biochemical signals that can direct a myriad of cellular processes including behavior, migration, growth, differentiation, and proliferation. In addition to chemical factors, there has been a growing body of literature showing that cell behavior can be modulated by biophysical cues. In tissues, the extracellular matrix (ECM) architecture is as influential in directing cell behavior as chemical factors presented to cells.

The ECM is composed of many different proteins with specific geometric, adhesive, and spatial properties. Many of the ECM proteins form fibrils that comprise the bulk architecture of the extracellular environment on the order of nanometers to micrometers. Collagen is one such protein found in many living tissues that forms fibrillar structures with a diameter from 20-200nm<sup>1</sup>, which in turn, can organize into microscale bundles. *In vitro* model microenvironments have been designed to mimic the geometry and length scale of the *in vivo* environment to gain insight into cell behavior and function (Fig. 1.1).

With recent advances in micro- and nanofabrication technologies, many studies have focused on how topography, particularly on the order of ECM fibril size, can influence cell behavior. Micro- and nanoscale grooves and ridges aligned in parallel arrays have been shown to induce cell alignment and elongation parallel to the pattern through contact guidance<sup>2-4</sup>. Fibroblasts aligned with microgrooves showed distinct nuclear morphology and chromosomal positioning that correlated with changes in protein and gene expression<sup>5</sup>. A symmetric array of micropits



**R** Gasiorowski JZ, et al. 2013.  
 Annu. Rev. Biomed. Eng. 15:155–76

Figure 1.1. *In vitro* model systems designed to mimic aspects, such as geometry and topography, elasticity, and compliance, of the *in vivo* environment of extracellular matrix to gain insights into cellular responses to biophysical cues. Micro- and nanofabrication have been used to create topographical cues of a scale similar to extracellular matrix protein fibers to align cell orientation and guide cell migration. Substrates to mimic tissue elasticity or cyclic stretch-relaxation cycles have been used to capture cellular responses to these dynamic processes. Elastic substrates have now been used widely to place cells in environments of physiological stiffness. In addition, platforms have been designed to provide a readout of mechanical forces exerted by cells on their environment, to help dissecting inside-out and outside-in signaling. Figure originally published in *Annual Review of Biomedical Engineering*, **15**: 155-176 (Gasiorowski et. al., 2013)<sup>6</sup>.

enhanced the formation and maturation of focal adhesions without affecting cell shape and spread area<sup>7</sup>. Corneal epithelial cells showed reduced rates of proliferation on nanogrooves similar in size to collagen fibers in the *in vivo* environment<sup>8</sup>. Additionally, neurites showed enhanced outgrowth parallel to aligned topographies, when responding to the depth/height of the grooves and ridges<sup>9,10</sup>. Nanopits were found to stimulate osteogenic differentiation of human mesenchymal stem cells (hMSCs) at depths around 100 nm<sup>11,12</sup>. Changes as small as tens of nanometers in the depth of nanogrooves or nanopits could significantly alter the observed cell behavior, suggesting cells are highly sensitive to nanoscale cues.

Microcontact printing has become an important and widely used tool in investigations of cell mechanosensing<sup>13,14</sup>. Various ECM proteins can be stamped onto a substrate in an ever expanding variety of patterns to influence cell behavior. Studies have shown that micropatterning cell size and shape can have a profound effect on cell phenotype, behavior, mechanical output, and signaling. For instance, confinement of cells to small micropatterned areas promoted cell apoptosis<sup>15</sup>. Micropatterning to increase aspect ratio of cells decreased proliferation rates of vascular smooth muscle cells<sup>16</sup> and promoted a prohealing M2 macrophage phenotype over the proinflammatory M1 phenotype<sup>17</sup>. Additionally, skeletal muscle cells preferentially aligned and fused on micropatterned lines of a specific width and spacing<sup>18</sup>.

Varying the geometry of the adhesive micropattern can significantly influence cellular physiology. Cells spread on square micropatterns extended lamellipodial, filopodial, and microspike protrusions preferentially from the corners. Cells also reoriented their cytoskeleton and focal adhesions such that traction forces were localized to the corners<sup>19,20</sup>. Altering the adhesive pattern while maintaining a constant spread area could drive preferential actin stress

fiber formation over non adhesive areas<sup>21</sup>. Changing the subcellular curvature of the adhesive pattern, between a flower and a star shape of the same overall area, was shown to direct stem cell differentiation towards adipocytes or osteoblasts respectively<sup>22</sup>. Increased resolution of micropatterning down to the nanoscale has allowed exploration of how physical parameters such as adhesive area size can affect focal adhesion assembly and force transduction<sup>23</sup>. In addition to studies on stationary cells, micropatterning can also be used to direct cell migration and study migration dependent behavior<sup>24,25</sup>. Cells migrating along thin lines displayed many characteristics of 3D cell migration and can be used as a simpler platform to study such migration<sup>26,27</sup>.

### **1.1.2 Cells respond to dynamic changes in the extracellular environment**

The above discussion indicates that the microenvironment can have a profound influence on cells. While these experimental cues are often static in their presentation, additional information can be gained from studying cellular responses to dynamic changes in the external environment. To this end, many studies have focused on creating dynamic or switchable microenvironments that can be controlled in real time while interacting with cells.

Thermally responsive shape memory polymers have been used to alter the landscape of the cellular microenvironment in real time. After an induced switch from microridges to a flat surface, aligned behavior was lost and cells reoriented in a random fashion<sup>28</sup>. Switching the orientation of nanogrooves by 90 degrees caused cells to reorient and align with the new pattern, which took place slowly, over about 48 hours<sup>29</sup>. Another platform to determine the effect of dynamic microtopography is a system for creating reversible wavy microfeatures on

polydimethylsiloxane (PDMS), which was used to align C2C12 myogenic cells reversibly and repeatedly at 24 hour intervals<sup>30</sup>.

Similarly, conditions in the body are dynamic, with forces exerted on cells through cycles of stretching and relaxation that can influence cell behavior. For fibroblasts plated on a surface of soft micropillars, 5% cyclic stretching at 10Hz increased cell spreading area and stress fiber formation, which persisted for up to 4 hours after stretching was halted<sup>31</sup>. U2OS cells reoriented actin stress fibers perpendicular to the direction of cyclic stretching<sup>32</sup>, while their focal adhesions and stress fibers were enriched upon confinement of the cell to micropatterned adhesive areas<sup>33</sup>. In addition to stretching, cells experience other forces in the body such as fluid shear stress from blood flow on endothelial cells lining blood vessels. Vascular endothelial cells showed enhanced migration in response to fluid flow<sup>34</sup>, and various other processes also showed a dependence on fluid shear including proliferation<sup>35</sup>, signaling<sup>36</sup>, haptotaxis<sup>37</sup>, cell morphology<sup>38</sup> and cytoskeletal arrangement<sup>39</sup>. Additionally, shear stress from transmural flow, fluid flowing out of the wall of a blood vessel, was shown to induce angiogenic sprouting<sup>40</sup>.

Advances in micropatterning techniques have allowed studies on cellular responses to changes in adhesive pattern in real time. For example, new substrates have been designed to contain cell repellent coatings that can be removed through UV exposure<sup>41</sup>. Pulsed UV laser exposure can be used to pattern new adhesive areas of nano- or microarrays, adjacent to a spread cell to determine how nano- or microscale geometries affect cell spreading and cytoskeletal reorganization compared to cells on continuously adhesive patches<sup>42</sup>. Initiation of collective cell migration can be studied when clusters of cells are released from confinement<sup>43</sup>.

Modulatable gels have also been created to study cellular responses to changes in substrate stiffness. Dynamic hyaluronic acid hydrogels tuned to stiffen over a period of days enhanced cardiac differentiation and induced a 3-fold increase in mature cardiac specific markers, compared with compliant static gels<sup>44</sup>. Hydrogels that undergo light mediated crosslinking can be used to quickly stiffen the substrate and caused an increase in cell area and in traction forces within hours<sup>45</sup>. Conversely, hydrogels prepared with a photocleavable crosslinker can be used to dynamically soften the substrate after exposure to UV light<sup>46</sup>. Global softening induced initial rapid retraction of cellular protrusions and a decrease in spread area after a few hours, while local softening at the leading edge of cells caused some cells to reverse polarity and migrate away from the softened area<sup>47</sup>. These studies also showed that, unlike changes in micro- or nanotopography, physiological response to substrate stiffness is a much faster process. Photocleavable groups have also been incorporated into 3D hydrogels to study the release of cells from 3D encapsulation<sup>48</sup>.

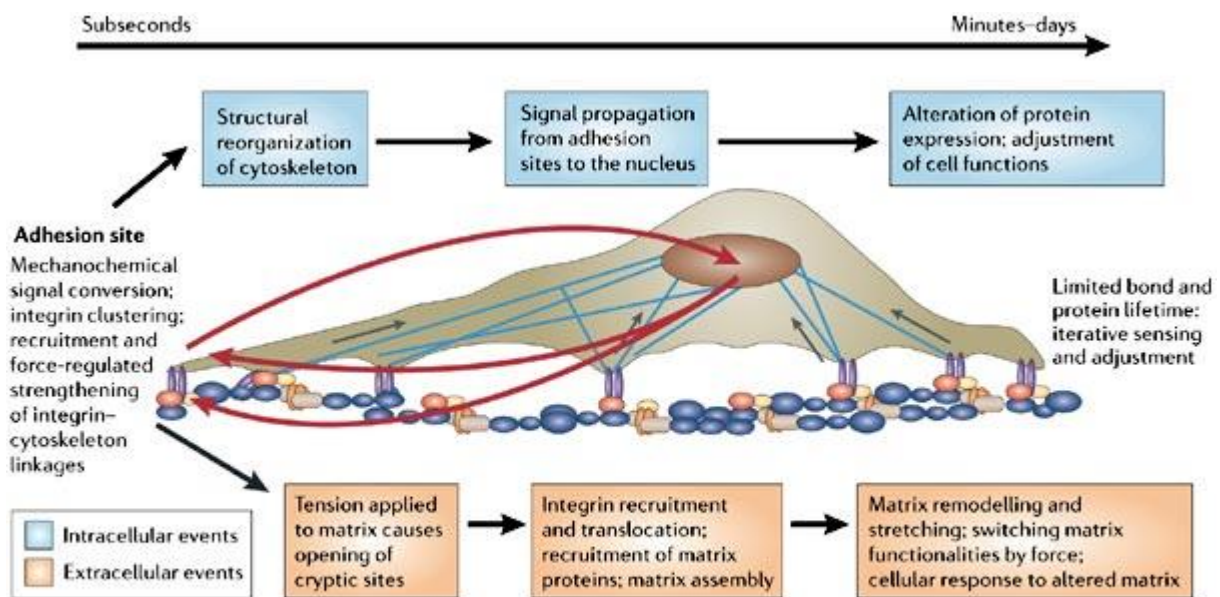
Of particular interest is how these parameters, both static and dynamic, can be used to control important processes such as cell growth, differentiation, migration, and gene expression. This knowledge will help biomedical engineers develop better scaffolds as they pursue increasingly complex tissue engineering constructs, such as the creation of artificial cardiac muscle to repair tissue damage from a cardiac infarct, the promotion of angiogenesis *in vitro* to enable development of larger scale replacement tissues, or the creation of better biomaterials that can promote faster wound healing or reconnection of severed nerves following severe spinal injuries. It may also allow the development of better drug therapies as we better understand the mechanical and signaling events that take place as cells sense the external environment.

## 1.2 The Influence of Substrate Rigidity

### 1.2.1 Substrate rigidity affects cellular physiology and behavior

Aside from geometrical/topographical features, such as nanotopography or micropatterning to control cell shape and adhesion, mechanical properties of the extracellular environment can also provide important cues that regulate cell behavior. It is now common practice to create elastic substrates using polyacrylamide<sup>49,50</sup>, PDMS<sup>51,52</sup>, or polyethylene glycol (PEG)<sup>53</sup> with varied amounts of crosslinker to control substrate compliance. Use of these systems has shown that cells are able to sense the stiffness of their external environment and regulate their behavior accordingly (Fig. 1.2).

Typically, on rigid substrates cells spread to a larger area and showed increased focal adhesion size, enhanced adhesion strength, and a more robust actin stress fiber network<sup>54,55</sup>. Measurement using atomic force microscopy of the stiffness of fibroblasts plated on polyacrylamide gels revealed that cells adapted their cytoskeletal stiffness to match the rigidity of the hydrogel substrate<sup>56</sup>. Cortical stiffening on rigid substrates was mediated by actin polymerization, cortical contractility, and stress fiber formation<sup>57,58</sup>. Assembly state of the intermediate filament vimentin is also modulated by physiologically relevant differences in substrate stiffness<sup>59</sup>. Recent reports have further suggested the involvement of microtubules in rigidity sensing, as microtubule stability was dependent on the stiffness of a 3D collagen matrix, showing reduced stability on stiffer matrices<sup>60</sup>. Recruitment of focal adhesion protein vinculin is modulated by myosin II in response to substrate rigidity<sup>61</sup>, while the turnover of focal adhesions is affected by ECM fiber stiffness in 3D matrix environments<sup>62</sup>. These morphological responses to substrate rigidity were mostly found to be dependent on actomyosin contractility<sup>63</sup>.



Copyright © 2006 Nature Publishing Group  
 Nature Reviews | Molecular Cell Biology

Figure 1.2. Schematic representation showing the timescale of various responses to substrate rigidity. Initial mechanosensing causes rapid signaling responses and strengthening of integrin-cytoskeleton linkages on a time scale of seconds. Following the generation of traction forces on the environment, structural reorganization and downstream signaling events take place on the order of minutes to days to alter protein expression or other cellular functions. Reprinted by permission from Macmillan Publishers Ltd: *Nature Reviews Molecular Cell Biology* 7: 265-275, Copyright 2006<sup>64</sup>.

The rigidity of the extracellular environment has been shown to regulate cell proliferation, apoptosis, and migration. Fibroblasts cultured on compliant substrates showed an increased rate of apoptosis and a decreased rate of DNA synthesis<sup>65,66</sup>. Additionally, cells migrated preferentially towards areas of stiffer substrate in a phenomenon known as durotaxis, which was initially discovered when migrating fibroblasts turned away from a border between a stiff and soft hydrogel opting to stay on the stiff side<sup>67</sup>. Many other cell types have also displayed durotactic behavior including vascular smooth muscle cells<sup>68</sup>, bovine endothelial cells<sup>69</sup>, and mesenchymal stem cells<sup>70</sup>, in a manner dependent on myosin II and cellular contractility<sup>71</sup>. Softer substrates promoted cell-cell adhesion over cell-substrate adhesion leading to aggregation and mock tissue formation<sup>72</sup>, while cell scattering was increased on stiffer substrates where cells migrated away from one another to favor cell-substrate adhesion<sup>73</sup>. Even platelets, enucleate cell fragments, have been shown to respond to substrate rigidity. Increased substrate stiffness enhanced platelet adhesion, spreading, and activation through Rac1 and the actomyosin contractility pathway<sup>74</sup>. It appears that stiffness sensing is a universal phenomenon across a wide variety of cell types, through a common mechanism involving actomyosin-mediated cellular contractility.

One important behavior, of particular interest to biomedical engineers, is rigidity-dependent regulation of stem cell differentiation. The seminal work on this phenomenon showed that substrates designed to mimic brain, muscle, and osteoid matrix stiffness, were able to direct differentiation of mesenchymal stem cells towards neurogenic, myogenic, and osteogenic lineages<sup>75</sup>. This process was also found to be regulated by Rho/ROCK signaling and myosin II mediated contractility, consistent with observations from recent studies that micropatterning or topography changes that increase cytoskeletal contractility can influence differentiation<sup>76-79</sup>.

Aside from differentiation, substrate rigidity has been shown to influence gene expression and other signaling pathways. YAP (Yes-associated protein) and TAZ (transcriptional coactivator with PDZ-binding motif) transcriptional regulators, have been identified as a possible relay of mechanical signals to the nucleus. Substrate rigidity, probed via cellular contractility, controls subcellular localization of YAP/TAZ, which localize to the nucleus in cells grown on rigid substrates and in the cytoplasm in cells grown on soft substrates<sup>80</sup>. Matrix rigidity also regulated the response of epithelial cells to transforming growth factor beta (TGF $\beta$ ). Soft matrices increased TGF $\beta$  induced cell apoptosis, while increased rigidity promoted epithelial to mesenchymal transition (EMT) and a more migratory phenotype<sup>81</sup>. These processes are likely the result of differential gene regulation in response to substrate stiffness. For instance, tissue specific markers were upregulated in response to substrate rigidity, leading to the commitment of stem cell lineages<sup>75,82</sup>. Other genes such as inflammatory markers and genes associated with extracellular matrix remodeling such as matrix metalloproteinases (MMPs) were also found to be regulated by substrate rigidity<sup>83,84</sup>.

### **1.2.2 The influence of matrix rigidity on disease progression**

It has become clear that a multitude of cellular signaling pathways leading to a variety of morphological or behavioral changes are regulated by substrate rigidity *in vitro*<sup>85-87</sup>. Different tissues each have their own characteristic stiffness, while changes in tissue stiffness represent a common marker of diseases. Consideration of substrate rigidity has become an essential aspect in not only tissue engineering<sup>86,88</sup>, but also in the understanding of disease progression and the development of disease treatment<sup>89-93</sup>.

Tissue engineering can benefit from an understanding of rigidity sensing to aid in the design of better biomimetic scaffolds or medical devices. For instance, platelet adhesion and activation was shown to be upregulated on stiffer surfaces<sup>74</sup>, information which may aid in the design of materials or coatings to reduce platelet adhesion on medical devices and prevent clotting at the tissue-device interface. Additionally, stem cell therapy has gained significant attention as an avenue to treat a variety of diseases<sup>94</sup>. Simply injecting stem cells into a diseased tissue with an altered microenvironment may not produce the desired restorative results, while a combination of stem cells and a scaffold to direct differentiation may represent a more promising avenue for achieving the desired outcome in implantable or injectable therapies<sup>95-98</sup>.

Matrix stiffening is a symptom associated with many disease pathologies<sup>99</sup>. After an acute myocardial infarction, cardiac fibroblast infiltration and healing fibrosis leads to an increased number of contractile myofibroblasts in the affected area<sup>100,101</sup>. Contractility and collagen production of myofibroblasts in turn causes stiffening of the heart muscle, which leads to scar tissue formation, diastolic dysfunction and heart failure<sup>102-104</sup>. As blood is pumped through the body, large blood vessels must be able to efficiently expand and contract in response to changes in pressure. Arterial stiffening can develop due to age, genetics, or other diseases, and is associated with an increased risk of many cardiovascular events<sup>105-107</sup>. Maintaining proper arterial compliance is important in the function and longevity of the cardiovascular system.

Liver fibrosis is another example of pathological change in tissue stiffness, when an acute or chronic injury to the liver leads to excessive accumulation of ECM proteins and tissue stiffening<sup>108</sup>. Increased matrix stiffness disrupts the maintenance and function of the endogenous population of hepatocytes, stellate cells, and portal fibroblasts, which can in turn lead to cirrhosis

or liver failure, eventually requiring a liver transplant<sup>109,110</sup>. Liver tissue stiffening was observed after an acute injury and before the start of fibrosis and associated increase in collagen synthesis and deposition. Inhibition of lysyl oxidase (LOX)-dependent collagen crosslinking can prevent this initial liver stiffening<sup>111</sup>, indicating that collagen crosslinking may play a role in promoting fibrosis and could be a viable candidate for therapeutic intervention.

With a growing body of literature on the importance of substrate rigidity in the cell niche for maintaining homeostasis, it is little wonder that ECM rigidity has been shown to influence the hallmark traits of cancers<sup>97</sup>. Increased matrix density and stiffness can cause abnormal proliferation by enabling tumor cells to overcome quiescence signals<sup>92,112–114</sup>. In addition, stiffened substrates reduced T-cell activation and proliferation, implying that the stiffer tumor environment may be responsible for suppressing anti-tumorigenic T-cell activities<sup>115</sup>. In breast cancer, increased mammogram density, often associated with an increase in tissue stiffness, was correlated with a higher risk of developing cancer<sup>116</sup>. A study using cell lines of varying malignancies derived from breast, prostate, and liver cancers showed a correlation between traction stress generation and malignancy, with more malignant cancers generating higher stresses<sup>117</sup>. Furthermore, an increase in substrate stiffness promoted EMT in response to growth factors, a process thought to be important in extravasion during cancer metastasis<sup>73,118–121</sup>. Recent studies have even shown that increased matrix stiffness decreased the response of cancer cells to chemotherapies<sup>114,122,123</sup>. Thus, growing evidence suggests that increased matrix rigidity in the tumor microenvironment may actively promote tumor progression and reduce susceptibility to the body's own immune response or chemotherapeutics.

## **1.3 How Cells Interact with the Extracellular Environment**

### **1.3.1 Cells “feel” the extracellular environment through the generation of traction forces**

In order for cells to respond to adhesion-mediated cues, cells must be able to “feel” the external environment and then be able to “read out” the consequences. The process of feeling extracellular environment involves the exertion of mechanical forces termed “traction forces”<sup>124</sup> (Fig. 1.3). It has become evident that these mechanical forces play a significant role in regulating cellular functions<sup>125,126</sup>. For example, regulation of traction forces is known to be important for dimension sensing, which was disrupted by aberrant or disorganized traction force generation in cells treated with myosin II inhibitors or in Ras-oncogene transformed fibroblasts<sup>24</sup>. Numerous studies, explored earlier, indicated the importance of myosin II driven cytoskeletal contractility in interactions with the extracellular environment, such as during durotaxis, nanogroove sensing, and the response to cyclic stretching. Disrupting the regulation of contractility can in turn alter cell phenotype and differentiation<sup>65</sup>.

Emerging evidence suggests that rigidity sensing may occur at multiple length scales. Cells plated on wrinkling films indicated the production of strain across the length of the cell<sup>127</sup>. Early reports on rigidity sensing showed a relationship between traction force generation and substrate stiffness<sup>67</sup>. Using an array of rigid islands grafted onto a soft hydrogel material, revealed that local rigidity beneath individual focal adhesions was insufficient to facilitate cell spreading. Instead, cells responded to substrate rigidity based on compliance across the cell length<sup>128</sup>. Building on that idea, a large scale mechanism for sensing substrate rigidity has been proposed based on cytoskeletal reorganization and contractility<sup>129</sup>. It was further suggested that durotaxis

involves a traction force imbalance within the cell from the softer to stiffer region, which causes polarization and migration towards the rigid domain<sup>129,130</sup>.

Focal adhesion components, particularly integrins, may play a role in modulating traction force output and rigidity sensing. Different integrins, expressed in different cell types, are known to preferentially bind different ECM proteins. For instance,  $\alpha_5\beta_1$  and  $\alpha_v\beta_3$  integrins preferentially bind RGD sequences on fibronectin<sup>131,132</sup>, while  $\alpha_1\beta_1$  and  $\alpha_2\beta_1$  are well known receptors mediating adhesion to collagen surfaces<sup>133</sup>. Studies have suggested that the type of ECM, and the engagement of specific integrins, modulates cell scattering by regulating cellular contractility<sup>73,134</sup>, with increased contractility on stiffer matrices favoring cell scattering<sup>119</sup>. Another study showed that engagement of different fibronectin binding integrins was sufficient to alter traction force generation. Breast myoepithelial cells can bind fibronectin through  $\alpha_5\beta_1$  integrins or  $\alpha_v\beta_6$  integrins, which are selectively upregulated during development or in cancers. Binding via  $\alpha_v\beta_6$  integrins increased force generation at physiological stiffness, thereby disrupting proper tensional homeostasis<sup>135</sup>.

Recent studies have suggested a more localized process for rigidity sensing involving contraction between neighboring adhesions or within single adhesions. Micron and submicron sized pillars have been used to further define the length scale of rigidity sensing. While forces exerted by cells on micron-scale pillars caused global inward deflections<sup>136</sup>, local contractions between pillars of submicron scale were found to point towards each other, possibly for the detection of stiffness in between<sup>137</sup>. It was suggested that these smaller pillar arrays can more closely mimic continuous surfaces for studying rigidity sensing and force generation. These local contractions appeared to be mediated by stepped contractions of myosin mini-filaments connecting adjacent

pillars. The stepped contraction proceeded until a force threshold of 20 pN was reached, at which time there was a pause in contraction coupled to reinforcement of focal adhesions and the actin cytoskeleton. This threshold force was reached more quickly on rigid pillars than softer pillars, while on very soft pillars forces could never build up sufficiently, which led to the breakage of adhesion and retraction<sup>138</sup>.

Still other studies have suggested that rigidity sensing can take place at the scale of focal adhesions. Using high resolution traction force microscopy to characterize the nanoscale organization of traction forces, one study revealed that larger mature adhesions, which appear static, could exist in one of two states: one where traction remained stationary and a second where internal force fluctuates along the length of focal adhesion, termed “tugging adhesions”. ECM rigidity and myosin II contractility controlled the switch between these focal adhesion states with tugging occurring more frequently when myosin activity was inhibited such as on softer substrates<sup>139</sup>. This study suggested that local tugging within single focal adhesions may serve as a way for cells to sample the rigidity of the environment.

### **1.3.2 How rigidity mediates intracellular signaling**

Our understanding of how cells probe the external environment and convert adhesion-mediated signals, such as substrate rigidity, into intracellular chemical events is still far from complete. Due to the fundamental role of rigidity in guiding a variety of cellular processes, it is important to understand the mechanism of rigidity sensing. Several subcellular structures, including actin filaments<sup>140,141</sup>, the cortical cytoskeleton<sup>142,143</sup>, the nucleus<sup>144</sup>, mechanosensitive ion channels<sup>145</sup>, or focal adhesions<sup>135,139,146</sup>, have been proposed as force sensors to allow the determination of the mechanical properties of the extracellular environment. Many reports, however, have pointed

toward an actomyosin contractility based mechanism, with forces transmitted through focal adhesions that link the extracellular environment and the cytoskeleton<sup>147-149</sup>. Elucidating the mechanism of contractility-driven rigidity sensing represents an active area of ongoing research.

Integrin-containing focal adhesions allow the cell to adhere to the external environment, and may serve as mechanosensors. One popular model to describe mechanosensing through integrins is a catch bond model. Most protein bonds can be classified as slip bonds, where the application of force can lower the activation energy necessary to transition between states<sup>150</sup>. In a catch bond, however, application of force acts to increase the bond strength and lifetime by increasing the activation energy necessary to transition from one state to another<sup>151,152</sup>. This idea is supported by the observation that increased substrate rigidity causes strengthening of the integrin linkage to the cytoskeleton via increased integrin clustering and focal adhesion size<sup>54,153</sup>.

The use of magnetic and optical tweezers to manipulate integrin-ligand coated beads provided early evidence that rigidity is sensed through integrin containing adhesions. Cells rapidly formed focal adhesions at the site of bead binding, and responded to the restraining force on the beads by locally strengthening those cytoskeletal linkages as the force was increased<sup>153-155</sup>. Use of various sizes of fibronectin coated beads revealed that initial adhesions, or focal complexes, were able to exert force upon the recruitment of vinculin to the adhesion<sup>156</sup>. Additionally, application of an external pulling force with a microneedle either directly on the cell<sup>157</sup> or indirectly via the adjacent substrate also induced an increase of focal adhesion size<sup>158</sup>.

Chemical effects, downstream of the readout of these mechanical responses, likely involve force-induced molecular conformational changes<sup>159,160</sup>. Vinculin is a likely candidate for a molecular

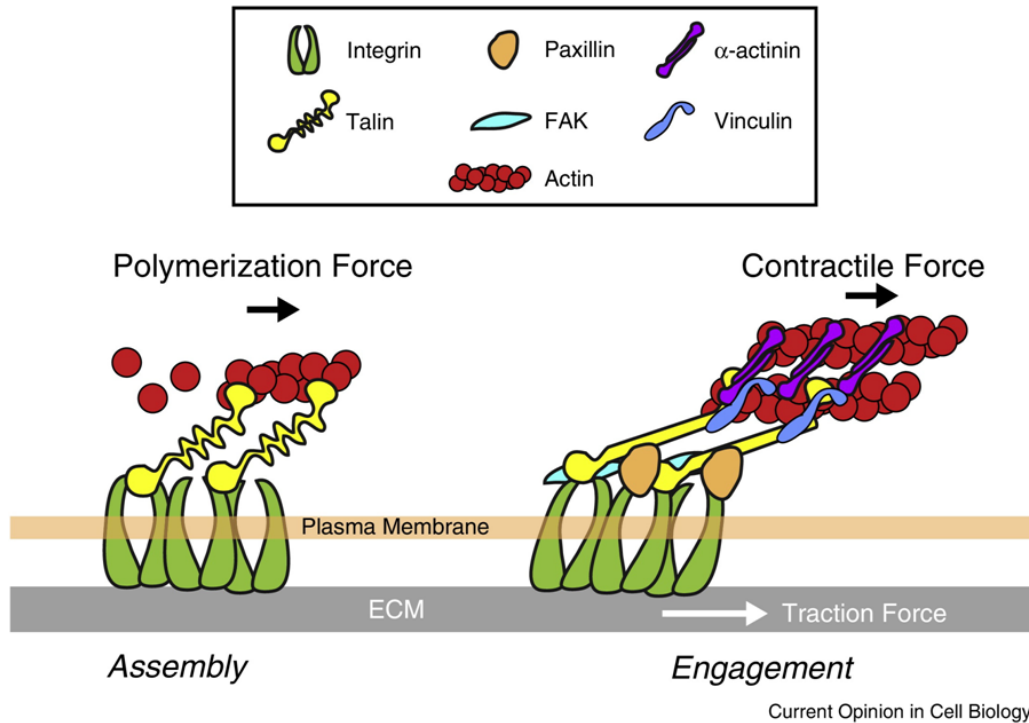


Figure 1.3. A schematic representation of force transmission during the assembly and maturation of focal adhesions. Nascent focal adhesions are first assembled to connect the cellular actin cytoskeleton to the extracellular matrix. Exertion of initial mechanical forces on these nascent adhesions is followed by the recruitment of additional focal adhesion elements and the production of strong traction forces. Adapted from *Current Opinion in Cell Biology*, Vol. 30, Oakes and Gardel, Stressing the limits of focal adhesion mechanosensitivity, pp. 68-73, Copyright 2014, with permission from Elsevier<sup>161</sup>.

force sensor as it is recruited early to newly forming adhesions and can bind the actin cytoskeleton to provide a mechanical link<sup>162</sup>. Recruitment of vinculin to focal adhesions is myosin II contractility dependent, possibly through the exposure of vinculin binding sites when talin is stretched under a mechanical load<sup>163</sup> (represented in Fig. 1.3). Measurements of the mechanical tension across vinculin using a FRET-based sensor revealed that vinculin can exist in a closed inactive state or an open active state due to applied mechanical tension<sup>164,165</sup>. In addition, high tension across vinculin was associated with the assembly of focal adhesions while low tension was associated with disassembly, and vinculin was required for adhesion stabilization under tension<sup>166</sup>.

Tyrosine phosphorylation and dephosphorylation are known to be critical in the formation of focal adhesions and rigidity-dependent signal transduction<sup>167</sup>. Focal adhesion kinase (FAK), receptor-like protein tyrosine phosphatase (RPTP), Src family kinases (SFK), and SH2 domain containing SHP-2 have all been identified as important signaling molecules in the response to rigidity<sup>146,158,168,169</sup>. FAK *-/-* cells were unable to properly regulate rigidity-dependent traction forces or to modulate focal adhesion formation in response to externally applied force<sup>158</sup>. SFKs can be rapidly activated by RPTP $\alpha$  at the leading edge of cells in response to local force application<sup>170,171</sup>. Activation of SFKs in turn initiates several downstream signaling cascades including activation of small G proteins, such as Rac1 and RhoA that are known to be important regulators of cell migration and cytoskeletal contractility<sup>172,173</sup>, and mitogen activated protein (MAP) kinases that are involved in proliferation, differentiation, motility, stress response, apoptosis, and survival<sup>174-176</sup>.

## 1.4 Organization of the Thesis

This thesis encompasses studies that seek to understand how adherent cells sense and respond to their extracellular environment. Part of the effort has focused on the development and application of innovative tools that combine materials, microfabrication, micromanipulation and pharmacological approaches, for controlling the environment of adherent cells and probing cellular functions that cannot be easily studied using conventional approaches.

A model experimental system for studying rigidity sensing was developed based on the "cell-on-a-chip" concept, using a micropatterned composite material that confines cells to a simulated rigidity border. I present in Chapter 2 a method for fabricating such composite substrates that incorporates micropatterned rigidity for studying durotaxis and rigidity sensing. I show that NIH 3T3 cells respond to the simulated rigidity border based on the rigidity of the underlying hydrogel, thereby validating the design. Work in this chapter has been published as a methods chapter in *Methods in Cell Biology*<sup>177</sup> and in *Proceedings of the National Academy of Sciences*<sup>178</sup> in conjunction with work in Chapter 3.

The phenomenon termed durotaxis was first discovered when fibroblasts were found to turn away from soft substrates as they migrated to an interface between a rigid and soft hydrogel. In Chapter 3, I utilize the previously developed composite substrate to investigate the mechanism behind the probing process that cells apply at a border to sense substrate rigidity. I demonstrate that migrating fibroblasts use filopodia to probe substrate rigidity in front of the leading edge, such that it "feels" its way based on the deformability of a material before occupying an area. Work in this chapter has been published in *Proceedings of the National Academy of Sciences*<sup>178</sup> in conjunction with work in Chapter 2.

Using our model experimental system, I show in Chapter 4 that FAK<sup>-/-</sup> cells, with a known defect in rigidity sensing, spread readily across a rigidity border. Upon the re-expression of FAK, cells once again remained confined to the rigid area. I then show that probing dynamics are impaired in FAK<sup>-/-</sup> cells and that protrusions are unable to retract properly in response to substrate strain. I find that increased Rho activity is responsible for the defect in rigidity sensing of FAK<sup>-/-</sup> cells, and that mDia1 rather than ROCK is likely the responsible downstream effector. These results suggest that the regulation of Rho activity is crucial to rigidity sensing in adherent cells and that studying cells on separate substrates of different but homogeneous stiffness may not be sufficient for capturing the full picture of rigidity sensing and durotaxis.

In Chapter 5, I have extended the study and methodology to dissect how cells use mechanosensing to detect the state of migration. Using a checkerboard pattern to prevent adhesion in part of the frontal region, I found that cells are able to produce stronger traction stress that persists for a longer period of time, and that peak stress is located further behind the leading edge than in cells migrating on continuous lines. This supports the hypothesis that the appearance of new traction forces and focal adhesions promotes the down-regulation of pre-existing forces at focal adhesions that lag behind.

## 1.5 References

1. Kim, D.-H., Provenzano, P. P., Smith, C. L. & Levchenko, A. Matrix nanotopography as a regulator of cell function. *J. Cell Biol.* **197**, 351–360 (2012).
2. Hu, J. *et al.* Enhanced Cell Adhesion and Alignment on Micro-Wavy Patterned Surfaces. *PLoS One* **9**, e104502 (2014).
3. Clark, P., Connolly, P., Curtis, a S., Dow, J. a & Wilkinson, C. D. Cell guidance by ultrafine topography in vitro. *J. Cell Sci.* **99** ( Pt 1), 73–77 (1991).
4. Karuri, N. W. *et al.* Biological length scale topography enhances cell-substratum adhesion of human corneal epithelial cells. *J. Cell Sci.* **117**, 3153–64 (2004).
5. McNamara, L. E. *et al.* The role of microtopography in cellular mechanotransduction. *Biomaterials* **33**, 2835–2847 (2012).
6. Gasiorowski, J. Z., Murphy, C. J. & Nealey, P. F. Biophysical cues and cell behavior: the big impact of little things. *Annu. Rev. Biomed. Eng.* **15**, 155–76 (2013).
7. Seo, C. H., Furukawa, K., Montagne, K., Jeong, H. & Ushida, T. The effect of substrate microtopography on focal adhesion maturation and actin organization via the RhoA/ROCK pathway. *Biomaterials* **32**, 9568–75 (2011).
8. Liliensiek, S., Campbell, S., Nealey, P. F. & Murphy, C. J. The scale of substratum topographical features modulates proliferation of corneal epithelial cells and corneal fibroblasts. *J. Biomed. Mater. Res. Part A* **79A**, 185–192 (2016).
9. Chua, J. S. *et al.* Extending neurites sense the depth of the underlying topography during neuronal differentiation and contact guidance. *Biomaterials* **35**, 7750–7761 (2014).
10. Rajnicek, A. M., Britland, S. & McCaig, C. D. Contact guidance of CNS neurites on grooved quartz: influence of groove dimensions, neuronal age and cell type. *J. Cell Sci.* **110** ( Pt 2), 2905–2913 (1997).
11. Dalby, M. J. *et al.* The control of human mesenchymal cell differentiation using nanoscale symmetry and disorder. *Nat. Mater.* **6**, 407–413 (2007).
12. Zouani, O. F. *et al.* Altered nanofeature size dictates stem cell differentiation. *J. Cell Sci.* **125**, 1217–1224 (2012).
13. Alom Ruiz, S. & Chen, C. S. Microcontact printing: A tool to pattern. *Soft Matter* **3**, 168 (2007).
14. Théry, M. Micropatterning as a tool to decipher cell morphogenesis and functions. *J. Cell Sci.* **123**, 4201–13 (2010).
15. Chen, C. S., Mrksich, M., Huang, S., Whitesides, G. M. & Ingber, D. E. Micropatterned surfaces for control of cell shape, position, and function. *Biotechnol. Prog.* **14**, 356–63 (1998).
16. Thakar, R. G. *et al.* Cell-shape regulation of smooth muscle cell proliferation. *Biophys. J.* **96**, 3423–3432 (2009).
17. McWhorter, F. Y., Wang, T., Nguyen, P., Chung, T. & Liu, W. F. Modulation of macrophage phenotype by cell shape. *Proc. Natl. Acad. Sci.* **110**, 17253–8 (2013).
18. Sun, Y., Duffy, R., Lee, A. & Feinberg, A. W. Optimizing the structure and contractility of engineered skeletal muscle thin films. *Acta Biomater.* **9**, 7885–7894 (2013).
19. Parker, K. K. *et al.* Directional control of lamellipodia extension by constraining cell shape and orienting cell tractional forces. *FASEB J.* **16**, 1195–204 (2002).
20. Wang, N., Ostuni, E., Whitesides, G. M. & Ingber, D. E. Micropatterning tractional forces in living cells. *Cell Motil. Cytoskeleton* **52**, 97–106 (2002).

21. Théry, M., Pépin, A., Dressaire, E., Chen, Y. & Bornens, M. Cell distribution of stress fibres in response to the geometry of the adhesive environment. *Cell Motil. Cytoskeleton* **63**, 341–55 (2006).
22. Kilian, K. a, Bugarija, B., Lahn, B. T. & Mrksich, M. Geometric cues for directing the differentiation of mesenchymal stem cells. *Proc. Natl. Acad. Sci.* **107**, 4872–7 (2010).
23. Coyer, S. R. *et al.* Nanopatterning Reveals an ECM Area Threshold for Focal Adhesion Assembly and Force Transmission that is regulated by Integrin Activation and Cytoskeleton Tension. *J. Cell Sci.* **125**, 5110–23 (2012).
24. Chang, S. S., Guo, W., Kim, Y. & Wang, Y. Guidance of cell migration by substrate dimension. *Biophys. J.* **104**, 313–21 (2013).
25. Zhang, J., Guo, W.-H. & Wang, Y.-L. Microtubules stabilize cell polarity by localizing rear signals. *Proc. Natl. Acad. Sci.* **111**, 16383–8 (2014).
26. Pouthas, F. *et al.* In migrating cells, the Golgi complex and the position of the centrosome depend on geometrical constraints of the substratum. *J. Cell Sci.* **121**, 2406–14 (2008).
27. Doyle, A. D., Wang, F. W., Matsumoto, K. & Yamada, K. M. One-dimensional topography underlies three-dimensional fibroblast cell migration. *J. Cell Biol.* **184**, 481–490 (2009).
28. Davis, K. A., Burke, K. A., Mather, P. T. & Henderson, J. H. Dynamic cell behavior on shape memory polymer substrates. *Biomaterials* **32**, 2285–2293 (2011).
29. Ebara, M., Uto, K., Idota, N., Hoffman, J. M. & Aoyagi, T. The taming of the cell: Shape-memory nanopatterns direct cell orientation. *Int. J. Nanomedicine* **9**, 117–126 (2014).
30. Lam, M. T., Clem, W. C. & Takayama, S. Reversible on-demand cell alignment using reconfigurable microtopography. *Biomaterials* **29**, 1705–1712 (2008).
31. Cui, Y. *et al.* Cyclic stretching of soft substrates induces spreading and growth. *Nat. Commun.* **6**, 6333 (2015).
32. Lee, C. F., Haase, C., Deguchi, S. & Kaunas, R. Cyclic stretch-induced stress fiber dynamics - Dependence on strain rate, Rho-kinase and MLCK. *Biochem. Biophys. Res. Commun.* **401**, 344–349 (2010).
33. Gadhari, N., Charnley, M., Marelli, M., Brugger, J. & Chiquet, M. Cell shape-dependent early responses of fibroblasts to cyclic strain. *Biochim. Biophys. Acta* **1833**, 3415–25 (2013).
34. Hsu, P.-P. *et al.* Effects of Flow Patterns on Endothelial Cell Migration into a Zone of Mechanical Denudation. *Biochem. Biophys. Res. Commun.* **285**, 751–759 (2001).
35. Lin, K. *et al.* Molecular mechanism of endothelial growth arrest by laminar shear stress. *Proc. Natl. Acad. Sci.* **97**, 9385–9 (2000).
36. Takahashi, M., Ishida, T., Traub, O., Corson, M. & Berk, B. Mechanotransduction in endothelial cells- temporal signaling events in response to shear stress. *J. Vasc. Res.* **34**, 212–219 (1997).
37. Hsu, S., Thakar, R., Liepmann, D. & Li, S. Effects of shear stress on endothelial cell haptotaxis on micropatterned surfaces. *Biochem. Biophys. Res. Commun.* **337**, 401–9 (2005).
38. Helmlinger, G., Geiger, R., Schreck, S. & Nerem, R. Effects of Pulsatile Flow on Cultured Vascular Endothelial Cell Morphology. *J. Biomech. Eng.* **113**, 123–131 (1991).
39. Blackman, B. R. & Gimbrone, M. A. A New In Vitro Model to Evaluate Differential Responses of Endothelial Cells to Simulated. *Image (Rochester, N.Y.)* **124**, 397–407 (2002).

40. Galie, P. a *et al.* Fluid shear stress threshold regulates angiogenic sprouting. *Proc. Natl. Acad. Sci.* **111**, (2014).
41. Nakanishi, J. *et al.* Spatiotemporal control of migration of single cells on a photoactivatable cell microarray. *J. Am. Chem. Soc.* **129**, 6694–5 (2007).
42. Vignaud, T. *et al.* Reprogramming cell shape with laser nano-patterning. *J. Cell Sci.* **125**, 2134–40 (2012).
43. Rolli, C. G. *et al.* Switchable adhesive substrates: Revealing geometry dependence in collective cell behavior. *Biomaterials* **33**, 2409–2418 (2012).
44. Young, J. L. & Engler, A. J. Hydrogels with time-dependent material properties enhance cardiomyocyte differentiation in vitro. *Biomaterials* **32**, 1002–9 (2011).
45. Guvendiren, M. & Burdick, J. a. Stiffening hydrogels to probe short- and long-term cellular responses to dynamic mechanics. *Nat. Commun.* **3**, 792 (2012).
46. Kloxin, A. M., Benton, J. a & Anseth, K. S. In situ elasticity modulation with dynamic substrates to direct cell phenotype. *Biomaterials* **31**, 1–8 (2010).
47. Frey, M. T. & Wang, Y. A photo-modulatable material for probing cellular responses to substrate rigidity. *Soft Matter* **5**, 1918–1924 (2009).
48. Kloxin, A. M., Kasko, A. M., Salinas, C. N. & Anseth, K. S. Photodegradable hydrogels for dynamic tuning of physical and chemical properties. *Science* **324**, 59–63 (2009).
49. Beningo, K. A. & Wang, Y. L. Flexible substrata for the detection of cellular traction forces. *Trends Cell Biol.* **12**, 79–84 (2002).
50. Tse, J. R. & Engler, A. J. Preparation of hydrogel substrates with tunable mechanical properties. *Curr. Protoc. Cell Biol.* **Chapter 10**, Unit 10.16 (2010).
51. Palchesko, R. N., Zhang, L., Sun, Y. & Feinberg, A. W. Development of Polydimethylsiloxane Substrates with Tunable Elastic Modulus to Study Cell Mechanobiology in Muscle and Nerve. *PLoS One* **7**, e51499 (2012).
52. Chen, C. S., Brown, X. Q., Ookawa, K. & Wong, J. Y. Evaluation of polydimethylsiloxane scaffolds with physiologically-relevant elastic moduli: interplay of substrate mechanics and surface chemistry effects on vascular smooth muscle cell response. *Biomaterials* **26**, 3123–3129 (2005).
53. Kloxin, A. M., Tibbitt, M. W. & Anseth, K. S. Synthesis of photodegradable hydrogels as dynamically tunable cell culture platforms. *Nat. Protoc.* **5**, 1867–1887 (2010).
54. Pelham, R. J. & Wang, Y. Cell locomotion and focal adhesions are regulated by substrate flexibility. *Cell* **94**, 13661–13665 (1997).
55. Yeung, T. *et al.* Effects of substrate stiffness on cell morphology, cytoskeletal structure, and adhesion. *Cell Motil. Cytoskeleton* **60**, 24–34 (2005).
56. Solon, J., Levental, I., Sengupta, K., Georges, P. C. & Janmey, P. A. Fibroblast Adaptation and Stiffness Matching to Soft Elastic Substrates. *Biophys. J.* **93**, 4453–4461 (2007).
57. Tee, S. Y., Fu, J., Chen, C. S. & Janmey, P. A. Cell shape and substrate rigidity both regulate cell stiffness. *Biophys. J.* **100**, L25–L27 (2011).
58. Byfield, F. J., Reen, R. K., Shentu, T.-P., Levitan, I. & Gooch, K. J. Endothelial actin and cell stiffness is modulated by substrate stiffness in 2D and 3D. *J. Biomech.* **42**, 1114–1119 (2009).
59. Murray, M. E., Mendez, M. G. & Janmey, P. a. Substrate stiffness regulates solubility of cellular vimentin. *Mol. Biol. Cell* **25**, 87–94 (2014).
60. Heck, J. N. *et al.* Microtubules regulate GEF-H1 in response to extracellular matrix

- stiffness. *Mol. Biol. Cell* **23**, 2583–2592 (2012).
61. Pasapera, A. M., Schneider, I. C., Rericha, E., Schlaepfer, D. D. & Waterman, C. M. Myosin II activity regulates vinculin recruitment to focal adhesions through FAK-mediated paxillin phosphorylation. *J. Cell Biol.* **188**, 877–90 (2010).
  62. Doyle, A. D., Carvajal, N., Jin, A., Matsumoto, K. & Yamada, K. M. Local 3D matrix microenvironment regulates cell migration through spatiotemporal dynamics of contractility-dependent adhesions. *Nat. Commun.* **6**, 8720 (2015).
  63. Even-Ram, S. *et al.* Myosin IIA regulates cell motility and actomyosin-microtubule crosstalk. *Nat. Cell Biol.* **9**, 299–309 (2007).
  64. Vogel, V. & Sheetz, M. Local force and geometry sensing regulate cell functions. *Nat. Rev. Mol. Cell Biol.* **7**, 265–75 (2006).
  65. Wang, H., Dembo, M. & Wang, Y. Substrate flexibility regulates growth and apoptosis of normal but not transformed cells. *Am. J. Physiol. Cell Physiol.* **279**, C1345–C1350 (2000).
  66. Klein, E. A. *et al.* Cell-Cycle Control by Physiological Matrix Elasticity and In Vivo Tissue Stiffening. *Curr. Biol.* **19**, 1511–1518 (2009).
  67. Lo, C. M., Wang, H., Dembo, M. & Wang, Y.-L. Cell movement is guided by the rigidity of the substrate. *Biophys. J.* **79**, 144–52 (2000).
  68. Wong, J. Y., Velasco, A., Rajagopalan, P. & Pham, Q. Directed Movement of Vascular Smooth Muscle Cells on Gradient-Compliant Hydrogels. *Langmuir* **19**, 1908–1913 (2003).
  69. Gray, D. S., Tien, J. & Chen, C. S. Repositioning of cells by mechanotaxis on surfaces with micropatterned Young 's modulus. *J. Biomed. Mater. Res.* 605–614 (2003).
  70. Vincent, L. G., Choi, Y. S., Alonso-Latorre, B., del Alamo, J. C. & Engler, A. J. Mesenchymal stem cell durotaxis depends on substrate stiffness gradient strength. *Biotechnol. J.* **8**, 472–484 (2013).
  71. Raab, M. *et al.* Crawling from soft to stiff matrix polarizes the cytoskeleton and phosphoregulates myosin-II heavy chain. *J. Cell Biol.* **199**, 669–83 (2012).
  72. Guo, W., Frey, M. T., Burnham, N. a & Wang, Y. Substrate rigidity regulates the formation and maintenance of tissues. *Biophys. J.* **90**, 2213–20 (2006).
  73. de Rooij, J., Kerstens, A., Danuser, G., Schwartz, M. a & Waterman-Storer, C. M. Integrin-dependent actomyosin contraction regulates epithelial cell scattering. *J. Cell Biol.* **171**, 153–64 (2005).
  74. Qiu, Y. *et al.* Platelet mechanosensing of substrate stiffness during clot formation mediates adhesion, spreading, and activation. *Proc. Natl. Acad. Sci.* **111**, 14430–14435 (2014).
  75. Engler, A. J., Sen, S., Sweeney, H. L. & Discher, D. E. Matrix elasticity directs stem cell lineage specification. *Cell* **126**, 677–89 (2006).
  76. Kolahi, K. S. *et al.* Effect of substrate stiffness on early mouse embryo development. *PLoS One* **7**, (2012).
  77. Keung, A. J., Asuri, P., Kumar, S. & Schaffer, D. V. Soft microenvironments promote the early neurogenic differentiation but not self-renewal of human pluripotent stem cells. *Integr. Biol. (Camb)*. **4**, 1049–1058 (2012).
  78. Keung, A. J., De Juan-Pardo, E. M., Schaffer, D. V. & Kumar, S. Rho GTPases mediate the mechanosensitive lineage commitment of neural stem cells. *Stem Cells* **29**, 1886–1897 (2011).
  79. Jungmann, P. M. *et al.* Nanomechanics of human adipose-derived stem cells: small

- GTPases impact chondrogenic differentiation. *Tissue Eng. Part A* **18**, 1035–44 (2012).
80. Dupont, S. *et al.* Role of YAP/TAZ in mechanotransduction. *Nature* **474**, 179–183 (2011).
  81. Leight, J. L., Wozniak, M. a, Chen, S., Lynch, M. L. & Chen, C. S. Matrix rigidity regulates a switch between TGF- $\beta$ 1-induced apoptosis and epithelial-mesenchymal transition. *Mol. Biol. Cell* **23**, 781–91 (2012).
  82. Lv, H. *et al.* Mechanism of regulation of stem cell differentiation by matrix stiffness. *Stem Cell Res. Ther.* **6**, 103 (2015).
  83. Forte, G. *et al.* Substrate stiffness modulates gene expression and phenotype in neonatal cardiomyocytes in vitro. *Tissue Eng. Part A* **18**, 1837–48 (2012).
  84. Zhang, Y. H., Zhao, C. Q., Jiang, L. S. & Dai, L. Y. Substrate stiffness regulates apoptosis and the mRNA expression of extracellular matrix regulatory genes in the rat annular cells. *Matrix Biol.* **30**, 135–144 (2011).
  85. Discher, D. E., Janmey, P. & Wang, Y.-L. Tissue cells feel and respond to the stiffness of their substrate. *Science* **310**, 1139–43 (2005).
  86. Mason, B. N., Califano, J. P. & Reinhart-king, C. A. in *Eng. Biomater. Regen. Med.* (Bhatia, S. K.) 19–38 (Springer New York, 2012). doi:10.1007/978-1-4614-1080-5
  87. Wells, R. G. The role of matrix stiffness in regulating cell behavior. *Hepatology* **47**, 1394–1400 (2008).
  88. Levy-Mishali, M., Zoldan, J. & Levenberg, S. Effect of scaffold stiffness on myoblast differentiation. *Tissue Eng. Part A* **15**, 935–44 (2009).
  89. Butcher, D. T., Alliston, T. & Weaver, V. M. A tense situation: forcing tumour progression. *Nat. Rev. Cancer* **9**, 108–22 (2009).
  90. Paszek, M. J. *et al.* Tensional homeostasis and the malignant phenotype. *Cancer Cell* **8**, 241–54 (2005).
  91. Tilghman, R. W. *et al.* Matrix rigidity regulates cancer cell growth and cellular phenotype. *PLoS One* **5**, e12905 (2010).
  92. Ulrich, T. a, de Juan Pardo, E. M. & Kumar, S. The mechanical rigidity of the extracellular matrix regulates the structure, motility, and proliferation of glioma cells. *Cancer Res.* **69**, 4167–74 (2009).
  93. Ingber, D. E. Mechanobiology and diseases of mechanotransduction. *Ann. Med.* **35**, 564–577 (2003).
  94. Trounson, A. & McDonald, C. Stem Cell Therapies in Clinical Trials: Progress and Challenges. *Cell Stem Cell* **17**, 11–22 (2015).
  95. Dib, N., Khawaja, H., Varner, S., McCarthy, M. & Campbell, A. Cell therapy for cardiovascular disease: A comparison of methods of delivery. *J. Cardiovasc. Transl. Res.* **4**, 177–181 (2011).
  96. Sakiyama-Elbert. Combining stem cells and biomaterial scaffolds for constructing tissues and cell delivery. *StemBook* 1–18 (2008). doi:10.3824/stembook.1.1.1
  97. Pickup, M. W., Mouw, J. K. & Weaver, V. M. The extracellular matrix modulates the hallmarks of cancer. *EMBO Rep* **15**, 1243–1253 (2014).
  98. Amy CY Lo, F. S. Collagen-Based Scaffolds for Cell Therapies in the Injured Brain. *J. Stem Cell Res. Ther.* **05**, (2015).
  99. Janmey, P. a & Miller, R. T. Mechanisms of mechanical signaling in development and disease. *J. Cell Sci.* **124**, 9–18 (2011).
  100. Midwood, K. S., Williams, L. V. & Schwarzbauer, J. E. Tissue repair and the dynamics of the extracellular matrix. *Int. J. Biochem. Cell Biol.* **36**, 1031–1037 (2004).

101. Camelliti, P., Borg, T. K. & Kohl, P. Structural and functional characterisation of cardiac fibroblasts. *Cardiovasc. Res.* **65**, 40–51 (2005).
102. Fishbein, M. C., Maclean, D. & Maroko, P. R. The histopathologic evolution of myocardial infarction. *Chest* **73**, 843–849 (1978).
103. Lerman, R. H. *et al.* Myocardial healing and repair after experimental infarction in the rabbit. *Circ. Res.* **53**, 378–388 (1983).
104. Kass, D. A., Bronzwaer, J. G. F. & Paulus, W. J. What mechanisms underlie diastolic dysfunction in heart failure? *Circ. Res.* **94**, 1533–1542 (2004).
105. O'Rourke, M. Arterial stiffness, systolic blood pressure, and logical treatment of arterial hypertension. *Hypertension* **15**, 339–347 (1990).
106. Ziemann, S. J., Melenovsky, V. & Kass, D. A. Mechanisms, pathophysiology, and therapy of arterial stiffness. *Arterioscler. Thromb. Vasc. Biol.* **25**, 932–943 (2005).
107. Cecelja, M. & Chowienczyk, P. Role of arterial stiffness in cardiovascular disease. *JRSM Cardiovasc. Dis.* **1**, 11 (2012).
108. Bataller, R. & Brenner, D. Liver fibrosis. *J. Clin. Invest.* **115**, 209–218 (2005).
109. Gabele, E., Brenner, D. & Rippe, R. Liver fibrosis: signals leading to the amplification of the fibrogenic hepatic stellate cell. *Front Biosci.* **1**, 69–77 (2003).
110. Friedman, S. L. Liver fibrosis - from bench to bedside. *J. Hepatol.* **38**, S38–S53 (2003).
111. Georges, P. C. *et al.* Increased stiffness of the rat liver precedes matrix deposition: implications for fibrosis. *Am. J. Physiol. Gastrointest. Liver Physiol.* **293**, 1147–1154 (2007).
112. Zahir, N. & Weaver, V. M. Death in the third dimension: Apoptosis regulation and tissue architecture. *Curr. Opin. Genet. Dev.* **14**, 71–80 (2004).
113. Gérard, C. & Goldbeter, A. The balance between cell cycle arrest and cell proliferation: control by the extracellular matrix and by contact inhibition. *Interface Focus* **4**, 20130075 (2014).
114. Schrader, J. *et al.* Matrix Stiffness Modulates Proliferation, Chemotherapeutic Response and Dormancy in Hepatocellular Carcinoma Cells. *Hepatology* **53**, 1192–1205 (2011).
115. O'Connor, R. S. *et al.* Substrate rigidity regulates human T cell activation and proliferation. *J. Immunol.* **189**, 1330–9 (2012).
116. Boyd, N. *et al.* Mammographic density and the risk and detection of breast cancer. *N Engl J Med* **356**, 227–236 (2007).
117. Kraning-Rush, C. M., Califano, J. P. & Reinhart-King, C. A. Cellular traction stresses increase with increasing metastatic potential. *PLoS One* **7**, e32572 (2012).
118. Lee, K. *et al.* Matrix compliance regulates Rac1b localization, NADPH oxidase assembly, and epithelial-mesenchymal transition. *Mol. Biol. Cell* **23**, 4097–108 (2012).
119. Hoj, J. P. *et al.* Cellular contractility changes are sufficient to drive epithelial scattering. *Exp. Cell Res.* **326**, 187–200 (2014).
120. Yilmaz, M. & Christofori, G. EMT, the cytoskeleton, and cancer cell invasion. *Cancer Metastasis Rev.* **28**, 15–33 (2009).
121. Brabletz, T. EMT and MET in Metastasis: Where Are the Cancer Stem Cells? *Cancer Cell* **22**, 699–701 (2012).
122. Tokuda, E. Y., Leight, J. L. & Anseth, K. S. Modulation of matrix elasticity with PEG hydrogels to study melanoma drug responsiveness. *Biomaterials* **35**, 4310–4318 (2014).
123. Lin, C.-H. *et al.* Microenvironment rigidity modulates responses to the HER2 receptor tyrosine kinase inhibitor lapatinib via YAP and TAZ transcription factors. *Mol. Biol. Cell*

- 26**, 3946–3953 (2015).
124. Dembo, M. & Wang, Y.-L. Stresses at the cell-to-substrate interface during locomotion of fibroblasts. *Biophys. J.* **76**, 2307–2316 (1999).
  125. Parsons, J. T., Horwitz, A. R. & Schwartz, M. A. Cell adhesion: integrating cytoskeletal dynamics and cellular tension. *Nat. Rev. Mol. Cell Biol.* **11**, 633–643 (2010).
  126. Rape, A. D., Guo, W. & Wang, Y. in *Mechanobiol. Cell-Cell Cell-Matrix Interact.* (Wagoner Johnson, A. & Harley, B. A. C.) 1–10 (Springer US, 2011). doi:10.1007/978-1-4419-8083-0
  127. Harris, A., Wild, P. & Stopak, D. Silicone rubber substrata: a new wrinkle in the study of cell locomotion. *Sci. Reports* **208**, 177–179 (1980).
  128. Hoffecker, I. T., Guo, W. & Wang, Y. Assessing the spatial resolution of cellular rigidity sensing using a micropatterned hydrogel-photoresist composite. *Lab Chip* **11**, 3538–44 (2011).
  129. Trichet, L. *et al.* Evidence of a large-scale mechanosensing mechanism for cellular adaptation to substrate stiffness. *Proc. Natl. Acad. Sci.* **109**, 6933–8 (2012).
  130. Breckenridge, M. T., Desai, R. a., Yang, M. T., Fu, J. & Chen, C. S. Substrates with Engineered Step Changes in Rigidity Induce Traction Force Polarity and Durotaxis. *Cell. Mol. Bioeng.* **7**, 26–34 (2013).
  131. Hynes, R. O. Integrins: versatility, modulation, and signaling in cell adhesion. *Cell* **69**, 11–25 (1992).
  132. Wu, C., Bauer, J. S., Juliano, R. L. & McDonald, J. A. The  $\alpha 5\beta 1$  integrin fibronectin receptor, but not the  $\alpha 5$  cytoplasmic domain, functions in an early and essential step in fibronectin matrix assembly. *J. Biol. Chem.* **268**, 21883–21888 (1993).
  133. Gullberg, D. *et al.* Analysis of  $\alpha 1\beta 1$ ,  $\alpha 2\beta 1$  and  $\alpha 3\beta 1$  integrins in cell - Collagen interactions: Identification of conformation dependent  $\alpha 1\beta 1$ , binding sites in collagen type I. *EMBO J.* **11**, 3865–3873 (1992).
  134. Shintani, Y., Wheelock, M. J. & Johnson, K. R. Kinase Signaling Mediates Collagen I – induced Cell Scattering and Up-Regulation of N-Cadherin Expression in Mouse Mammary Epithelial Cells □. *Mol. Biol. Cell* **17**, 2963–2975 (2006).
  135. Elosegui-Artola, A. *et al.* Rigidity sensing and adaptation through regulation of integrin types. *Nat. Mater.* **13**, 631–7 (2014).
  136. Tan, J. L. *et al.* Cells lying on a bed of microneedles : An approach to isolate mechanical force. *Proc. Natl. Acad. Sci.* **100**, 1484–1489 (2002).
  137. Ghassemi, S. *et al.* Cells test substrate rigidity by local contractions on submicrometer pillars. *Proc. Natl. Acad. Sci.* **109**, 5328–5333 (2012).
  138. Wolfenson, H. *et al.* Tropomyosin controls sarcomere-like contractions for rigidity sensing and suppressing growth on soft matrices. *Nat. Cell Biol.* **18**, 33–42 (2015).
  139. Plotnikov, S. V, Pasapera, A. M., Sabass, B. & Waterman, C. M. Force Fluctuations within Focal Adhesions Mediate ECM-Rigidity Sensing to Guide Directed Cell Migration. *Cell* **151**, 1513–27 (2012).
  140. Hayakawa, K., Tatsumi, H. & Sokabe, M. Actin filaments function as a tension sensor by tension-dependent binding of cofilin to the filament. *J. Cell Biol.* **195**, 721–727 (2011).
  141. Galkin, V. E., Orlova, A. & Egelman, E. H. Actin filaments as tension sensors. *Curr. Biol.* **22**, R96–R101 (2012).
  142. Byfield, F. J. *et al.* Absence of filamin A prevents cells from responding to stiffness gradients on gels coated with collagen but not fibronectin. *Biophys. J.* **96**, 5095–5102

- (2009).
143. Ehrlicher, A. J., Nakamura, F., Hartwig, J. H., Weitz, D. A. & Stossel, T. P. Mechanical strain in actin networks regulates FilGAP and integrin binding to filamin A. *Nature* **478**, 260–263 (2011).
  144. Kim, D.-H. *et al.* Actin cap associated focal adhesions and their distinct role in cellular mechanosensing. *Sci. Rep.* **2**, 555 (2012).
  145. Kobayashi, T. & Sokabe, M. Sensing substrate rigidity by mechanosensitive ion channels with stress fibers and focal adhesions. *Curr. Opin. Cell Biol.* **22**, 669–76 (2010).
  146. Jiang, G., Huang, A. H., Cai, Y., Tanase, M. & Sheetz, M. P. Rigidity sensing at the leading edge through  $\alpha$ 5 $\beta$ 3 integrins and RPTP $\alpha$ . *Biophys. J.* **90**, 1804–9 (2006).
  147. Hoffman, B. D., Grashoff, C. & Schwartz, M. a. Dynamic molecular processes mediate cellular mechanotransduction. *Nature* **475**, 316–23 (2011).
  148. Plotnikov, S. V & Waterman, C. M. Guiding cell migration by tugging. *Curr. Opin. Cell Biol.* 1–8 (2013). doi:10.1016/j.ceb.2013.06.003
  149. Shemesh, T., Geiger, B., Bershadsky, A. D. & Kozlov, M. M. Focal adhesions as mechanosensors: a physical mechanism. *Proc. Natl. Acad. Sci. U. S. A.* **102**, 12383–12388 (2005).
  150. Bell, G. Models for the specific adhesion of cells to cells. *Science* **200**, 618–627 (1978).
  151. Thomas, W. E., Vogel, V. & Sokurenko, E. Biophysics of catch bonds. *Annu. Rev. Biophys.* **37**, 399–416 (2008).
  152. Prezhdov, O. V. & Pereverzev, Y. V. Theoretical aspects of the biological catch bond. *Acc. Chem. Res.* **42**, 693–703 (2009).
  153. Choquet, D., Felsenfeld, D. P. & Sheetz, M. P. Extracellular Matrix Rigidity Causes Strengthening of Integrin–Cytoskeleton Linkages. *Cell* **88**, 39–48 (1997).
  154. Wang, N., Butler, J. P., Ingber, D. E. & Donald, E. Mechanotransduction across the cell surface and through the cytoskeleton. *Sci. Reports* **260**, 1124–1127 (1993).
  155. Plopper, G. & Ingber, D. E. Rapid induction and isolation of focal adhesion complexes. *Biochem. Biophys. Res. Commun.* **193**, 571–578 (1993).
  156. Galbraith, C. G., Yamada, K. M. & Sheetz, M. P. The relationship between force and focal complex development. *J. Cell Biol.* **159**, 695–705 (2002).
  157. Rivelino, D. *et al.* Focal contacts as mechanosensors: externally applied local mechanical force induces growth of focal contacts by an mDia1-dependent and ROCK-independent mechanism. *J. Cell Biol.* **153**, 1175–86 (2001).
  158. Wang, H., Dembo, M., Hanks, S. K. & Wang, Y. Focal adhesion kinase is involved in mechanosensing during fibroblast migration. *Proc. Natl. Acad. Sci.* **98**, 11295–300 (2001).
  159. Schoen, I., Pruitt, B. L. & Vogel, V. The Yin-Yang of Rigidity Sensing: How Forces and Mechanical Properties Regulate the Cellular Response to Materials. *Annu. Rev. Mater. Res.* **43**, 589–618 (2013).
  160. Moore, S. W., Roca-Cusachs, P. & Sheetz, M. P. Stretchy proteins on stretchy substrates: the important elements of integrin-mediated rigidity sensing. *Dev. Cell* **19**, 194–206 (2010).
  161. Oakes, P. W. & Gardel, M. L. Stressing the limits of focal adhesion mechanosensitivity. *Curr. Opin. Cell Biol.* **30**, 68–73 (2014).
  162. Humphries, J. D. *et al.* Vinculin controls focal adhesion formation by direct interactions with talin and actin. *J. Cell Biol.* **179**, 1043–57 (2007).

163. Rio, A. *et al.* Stretching Single Talin Rod Modulates Activates Vinculin Binding. *Sci. Reports* **323**, 638–641 (2009).
164. Chen, H., Cohen, D. M., Choudhury, D. M., Kioka, N. & Craig, S. W. Spatial distribution and functional significance of activated vinculin in living cells. *J. Cell Biol.* **169**, 459–70 (2005).
165. Case, L. B. *et al.* Molecular mechanism of vinculin activation and nanoscale spatial organization in focal adhesions. *Nat. Cell Biol.* **17**, 880–892 (2015).
166. Grashoff, C. *et al.* Measuring mechanical tension across vinculin reveals regulation of focal adhesion dynamics. *Nature* **466**, 263–6 (2010).
167. Schoenwaelder, S. M. & Burridge, K. Bidirectional signaling between the cytoskeleton and integrins. *Curr. Opin. Cell Biol.* **11**, 274–86 (1999).
168. Von Wichert, G., Haimovich, B., Feng, G. S. & Sheetz, M. P. Force-dependent integrin-cytoskeleton linkage formation requires downregulation of focal complex dynamics by Shp2. *EMBO J.* **22**, 5023–5035 (2003).
169. Felsenfeld, D. P., Schwartzberg, P. L., Venegas, a, Tse, R. & Sheetz, M. P. Selective regulation of integrin--cytoskeleton interactions by the tyrosine kinase Src. *Nat. Cell Biol.* **1**, 200–206 (1999).
170. von Wichert, G. *et al.* RPTP-alpha acts as a transducer of mechanical force on alphav/beta3-integrin-cytoskeleton linkages. *J. Cell Biol.* **161**, 143–53 (2003).
171. Wang, Y. *et al.* Visualizing the mechanical activation of Src. *Nature* **434**, 1040–1045 (2005).
172. Huveneers, S. & Danen, E. H. J. Adhesion signaling - crosstalk between integrins, Src and Rho. *J. Cell Sci.* **122**, 1059–1069 (2009).
173. Tamada, M., Sheetz, M. P. & Sawada, Y. Activation of a signaling cascade by cytoskeleton stretch. *Dev. Cell* **7**, 709–718 (2004).
174. Sawada, Y. *et al.* Rap1 is involved in cell stretching modulation of p38 but not ERK or JNK MAP kinase. *J. Cell Sci.* **114**, 1221–1227 (2001).
175. Plotnikov, A., Zehorai, E., Procaccia, S. & Seger, R. The MAPK cascades: Signaling components, nuclear roles and mechanisms of nuclear translocation. *Biochim. Biophys. Acta - Mol. Cell Res.* **1813**, 1619–1633 (2011).
176. Cargnello, M. & Roux, P. P. Activation and function of the MAPKs and their substrates, the MAPK-activated protein kinases. *Microbiol. Mol. Biol. Rev.* **75**, 50–83 (2011).
177. Wong, S., Guo, W., Hoffecker, I. T. & Wang, Y. in *Methods Cell Biol.* (2014).
178. Wong, S., Guo, W.-H. & Wang, Y.-L. Fibroblasts probe substrate rigidity with filopodia extensions before occupying an area. *Proc. Natl. Acad. Sci.* **111**, 1–6 (2014).

## Chapter 2

# Preparation of a Micropatterned Rigid-Soft Composite Substrate for Probing Cellular Rigidity Sensing

Substrate rigidity has been recognized as an important property of the extracellular environment that affects cellular physiology and functions. While the phenomenon has been well recognized, understanding the underlying mechanism may be greatly facilitated by creating a microenvironment with designed rigidity patterns. This chapter describes in detail an optimized method for preparing, troubleshooting, and testing substrates with micropatterned rigidity. We utilize a method for preparing a composite substrate that takes advantage of the ability to dehydrate polyacrylamide gels for micropatterning with photolithography, and subsequently rehydrate the gel to regain the original elastic state. While a wide range of micropatterns may be prepared, we have developed a model experimental system that confines cells to a micropatterned area with a rigidity border. The system consists of a rigid domain of one large adhesive island, adjacent to a soft domain of small adhesive islands grafted on non-adhesive soft gels. Depending on the stiffness of the underlying polyacrylamide hydrogel, these islands may or may not be displaceable by cellular traction forces. NIH 3T3 cells responded to the composite substrate by preferentially locating to the large island after culturing overnight on the composite substrate with a soft underlying hydrogel, while cells on composite substrates with a stiff underlying hydrogel were able to occupy most of the small islands. This composite material facilitates systematic investigation of rigidity sensing and durotaxis.

## 2.1 Introduction

Micropatterning has been utilized during the past two decades to create microenvironments of defined geometry at a micron scale<sup>1</sup>. It allows systematic testing of specific features of the *in vivo* environment for their biological effects. By controlling the geometry of adhesive areas on glass, previous micropatterning studies have demonstrated the effects of cell shape and size on events such as apoptosis, proliferation, differentiation, and migration<sup>2-7</sup>.

An important parameter that would benefit from micropatterning studies is substrate rigidity, which is known to cause profound cellular responses<sup>8-10</sup>. Most studies of cellular rigidity sensing have relied on the use of either elastic polymers or bendable micropost arrays as the substrate. The former included PDMS<sup>11,12</sup>, polyacrylamide<sup>13,14</sup>, or PEG based systems<sup>15</sup>, where the elasticity may be controlled over a wide range by altering the concentration of the crosslinker and/or the base material. The latter involved the preparation of PDMS pillars with bending moduli varied over a limited range by changing the diameter or height of the pillars<sup>16,17</sup>, or over a wider range by changing both the rigidity of PDMS used for pillar fabrication and dimension of the pillars<sup>18</sup>.

Both elastic polymers and micropost arrays may be micropatterned by selectively coating the surface with adhesive proteins, to control cell size, shape, and migration. Methods used to micropattern adhesive domains include microstencils<sup>5</sup>, microcontact printing<sup>19,20</sup>, activation with deep UV-exposure through a mask<sup>21</sup>, and microcontact printing of activated proteins on glass followed by transfer of the pattern to the elastic substrate during polymerization<sup>22</sup>. What has been lacking, however, is a method to create micropatterns of mixed rigidity at the scale of a single cell, given the importance of studying cellular responses at a rigidity interface such as in

durotaxis<sup>23</sup>. Previous methods to address durotaxis have involved the creation of a border of rigidity across a substrate surface<sup>17,24</sup>, with serious limitations in the number cells that may be studied at the border.

Methods that have been developed for creating a rigidity interface include polymerization of hydrogels using photosensitive reactions with patterned UV illumination<sup>25,26</sup>, or overlay of a thin hydrogel layer on micron-sized rigid topographic features<sup>27,28</sup>. Rigidity changes may also be created locally in real time using hydrogels formed with photo-labile crosslinkers<sup>29,30</sup>. While these methods create fixed rigidity domains of similar adhesiveness, different questions may be addressed by creating small islands of rigid adhesive materials grafted onto soft non-adhesive surfaces. In the initial study using this approach, we showed that long-range substrate strain between the islands dominates over local rigidity, in determining cellular responses<sup>31</sup>.

To prepare such composite substrates, we dehydrate polyacrylamide hydrogels for attachment of photoresist via micropatterning using standard photolithography techniques, and subsequently rehydrate the hydrogel to regain the original elastic property<sup>31</sup>. The polyacrylamide surface remains non-adhesive to cells, while the photoresist may be treated with ECM proteins to enhance cell adhesion. I present in this chapter a detailed method for generating this material using only inexpensive equipment without a clean room, as well as the design and testing of a pattern to trap cells at a rigidity border to study rigidity sensing.

## **2.2 Experimental Methods**

### **2.2.1 Cell culture**

NIH 3T3 cells (ATCC, Bethesda, MD) were maintained in Dulbecco's modified Eagle's medium (DMEM; Life Technologies, Waltham, MA) supplemented with 10% adult donor bovine serum (Thermo Scientific, Waltham, MA), 2 mM L-glutamine, 50 µg/mL streptomycin, and 50 U/mL penicillin (Life Technologies). MDCK cells (ATCC) were maintained in DMEM (Life Technologies) supplemented with 10% fetal bovine serum (Thermo Scientific), 2 mM L-glutamine, 50 µg/mL streptomycin, and 50 U/mL penicillin (Life Technologies). NRK52E cells (ATCC) were maintained in a 1:1 ratio of Dulbecco's modified Eagle's medium: Nutrient Mixture F-12 (DMEM/F12; Life Technologies) supplemented with 10% fetal bovine serum (Thermo Scientific), 2 mM L-glutamine, 50 µg/mL streptomycin, and 50 U/mL penicillin (Life Technologies).

### **2.2.2 Microscopy and image analysis**

Phase contrast images of cells on the composite material were collected after 16 hours of incubation with a Nikon Eclipse Ti microscope using a 40x Plan Fluor 0.75 N.A. dry objective. Only single cells were counted for the analysis. For the micromanipulation of SU-8 islands, a microneedle prepared with a vertical micropipette puller (Model 720, David Kopf Instruments, Tujunga, CA) was mounted on a Leitz micromanipulator to allow precise positioning of the tip (Leitz, Deerfield, IL). Phase contrast images were collected with a Zeiss Axiovert 200M using a 40x Plan Neofluar 0.75 N.A. dry objective. Images were collected before, during, and after microneedle manipulation to determine the elastic recovery of island position.

### **2.2.3 Characterization of composite substrates**

To quantify the relative amount of matrix protein adsorbed on the SU-8, Alexa fluor 546 (Life Technologies) conjugated fibronectin (Sigma, St. Louis, MO) or gelatin (Sigma) was prepared according to manufacturer's instruction. 10 µg/mL fibronectin solution or 0.1% gelatin solution was incubated on control or testing substrates for 30 minutes. The substrates were rinsed 3 times with PBS, and fluorescence images of the islands were detected using a Zeiss Axiovert 200M with a 40x Plan Neofluar 0.75 N.A. dry objective lens. Fluorescence intensity was quantified using ImageJ.

To measure the height of SU-8 islands, autofluorescence of SU-8 was used for optical sectioning and Z-stacks of 0.5 µm slices were collected using a Zeiss LSM 700 confocal microscope with a 63x Plan-Apo 1.40 N.A. oil immersion objective lens. The height of orthogonal projection of the stacks was measured using ImageJ.

## 2.3 Creation of a Model Experimental System

### 2.3.1 Design of a durotaxis pattern

Our previous study using this composite substrate indicated that the deformation of a soft hydrogel between islands should lead cells to interpret the region occupied by an array of small islands as being soft<sup>31</sup>. We designed a micropattern, as shown in Figure 2.1, which consists of one large rectangular adhesive island of rigid photoresist,  $45.5 \times 19.5 \mu\text{m}^2$  in area, flanked by two rows of four small square islands of  $6.5 \times 6.5 \mu\text{m}^2$ , grafted on top of a non-adhesive polyacrylamide hydrogel. When grafted on a soft hydrogel the array of small islands functions as a soft domain, while the large island provides an adjacent rigid domain of a similar area. This combination creates a testing substrate that traps cells at or near a rigidity border. The same pattern of islands grafted on a stiff hydrogel creates a control substrate of a similar chemical composition without a rigidity transition. The pattern was designed so that the overall area was  $\sim 2,000 \mu\text{m}^2$ , which is within the normal range of spreading for fibroblasts on rigid adhesive substrates. Therefore, under normal conditions, we expect the cell to cover the overall square area without experiencing a serious constraint.

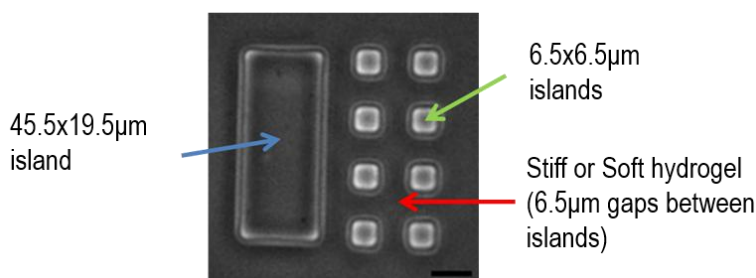


Figure 2.1. The testing substrate consists of a soft hydrogel (red arrow), grafted with one large  $45.5 \times 19.5 \mu\text{m}$  rectangular island to create the rigid domain (blue arrow), and two rows of four  $6.5 \times 6.5 \mu\text{m}$  islands to create the soft domain (green arrow). Control substrates are prepared by grafting the same pattern of islands onto a rigid hydrogel.

Our method for fabricating a composite substrate involves the following steps:

- A. Preparation of thin sheets of polyacrylamide of defined rigidity covalently bound to a glass coverslip for stability (Figure 2.2A).
- B. Dehydration of the polyacrylamide sheet to allow grafting and micropatterning of SU-8 using photolithography (Figure 2.2B-D).
- C. Rehydration of the polyacrylamide sheet and coating of the surface of SU-8 to promote cell adhesion (Figure 2.2E). The pattern of SU-8 grafted to the polyacrylamide gel may be easily seen using transmitted optics (Figure 2.2F).

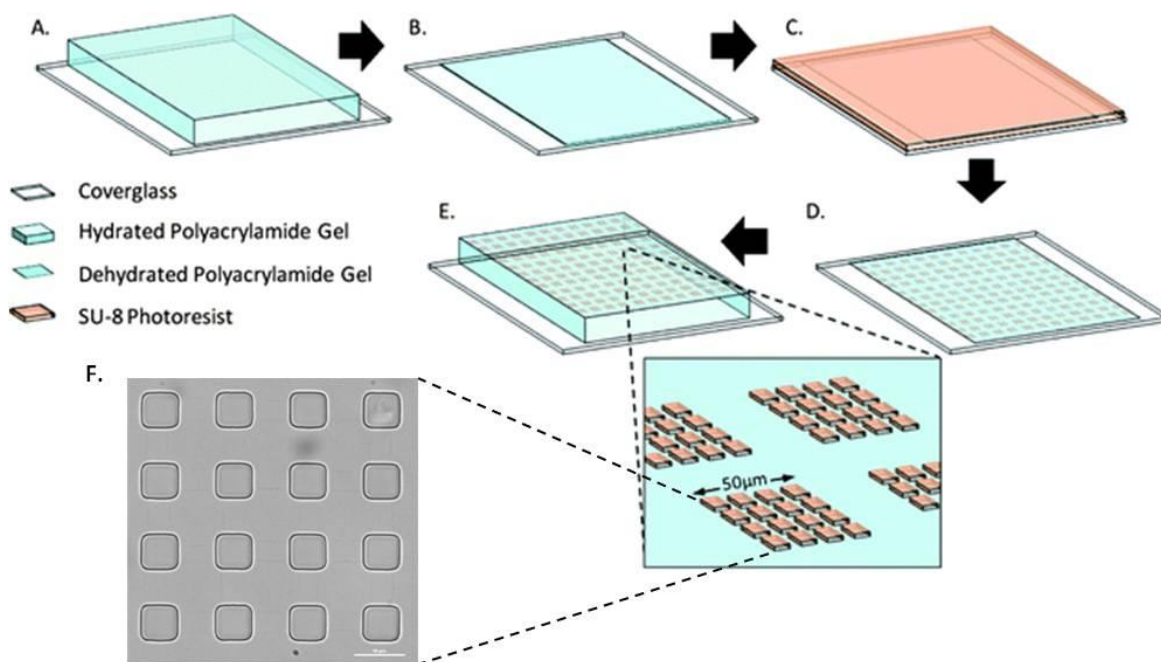


Figure 2.2. Schematic depicting the steps involved in composite substrate fabrication. Polyacrylamide hydrogels are polymerized on bind-silane activated glass coverslips (A). Hydrogels are air dried to dehydrate and flatten the hydrogel before micropatterning (B). A thin layer of SU-8 is spin coated on the dehydrated hydrogel surface (C). The surface is patterned by UV exposure through a photomask containing the desired pattern and development to remove unexposed regions of SU-8 leaving behind the desired pattern (D). Rehydration of the polyacrylamide in PBS allows the hydrogel to regain the original volume, with the patterned SU-8 islands grafted on the surface (E). Phase contrast image of the composite substrate consisting of a 4x4 array of small SU-8 islands on a polyacrylamide gel surface (F). Scale bar, 10  $\mu\text{m}$ . Reproduced from (Hoffecker et al., 2011)<sup>31</sup> with permission of The Royal Society of Chemistry.

### 2.3.2 Preparation of the polyacrylamide gel base

A thin sheet of polyacrylamide gel served as an elastic base for anchoring rigid islands of SU-8 photoresist, such that translocation of the islands is determined by the rigidity of polyacrylamide, the size of the islands, and forces applied by cells to the adhesive islands. The sheet of polyacrylamide must be covalently bound to a glass surface during dehydration, when the hydrogel sheet would otherwise shrink and detach from the surface. Bonding was established by pre-treating the glass surface with bind silane ( $\gamma$ -methacryloxypropyltrimethoxysilane), which reacts with glass through the trimethoxysilane moiety and copolymerizes with acrylamide through the methacryl moiety. For this procedure, one side of a coverslip (45x50 mm for our applications) was marked with a diamond tip pen for identification, the marked side was passed through the plasma of a Bunsen burner flame to render the surface hydrophilic, and 30  $\mu$ L of bind silane working solution was smeared evenly over the flamed side of the coverslip, in a fume hood, using the side of a pipette tip. After 15 minutes at room temperature, when the surface had fully dried, the treated side is rinsed with 70% ethanol and allowed to air dry. These activated coverslips can be stored at room temperature in a desiccator for at least 3 months.

A solution of acrylamide and bis-acrylamide was then polymerized on the activated glass surface. A thin uniform sheet was formed by polymerizing a small volume underneath a top coverslip (25mm circular or square in our applications). The use of a top coverslip also restricts oxygen exposure, which would inhibit the polymerization of acrylamide. A very thin sheet, formed by using a volume of 0.03-0.04  $\mu$ L per  $\text{mm}^2$  surface area during polymerization, is desirable for compatibility with microscope optics. In addition, a thin gel barely rises above the glass surface after dehydration, which facilitates spin coating during subsequent photolithography.

To facilitate removal of the top coverslip the surface can be coated with either Rain-X (to increase hydrophobicity) or 50% sucrose solution (to serve as a sacrificial layer). Such treatment is essential to minimize accidental adhesion of the polyacrylamide surface to the top coverslip, which could otherwise introduce defects on the gel surface, particularly for soft gels, during the removal of the top coverslip. Surface defects in turn compromise the quality of micropatterning and interfere with microscopy. Rain-X solution was smeared over the coverslip and wiped away with a Kimwipe. The surface was then rinsed with distilled water and wiped until clear. It is important to ensure complete treatment of the surface with Rain-X to prevent any local adhesion of the coverslip to polyacrylamide.

To coat the surface with sucrose solution, one side of a top coverslip was marked with a permanent marker and the unmarked side was passed through the plasma of a Bunsen burner flame to render the surface hydrophilic and ensure an even coating of sucrose solution. Approximately 100  $\mu\text{L}$  of 50% w/v sucrose solution was then placed on the flamed side of the coverslip and spread over the entire surface. Uniform coating was achieved by spin-coating the sample at 5,000 rpm for 15 seconds.

The rigidity of the polyacrylamide sheet can be controlled by changing the concentration of acrylamide and/or bis-acrylamide<sup>8</sup>. Calculated volumes of acrylamide, bis-acrylamide, and 0.1 mL of 10x PBS, were mixed with distilled water to reach a total volume of 1 mL, then placed in a sealed chamber under house vacuum to degas for 30 minutes. Skin contact with unpolymerized acrylamide should be avoided as it is a neurotoxin. Freshly prepared solution of 10% w/v APS and TEMED were then added at a volume of 6  $\mu\text{L}$  and 4  $\mu\text{L}$  respectively, and mixed by gentle tapping or pipetting. A 20  $\mu\text{L}$  droplet of solution was pipetted immediately onto a bind silane-

activated coverslip and a Rain-X or sucrose-coated top coverslip was placed on top using a pair of fine tweezers, with the coated side facing the acrylamide solution. The acrylamide solution should spread uniformly underneath the top coverslip; if not, the coverslip was gently moved with a pair of tweezers to help the solution spread. When using a sucrose-coated top coverslip, the coverslip assembly was turned upside down during polymerization to avoid the settling of sucrose into the acrylamide solution due to its higher density. The solution was allowed to polymerize for at least 30 minutes at 25°C.

Following polymerization, the sandwich was turned right side up and the top coverslip removed carefully. Rain-X treated coverslips were removed by flooding the surface of the coverslip with distilled water and waiting for at least 15 minutes to allow water to seep in. A razor blade was then used to lift the top coverslip very slowly off the polyacrylamide gel, with the gel staying submerged in water, to prevent the gel from cracking due to strain. Sucrose-coated coverslips were easier to remove and are recommended for soft gels to avoid surface cracking. They may be removed by immersing the sandwich in hot distilled water in a Petri dish to dissolve the sucrose. The coverslip should release in 20-30 minutes. Following removal of the top coverslip, the gel was washed with distilled water in a Petri dish for 30 minutes on a shaker. This helped prevent the formation of residual sucrose crystals during the subsequent drying.

The edges of the polyacrylamide gel often show a slight lip that could disrupt proper micropatterning. These may be removed using a razor blade to cut away ~1 mm along the edge while keeping the gel hydrated under distilled water. The gel is then rinsed with water to remove any bits of polyacrylamide gel and allowed to air dry overnight. Complete drying of the gel is essential for the subsequent spin coating with SU-8 and photolithography.

### **2.3.3 Micropatterning the polyacrylamide surface with SU-8 photoresist**

Once the polyacrylamide sheet was dry, the surface was micropatterned using SU-8, a negative photoresist that polymerizes upon UV exposure (Figure 2.2). Photomasks with a desired pattern may be obtained on either plastic transparencies (for patterns larger than 10  $\mu\text{m}$ ) or chrome plated lime glass (for high resolution patterns), from companies such as CAD/Art services (Bandon, OR) or Photo-Sciences (Torrance, CA), respectively, which accept CAD file formats such as dwt. Areas for SU-8 coverage should be clear, while areas in between should be masked.

Micropatterning was performed following standard photolithography procedures. The coverslip was first baked on a temperature-regulated heating plate for 1 minute at 95°C, to ensure that the gel surface was completely dry. After cooling to room temperature, approximately 300  $\mu\text{L}$  of SU-8 photoresist solution was spread on the coverslip to cover the dehydrated gel surface. The coverslip was placed in a spin coater and spun at 5,000 rpm for 20 seconds, then baked for 2-3 minutes at 95°C and cooled to room temperature. Using SU-8 2002, this procedure should create a uniform layer ~2-3  $\mu\text{m}$  in thickness.

Contact exposure represents the most economical way to transfer the pattern from the photomask onto the SU-8 photoresist. The coverslip was placed on a platform stand underneath a UV light source with the SU-8 side facing up, overlaid with the photomask with the patterned side facing down, and covered with a piece of plate glass 3 mm in thickness that has an area matching that of the platform. Several binder clips were placed around the plate glass to clamp the plate glass to the stand to ensure tight contact between the photomask and the coverslip. The source of UV may range from an arc lamp with collimated optics for uniform exposure (OAI; San Jose, CA), to inexpensive 360 nm UV photodiodes (Jelight; Irvine, CA). The latter was used in conjunction

with an orbital shaker, which rotates the coverslip assembly underneath the light beam to achieve uniform exposure. The exposure time is dependent on both the power of the UV source and the distance between the lamp and the coverslip, which must be determined by trial and error to ensure adequate patterning. At a light power of  $100 \text{ nJ}\cdot\text{cm}^{-2}$  at the sample, the optimal exposure time was around 60 seconds.

After exposure, the coverslip was baked for 2-3 minutes at  $95^\circ\text{C}$  and allowed to cool to room temperature. It was then immersed in the SU-8 developer in a Petri dish for 90 seconds with agitation, rinsed briefly with ethanol from a squirt bottle, and immersed in a separate Petri dish of ethanol for  $\sim 30$  seconds. After air drying, the micropattern should be easily visible under a microscope. There should be no speckles or films between the intended areas of SU-8, which indicate residual SU-8 due to incomplete development. In addition to potential problems with imaging, residual SU-8 may cause cell adhesion to an otherwise non-adhesive polyacrylamide surface. It may be removed by additional treatment with SU-8 developer, for approximately 10 seconds, and ethanol rinse as described above.

It is essential that all traces of SU-8 developer be removed from the hydrogel to mitigate the risk of cytotoxicity. For immediate use, the coverslip was washed with PBS in a Petri dish for an hour with shaking, to allow both rehydration of the gel and removal of residual developer. Alternatively, the coverslip may be baked for 4 hours at  $95^\circ\text{C}$  to evaporate the residual developer, and then stored in a dessicator at room temperature for up to 3 weeks. Repeated cycles of gel hydration and dehydration should be avoided as they can introduce microcracks on the gel surface.

### 2.3.4 Surface coating with ECM proteins and cell seeding

Before use, the composite substrate was submersed in PBS for approximately 1 hour at room temperature to rehydrate the polyacrylamide hydrogel, then sterilized under the UV of a biosafety cabinet for 15-20 minutes. SU-8 is known to have a biofouling surface<sup>32</sup>, which passively adsorbs proteins from serum containing media. Thus, cells may attach to the SU-8 surface to some extent without any additional treatment with ECM proteins. Cell adhesion to SU-8 surfaces may be optimized, however, by incubation with an ECM protein such as fibronectin, while the polyacrylamide surfaces should remain non-adhesive regardless of the incubation. A twenty-minute incubation at room temperature with the protein of interest (e.g. 10  $\mu\text{g/ml}$  fibronectin in PBS) is usually sufficient for the promotion of cell adhesion.

Coating of SU-8 surface with ECM protein was performed by incubating the surface with a solution of fluorescently tagged fibronectin at 10  $\mu\text{g/mL}$  or 0.1% gelatin for 30 minutes. No differences in fluorescent intensity were observed on the islands between control and testing substrates (Fig. 2.3A and B), indicating that adsorption of protein to the SU-8 surface was unaffected by the composition of the underlying hydrogel.

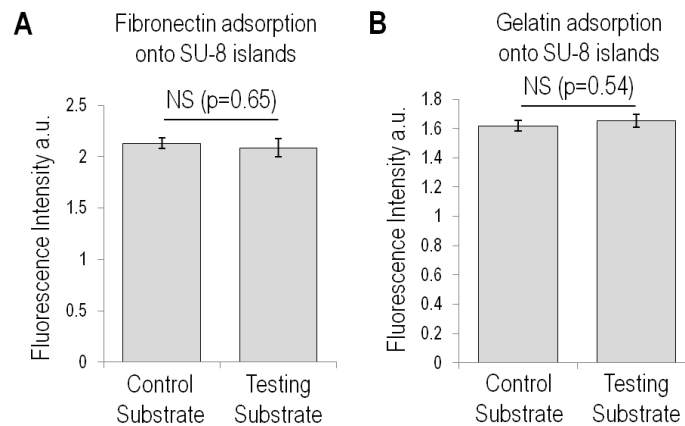


Figure 2.3. Adsorption of fluorescently tagged fibronectin (A) or gelatin (B) to SU-8 islands is unaffected by the stiffness of the underlying hydrogel (N=30 for all). Error bars represent S.E.M.

Before plating cells, the composite substrate was equilibrated with culture media for at least 30 minutes in a CO<sub>2</sub> incubator. Following inoculation, cells attached to areas occupied by SU-8 within 15 minutes. While the SU-8 pattern and adhered cells were easily visible at a low magnification with phase contrast or bright field optics, the use of a high magnification, oil immersion lens may be limited by the combined thickness of the hydrogel and photoresist. A lens of long working distance is therefore essential, and better resolution may be achieved with a water immersion lens to avoid spherical aberrations. It is also noteworthy that SU-8 emits autofluorescence when excited at 488nm, therefore fluorophores with a long wavelength are preferred over probes such as GFP.

The islands were of a similar height regardless of the composition of the underlying polyacrylamide (Table 2.1), which suggests that spin coating and the photochemical curing of SU-8 was also unaffected.

	Average SU-8 Thickness (μm)
<b>Control Substrate</b>	2.8 ± 0.2 (n = 30)
<b>Testing Substrate</b>	2.6 ± 0.4 (n = 29)
<b>p-value</b>	p = 0.10

Table 2.1. Average height of SU-8 islands on control and testing substrates, measured using laser confocal microscopy.

### 2.3.5 Troubleshooting

Although the present method may seem straightforward, problems may arise from the improper execution of a few crucial steps.

Poor micropatterning: After development, the micropattern may not look as expected; a good pattern is shown in Figure 2.4A. Poor contact between the photomask and SU-8 can create

poorly shaped micropatterns with ill-defined borders (Fig. 2.4B). Debris on a dirty photomask, or beading of the edge of polyacrylamide or SU-8 (from poor spin coating) can create space between the photomask and SU-8 and prevent tight contact. In addition, over-exposure can cause SU-8 areas to appear larger than expected with poorly defined edges (Fig. 2.4C), while under exposing or over developing would cause SU-8 areas to appear smaller with rounded corners (Fig. 2.4D).

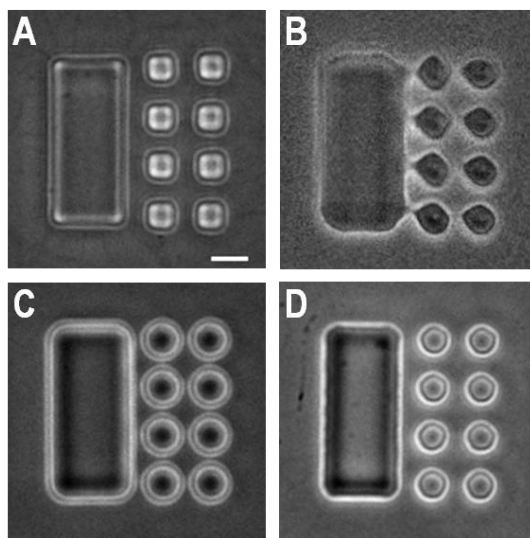


Figure 2.4. Poor micropatterning can result from a variety of factors during the photolithography process. The pattern as it should appear (A). Bad patterning can result from poor contact between the photomask and SU-8 surface (B), over-exposure (C), underexposure or over-developing (D). Scale bar, 10  $\mu\text{m}$ .

Poor association of SU-8 with the polyacrylamide surface: During development, the micropattern may become detached from the polyacrylamide surface, most likely because the SU-8 is underexposed or insufficiently heated after exposure. Underexposure prevents proper formation of crosslinks within the SU-8 layer all the way down to the polyacrylamide surface, which grafts the photoresist to the gel surface and provides the resistance against the shear during development. Increased exposure times may be necessary when using an old batch of SU-8 to ensure proper crosslinking. Insufficient baking after UV exposure also prevents exposed regions

of SU-8 from curing properly, while too thick a layer of polyacrylamide may slow down heat conduction and require a longer period of baking.

Adhesion of cells to supposedly non-adhesive areas of polyacrylamide: When cells are plated they may attach in between SU-8 islands to the hydrogel surface. Most likely this is due to insufficient development of SU-8, which causes a thin film or bits of unexposed SU-8 to remain on the surface of the polyacrylamide gel. This residual film then adsorbs proteins and mediates cell adhesion (Fig. 2.5). The problem may be rectified by additional treatment with SU-8 developer as noted earlier.

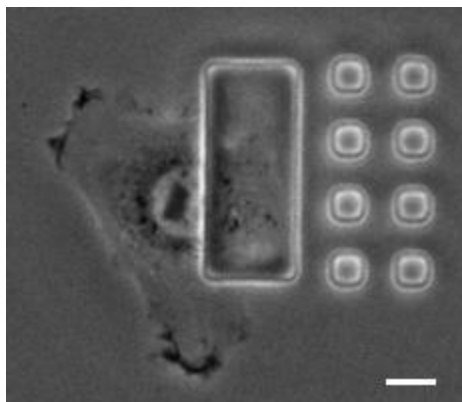


Figure 2.5. Incomplete development of SU-8 can leave behind a thin layer capable of facilitating cell adhesion and spreading off the desired pattern. Scale bar, 10  $\mu\text{m}$ .

Cracking of the gel beneath SU-8: After rehydration cracks might become easily visible on the hydrogel surface between SU-8 islands (Fig. 2.6A), which can cause islands to shift or rotate out of the plane to various extents (Fig. 2.6B and C). The most likely cause is adhesion of the top coverslip to the gel during removal, which causes strain across the surface, due to incomplete coverage of the top coverslip with Rain-X or sucrose solution. In addition to ensuring complete coverage, increasing the concentration of bis-acrylamide and decreasing the concentration of

acrylamide may alleviate this problem by increasing gel stability while maintaining the same elastic modulus.

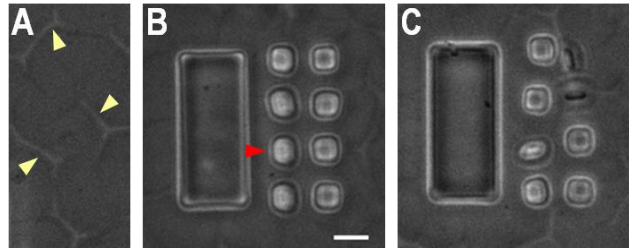


Figure 2.6. Cracking of the polyacrylamide hydrogel layer (A, yellow arrowheads) can cause tilting of the islands. Smaller cracks may cause minor deflections (B, red arrowhead), while more severe cracks can cause complete disruption of the pattern (C). Scale bar, 10  $\mu\text{m}$ .

Poor cell adhesion: Following inoculation the cells may not quickly adhere to the SU-8 islands.

If plated cells fail to attach to SU-8 within 20-30 minutes, a likely cause is insufficient incubation time with ECM proteins or serum containing medium.

## 2.4 Testing and Characterization of the Micropatterned Rigidity Border

### 2.4.1 Validating robust grafting of SU-8 islands to the underlying polyacrylamide gel

To determine if small SU-8 islands dislodge from the surface of polyacrylamide hydrogels upon the application of forces, and if the hydrogel maintains elasticity following dehydration and rehydration, a small island on a soft hydrogel was pushed with a microneedle by a few micrometers. The island returned to its original positions upon removal of the microneedle (Fig. 2.7). The process may be repeated multiple times without dislodging the island from the underlying hydrogel, indicating that the SU-8 islands are well adhered to the polyacrylamide hydrogel, and that cellular traction forces are unlikely to cause slippage between the gel and islands.

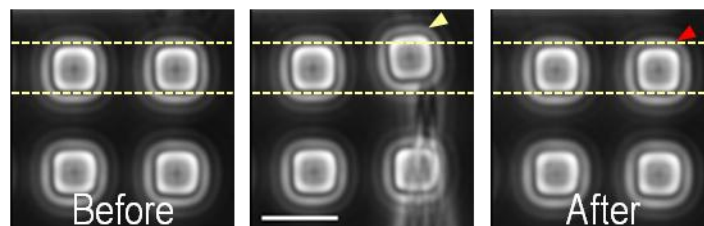


Figure 2.7. To test if SU-8 islands are well adhered to the underlying hydrogel, an island was pushed with a microneedle by a few micrometers. Displacement of the island is evident, (middle panel, yellow lines and yellow arrowhead). After removal of the microneedle, the island recovers immediately to its original position (right panel, yellow line and red arrowhead), indicating that the gel is elastic and that the island is not dislodged from the gel by the exerted force. Scale bar, 10  $\mu\text{m}$ .

### 2.4.2 Response of NIH 3T3 cells to a micropatterned rigidity border

NIH 3T3 cells were allowed to adhere to the composite substrate for 16 hours before imaging. Cells on control substrates readily crossed from the large island to occupy some or all adjacent

small islands, such that <1% of cells remained confined entirely to the large island after 16 hours. In contrast, 74% of cells plated on testing substrates remained completely confined to the large island (Fig. 2.8A and B). By varying the rigidity of the polyacrylamide layer, we found that the transition took place at around 1,000 Pa. Substrates with gels softer than 1,000 Pa inhibited cell spreading (Fig. 2.8A-C), while substrates with gels stiffer than 1,000 Pa allowed cell spreading. These results confirmed that cells were indeed able to sense the difference in rigidity in the present model system, as they do on conventional rigid or soft substrates.

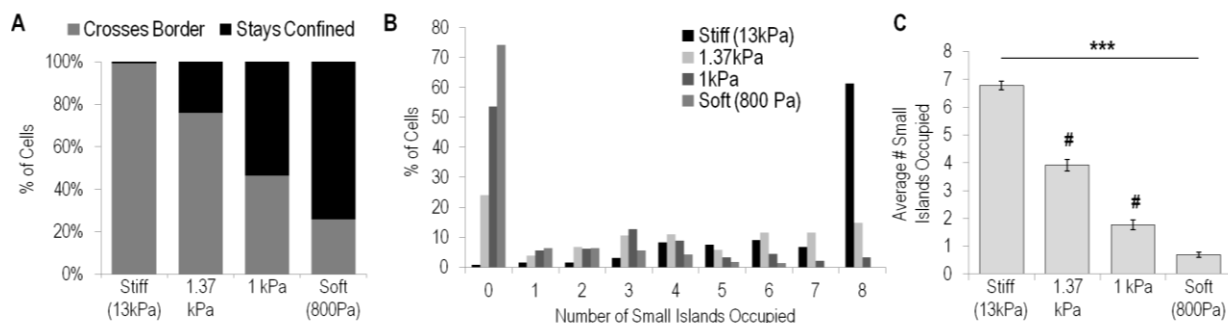
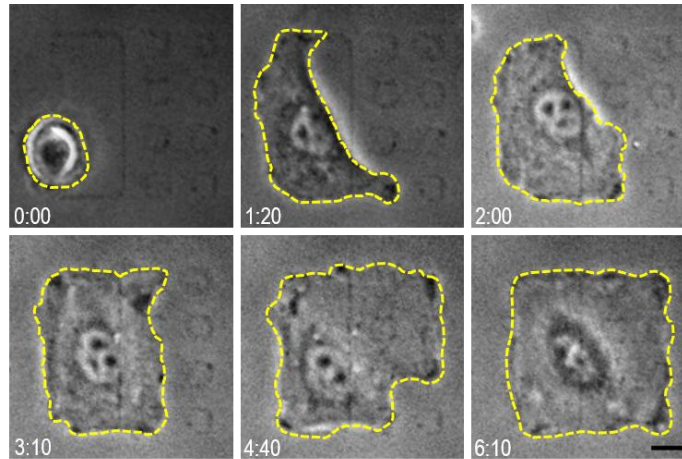


Figure 2.8. Bar graph shows that almost all the cells are able to cross the border between large and small islands on control substrates (A, leftmost bar and B, black bars, N=132), whereas most cells are confined to the large island on testing substrates (A and B, gray bars, N=233). Hydrogels of increasing rigidity cause progressively more cells to spread beyond the large island (A-C, middle bars, N=208, 181). After 16 hours of plating, cells on control substrates are able to spread over many more small islands (C, left bar) than cells on testing substrates (C, right bar). Error bars represent S.E.M. \*\*\*p<0.001. # statistically significant from both stiff and soft conditions p<0.001.

To ensure that the composite materials used in our substrates did not significantly affect cell spreading behavior, NIH 3T3 cells were plated on uniformly rigid polyacrylamide gels coated with adhesion proteins in the same micropattern as for the composite substrate. Cell spreading on these substrates followed a similar time course and reached a similar extent as for cells on control composite substrates (Fig. 2.9). Thus, although the 3D topography of SU-8 islands may affect some properties of the cell, it did not affect the extent or rate of cells spreading, which is the focus of this study.



	Control Substrate	Patterned Gel	p value
Time to fully spread over pattern area (hrs)	8.0 ± 0.4 (n = 48)	8.7 ± 0.5 (n = 47)	p = 0.26
Average # Small Islands Occupied	6.8 ± 0.2 (n = 129)	6.4 ± 0.2 (n = 132)	p = 0.12
Spreading Area (um <sup>2</sup> )	1667 ± 25 (n = 129)	1650 ± 27 (n = 132)	p = 0.64

Figure 2.9. NIH 3T3 cells display similar spreading behavior on composite control substrates and on uniformly rigid substrates. Uniformly rigid polyacrylamide gels prepared with 8% acrylamide and 0.2% bis-acrylamide were conjugated with gelatin in the same island pattern as for the composite substrates. Time lapse phase contrast microscopy indicates that cells spread to cover all the islands following a time course similar to that for cells on composite control substrates. Numbers at the bottom of each image indicate the lapse time in hours and minutes after initial cell attachment to the large island. Cell outlines are indicated by yellow dashed lines. Other aspects of the spreading kinetics are also similar between composite and homogeneous substrates with the island pattern, with no statistical differences found. Scale bar, 10  $\mu\text{m}$ .

### 2.4.3 Additional considerations when fabricating patterns

Several aspects deserve consideration when designing a micropatterned rigidity border for a particular cell type, including the spreading area of the cell, the distance between islands, and the effect of gel swelling. We found that Normal Rat Kidney (NRK) epithelial cells were unable to occupy all the islands on control substrates designed for NIH 3T3 fibroblasts. In time lapse videos, only 2 of the 18 NRK cells recorded were able to occupy an additional island over a period of up to 16 hours (Fig. 2.10A and B). Most likely these cells were unable to reach across

the islands since the total area of the pattern fell well within the typical spreading area for NRK cells on glass or unpatterned stiff polyacrylamide<sup>33</sup>. In contrast, MDCK cells were able to easily bridge non-adhesive areas but had difficulty covering the entire patterned area. Their constant migration around the islands (Fig. 2.10C) suggests that the incomplete coverage was due to a typical spreading area smaller than the designed pattern<sup>34</sup>.

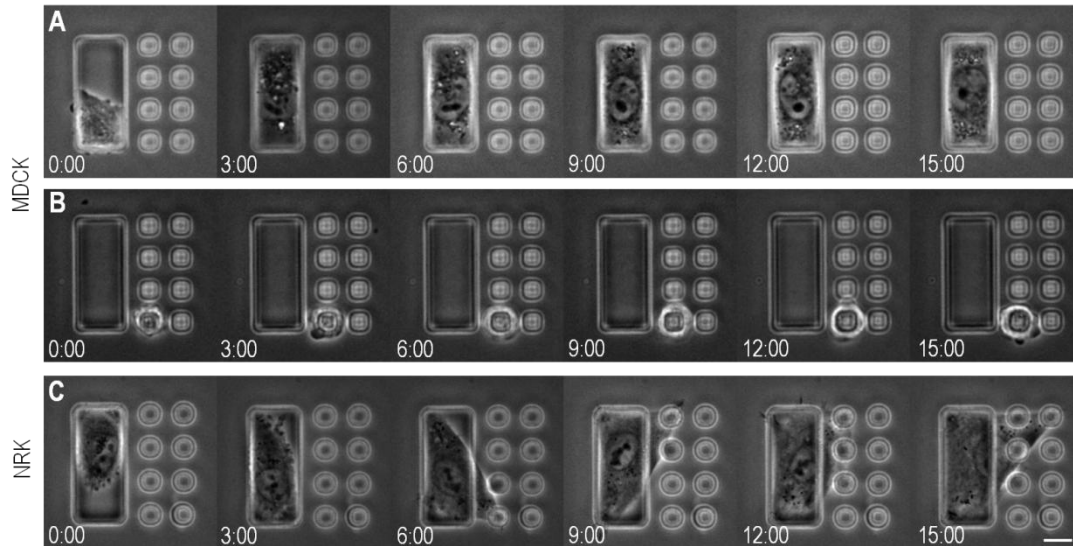


Figure 2.10. NRK cells are unable to reach across the non-adhesive polyacrylamide to spread to adjacent islands on control substrate. This was observed for both cells starting on a large island (A) and small island (B). In contrast, MDCK cells readily spread between islands and move around continuously, but are unable to occupy the full pattern (C). 0:00 is the starting time of imaging approximately 1 hour after plating cells. Scale bar, 10  $\mu\text{m}$ .

## 2.5 Discussion

Recent studies have demonstrated the importance of mechanical microenvironments in regulating cell physiology, differentiation, migration, and organization<sup>9,10</sup>. Micropatterning methods are emerging as an important tool for engineering microenvironments *in vitro* to mimic the conditions *in vivo*, or dissect the effects of specific parameters. Using the present composite system, both the stiffness of the hydrogel base and the pattern of adhesive photoresist can be varied according to the experimental design. For example, using a matrix of small islands, the spatial resolution for cellular rigidity sensing may be assessed by varying the size of the island and the distance between islands. The results demonstrated that long-range strains dominate cellular responses over local rigidity<sup>17,31</sup>, although other approaches suggested that local rigidity may also play a role under some conditions<sup>18,35</sup>. Future applications of composite substrates may help dissect the mechanism of rigidity sensing at both spatial regimes.

The effects of the above procedures on rheological properties of the polyacrylamide hydrogel have been previously assessed with sheets ~500  $\mu\text{m}$  in thickness using a Bohlin Gemini Advanced Rheometer (Malvern Instruments Inc, NJ). No significant difference in shear modulus was found between untreated hydrogels and hydrogels subjected to the micropatterning procedure without UV exposure (thus removal of the entire layer of SU-8 during the development), suggesting that the process of micropatterning, including dehydration and rehydration, does not affect mechanical properties of the hydrogel<sup>31</sup>.

Fabrication of composite substrates for the investigations of rigidity sensing is a straightforward process, requiring only inexpensive equipment such as a high flux UV-LED as the light source in conjunction with an orbital shaker for uniform illumination<sup>36</sup>. As pointed out by Tsai et al.<sup>37</sup>,

most biological applications can tolerate some defects in the micropattern, which allows photolithography to be performed without a clean room facility. The material can be easily treated with a variety of ECM proteins to facilitate adhesion. Additionally, the raised islands did not significantly affect the extent or rate of cell spreading.

NIH 3T3 cells exhibited strikingly different behavior on testing substrates (with a soft underlying gel to create a rigidity border) versus control substrates (with a rigid underlying gel to create a non-deformable surface across). On control substrates, many cells were able to occupy the majority of small islands. In contrast, on testing substrates, 74% of the cells remained completely confined to the rigid domain after 16 hours of culture. In the present experiment, this transition in response took place at an underlying hydrogel rigidity of 1,000 Pa. However, since on composite substrates cell extensions must move an island much larger in area as opposed to homogenous substrates where direct mechanical interactions with the substrate are confined to a small area, this value cannot be directly compared with the transition of rigidity response for cells plated on homogeneous substrates. Therefore, the equivalent rigidity threshold on homogeneous substrates may be 1-2 orders of magnitude higher, or between 10 and 100 kPa.

Rigidity sensing has emerged as an important factor in many biological processes. Various hydrogel-based experimental approaches, including spatial borders and temporal modulation of rigidity, have been used to study rigidity sensing<sup>17,25,29,38</sup>. However, many of these systems require lengthy time-lapse recording over a wide area in order to capture the brief moment when a cell encounters a rigidity border. While some recent studies have developed substrates with micropatterned rigidity<sup>26-28,39</sup>, the present composite substrate has several distinct advantages. First, it traps single cells at a simulated rigidity border, which allows prolonged observation of

cell behavior. Second, it allows a large number of cells to be studied under the same condition, which provides reproducible results and allows efficient screening of conditions that affect rigidity sensing. Third, the presence of non-adhesive polyacrylamide gels between adhesive islands allows the analysis of cellular responses to substrate rigidity at a distance from the cell body, as described in the following Chapter.

## 2.6 References

1. Whitesides, G. M., Ostuni, E., Takayama, S., Jiang, X. & Ingber, D. E. Soft lithography in biology and biochemistry. *Annu. Rev. Biomed. Eng.* **3**, 335–73 (2001).
2. Singhvi, R. *et al.* Engineering cell shape and function. *Science* **264**, 696–8 (1994).
3. Chen, C. S. Geometric Control of Cell Life and Death. *Science* **276**, 1425–1428 (1997).
4. Dike, L. E. *et al.* Geometric control of switching between growth, apoptosis, and differentiation during angiogenesis using micropatterned substrates. *In Vitro Cell. Dev. Biol. Anim.* **35**, 441–8 (1999).
5. Wang, N., Ostuni, E., Whitesides, G. M. & Ingber, D. E. Micropatterning tractional forces in living cells. *Cell Motil. Cytoskeleton* **52**, 97–106 (2002).
6. McBeath, R., Pirone, D. M., Nelson, C. M., Bhadriraju, K. & Chen, C. S. Cell shape, cytoskeletal tension, and RhoA regulate stem cell lineage commitment. *Dev. Cell* **6**, 483–95 (2004).
7. Pouthas, F. *et al.* In migrating cells, the Golgi complex and the position of the centrosome depend on geometrical constraints of the substratum. *J. Cell Sci.* **121**, 2406–14 (2008).
8. Pelham, R. J. & Wang, Y. Cell locomotion and focal adhesions are regulated by substrate flexibility. *Cell* **94**, 13661–13665 (1997).
9. Discher, D. E., Janmey, P. & Wang, Y.-L. Tissue cells feel and respond to the stiffness of their substrate. *Science* **310**, 1139–43 (2005).
10. Engler, A. J., Sen, S., Sweeney, H. L. & Discher, D. E. Matrix elasticity directs stem cell lineage specification. *Cell* **126**, 677–89 (2006).
11. Palchesko, R. N., Zhang, L., Sun, Y. & Feinberg, A. W. Development of Polydimethylsiloxane Substrates with Tunable Elastic Modulus to Study Cell Mechanobiology in Muscle and Nerve. *PLoS One* **7**, e51499 (2012).
12. Chen, C. S., Brown, X. Q., Ookawa, K. & Wong, J. Y. Evaluation of polydimethylsiloxane scaffolds with physiologically-relevant elastic moduli: interplay of substrate mechanics and surface chemistry effects on vascular smooth muscle cell response. *Biomaterials* **26**, 3123–3129 (2005).
13. Tse, J. R. & Engler, A. J. Preparation of hydrogel substrates with tunable mechanical properties. *Curr. Protoc. Cell Biol.* **Chapter 10**, Unit 10.16 (2010).
14. Beningo, K. A. & Wang, Y. L. Flexible substrata for the detection of cellular traction forces. *Trends Cell Biol.* **12**, 79–84 (2002).
15. Kloxin, A. M., Kasko, A. M., Salinas, C. N. & Anseth, K. S. Photodegradable hydrogels for dynamic tuning of physical and chemical properties. *Science* **324**, 59–63 (2009).
16. Tan, J. L. *et al.* Cells lying on a bed of microneedles : An approach to isolate mechanical force. *Proc. Natl. Acad. Sci.* **100**, 1484–1489 (2002).
17. Trichet, L. *et al.* Evidence of a large-scale mechanosensing mechanism for cellular adaptation to substrate stiffness. *Proc. Natl. Acad. Sci.* **109**, 6933–8 (2012).
18. Sun, Y., Jiang, L.-T., Okada, R. & Fu, J. UV-modulated substrate rigidity for multiscale study of mechanoresponsive cellular behaviors. *Langmuir* **28**, 10789–96 (2012).
19. Théry, M. & Piel, M. Adhesive Micropatterns for Cells: A Microcontact Printing Protocol. *Cold Spring Harb. Protoc.* **4**, 888–898 (2009).
20. Damljjanovic, V. *et al.* Bulk and micropatterned conjugation of extracellular matrix proteins to characterized polyacrylamide substrates for cell mechanotransduction assays. *Biotechniques* **39**, 847–851 (2005).

21. Tseng, Q. *et al.* A new micropatterning method of soft substrates reveals that different tumorigenic signals can promote or reduce cell contraction levels. *Lab Chip* **11**, 2231–40 (2011).
22. Rape, A. D., Guo, W.-H. & Wang, Y.-L. The regulation of traction force in relation to cell shape and focal adhesions. *Biomaterials* **32**, 2043–51 (2011).
23. Lo, C. M., Wang, H., Dembo, M. & Wang, Y.-L. Cell movement is guided by the rigidity of the substrate. *Biophys. J.* **79**, 144–52 (2000).
24. Wang, H., Dembo, M., Hanks, S. K. & Wang, Y. Focal adhesion kinase is involved in mechanosensing during fibroblast migration. *Proc. Natl. Acad. Sci.* **98**, 11295–300 (2001).
25. Wong, J. Y., Velasco, A., Rajagopalan, P. & Pham, Q. Directed Movement of Vascular Smooth Muscle Cells on Gradient-Compliant Hydrogels. *Langmuir* **19**, 1908–1913 (2003).
26. Nemir, S., Hayenga, H. N. & West, J. L. PEGDA hydrogels with patterned elasticity: Novel tools for the study of cell response to substrate rigidity. *Biotechnol. Bioeng.* **105**, 636–44 (2010).
27. Gray, D. S., Tien, J. & Chen, C. S. Repositioning of cells by mechanotaxis on surfaces with micropatterned Young 's modulus. *J. Biomed. Mater. Res.* 605–614 (2003).
28. Choi, Y. S. *et al.* The alignment and fusion assembly of adipose-derived stem cells on mechanically patterned matrices. *Biomaterials* **33**, 6943–51 (2012).
29. Frey, M. T. & Wang, Y. A photo-modulatable material for probing cellular responses to substrate rigidity. *Soft Matter* **5**, 1918–1924 (2009).
30. Kloxin, A. M., Benton, J. a & Anseth, K. S. In situ elasticity modulation with dynamic substrates to direct cell phenotype. *Biomaterials* **31**, 1–8 (2010).
31. Hoffecker, I. T., Guo, W. & Wang, Y. Assessing the spatial resolution of cellular rigidity sensing using a micropatterned hydrogel-photoresist composite. *Lab Chip* **11**, 3538–44 (2011).
32. Voskerician, G. *et al.* Biocompatibility and biofouling of MEMS drug delivery devices. *Biomaterials* **24**, 1959–1967 (2003).
33. Liu, W. F., Nelson, C. M., Pirone, D. M. & Chen, C. S. E-cadherin engagement stimulates proliferation via Rac1. *J. Cell Biol.* **173**, 431–441 (2006).
34. Sim, J. Y. *et al.* Spatial distribution of cell-cell and cell-ECM adhesions regulates force balance while main taining E-cadherin molecular tension in cell pairs. *Mol. Biol. Cell* **26**, 2456–2465 (2015).
35. Ghassemi, S. *et al.* Cells test substrate rigidity by local contractions on submicrometer pillars. *Proc. Natl. Acad. Sci.* **109**, 5328–5333 (2012).
36. Guo, W. & Wang, Y.-L. in *Cold Spring Harb. Protoc.* **2011**, prot5582 (2010).
37. Tsai, I. Y., Crosby, A. J. & Russell, T. P. in *Methods Cell Biol. Cell Mech.* 67–87 (2007).
38. Sunyer, R., Jin, A. J., Nossal, R. & Sackett, D. L. Fabrication of hydrogels with steep stiffness gradients for studying cell mechanical response. *PLoS One* **7**, e46107 (2012).
39. Kawano, T. & Kidoaki, S. Elasticity boundary conditions required for cell mechanotaxis on microelastically-patterned gels. *Biomaterials* **32**, 2725–33 (2011).

## Chapter 3

# Fibroblasts Probe Substrate Rigidity with Filopodia Extensions before Occupying an Area

Rigidity sensing and durotaxis are thought to be important elements in wound healing, tissue formation, and cancer treatment. It has been challenging, however, to study the underlying mechanism due to difficulties in capturing cells during the transient response to a rigidity interface. We utilize an experimental system that confines cells to a micropatterned area with a rigidity border. This configuration allowed us to test rigidity sensing away from the cell body during probing and spreading. NIH 3T3 cells used filopodia extensions to probe substrate rigidity at a distance in front of the leading edge and regulated their responses based on the strain of the intervening substrate. Soft substrates inhibited focal adhesion maturation and promoted cell retraction, while rigid substrates allowed stable adhesion formation and cell spreading. Myosin II was required for not only the generation of probing forces but also the retraction in response to soft substrates. We suggest that a myosin II-driven, filopodia-based probing mechanism ahead of the leading edge allows cells to migrate efficiently, by sensing physical characteristics before moving over a substrate to avoid back-tracking.

### 3.1 Introduction

Substrate rigidity has been shown to influence cell growth, differentiation, and migration *in vitro*<sup>1-3</sup>. Different tissues show different characteristic stiffness, and changes in tissue stiffness represent a common marker of diseases including cancer, liver fibrosis, and arteriosclerosis. Consideration of substrate rigidity has become an essential aspect in not only disease treatment, such as the prevention of cancer metastasis<sup>4-7</sup>, but also tissue engineering<sup>8,9</sup>.

There has been intense interest in understanding rigidity sensing at the cellular and molecular level. Of particular interest are cellular responses to spatial or temporal changes in rigidity, such as the ability of fibroblasts to migrate preferentially toward stiffer substrates at a rigidity interface known as durotaxis<sup>10</sup>. However, limitations in the experimental system have hampered the understanding of how cells detect and respond to a spatial or temporal transition in substrate rigidity. Most studies on cellular response to substrate rigidity have been performed with cells on a surface of homogeneous rigidity<sup>11-13</sup>. While some studies have examined cellular responses to changing rigidity, few have focused on the dynamic behavior of how cells probe and respond to temporal or spatial changes in substrate rigidity. One such study, which involved pushing and pulling a deformable substrate by micromanipulation to simulate changes in substrate rigidity, showed that cells extended protrusions and moved towards the direction of increased tension and recoiled from the direction of reduced tension<sup>10</sup>. A more recent study utilizing a similar approach further indicated that durotaxis involved dynamic tugging of adhesions<sup>14</sup>, however, this micromanipulation approach was time and labor intensive.

Alternatively, rigidity responses may be studied by placing migrating cells on engineered substrates with juxtaposed elastic and rigid domains<sup>15-17</sup>. One study used micropost arrays of

different dimensions to create a rigidity border<sup>18</sup>. However, as in the original study of durotaxis, this system still relied on spontaneous, time consuming migration of cells to the rigidity border, where the cell stays for only a limited period of time in the actual area of interest. In addition, it was often difficult to create sufficiently soft substrates with microposts. Studies utilizing this, and other approaches, have suggested that the cytoskeleton and actomyosin contractility are crucial for rigidity sensing during durotaxis<sup>18,19</sup>. A recent study with patterned microposts further suggested that a traction force imbalance at a rigidity border contributes to durotaxis<sup>20</sup>.

Using a novel approach that traps cells at a micropatterned rigidity border, we report here a rigidity sensing mechanism based on filopodia extensions that allows cells to probe substrate rigidity ahead of their leading edge. We have previously described a method for micropatterning arrays of micron-sized adhesive photoresist islands on the surface of non-adhesive polyacrylamide hydrogels<sup>21</sup>. The study indicated that long range strain rather than local rigidity underneath individual focal adhesions determines cellular rigidity responses. Thus, soft substrates may be created by an array of small rigid adhesive islands grafted onto soft non-adhesive hydrogels, while a rigidity border may be generated by juxtaposing such an island array with a large island, each covering half of the spreading area of a cell. In combination, the pattern provides a novel tool to assess rigidity sensing by trapping cells at a rigidity border, thereby avoiding prolonged recording waiting for the transient localization of cells to the transition region. Another advantage of this system is that the non-adhesive hydrogel that separates the adhesive islands allows the investigation of whether, and how, cells probe material rigidity across a distance beyond their border.

## 3.2 Experimental Methods

### 3.2.1 Preparation of composite substrates

Composite substrates with micropatterned islands of SU-8 photoresist grafted on the surface of polyacrylamide hydrogels were prepared as described in Chapter 2 and previously<sup>21,22</sup>. Briefly, a coverglass was activated with 30  $\mu\text{L}$  of bind-silane working solution according to the instruction of the manufacturer (GE Healthcare, Waukesha, WI), to allow bonding of the polyacrylamide gel to the glass surface during polymerization. Polyacrylamide hydrogels of two different rigidities were prepared: a stiff gel of approximately 13 kPa was prepared with a final concentration of 8% acrylamide (Bio-Rad, Hercules, CA) and 0.2% bis-acrylamide (Bio-Rad), while a soft gel of approximately 800 Pa was prepared with a final concentration of 3% acrylamide and 0.08% bis-acrylamide<sup>23,24</sup>. Polymerization was induced by adding 6  $\mu\text{L}$  freshly prepared 10% ammonium persulfate (Sigma) and 4  $\mu\text{L}$  N,N,N',N' tetramethylethylenediamine (Bio-Rad) to the 1 mL of acrylamide solution after degassing, and a 30  $\mu\text{L}$  drop was pipetted onto the bind-silane activated coverslip. A 25 mm circular coverslip, spin-coated with 50% w/v sucrose solution, was inverted onto the acrylamide drop. After 1 hour of polymerization, the sucrose solution was dissolved to allow gentle removal of the circular coverslip. The gel was equilibrated in deionized water for 30 minutes then dehydrated overnight.

Arrays of rigid islands were grafted onto dried polyacrylamide gels using a negative photoresist SU-8 2000 (Microchem, Newton, MA). Briefly, coverslips with dried hydrogel were baked at 95°C for 1 minute and cooled to room temperature before coating with 300  $\mu\text{L}$  of SU-8 using a spin coater at 5,000 rpm for 20 seconds (WS-6505-6NPP-LITE, Laurell Technologies, North Wales, PA). The coverslips were baked for 3 minutes, cooled to room temperature, then exposed

to ultraviolet light (360 nm, 100 mJ•cm<sup>-2</sup>) underneath a photomask with designed pattern (Photo-Sciences, Torrance, CA) for 90 seconds, then baked for another 3 minutes at 95°C before immersion in the SU-8 developer (Microchem) for 90 seconds to generate the pattern. Developed coverslips were rinsed twice with 95% ethanol, then baked at 95°C for 4 hours to ensure removal of any residual developer. Before use, the hydrogel was rehydrated in phosphate buffered saline for 1 hour.

### **3.2.2 Cell culture and pharmacological treatments**

NIH 3T3 cells (ATCC) were maintained in Dulbecco's modified Eagle's medium (DMEM; Life Technologies) supplemented with 10% adult donor bovine serum (Thermo Scientific), 2 mM L-glutamine, 50 µg/mL streptomycin, and 50 U/mL penicillin (Life Technologies). To inhibit myosin contractility, cells were treated with 10 µM blebbistatin (Calbiochem, San Diego, CA) for either 30 minutes prior to the microneedle experiment, or 16 hours before quantitative analysis of pattern occupancy. For inhibition studies, cells were treated with 10 µM ML-141 to inhibit Cdc42 (Tocris, Bristol, UK), 10 µM SMIFH2 to inhibit formins (EMD Millipore, Darmstadt, Germany), 10 µM CK666 to inhibit Arp2/3 (EMD Millipore), or 100 µM NSC-23766 to inhibit Rac1 (Tocris) for either 30 minutes before starting time lapse imaging or 16 hours before quantitative analysis of pattern occupancy. The number of cells analyzed for each graph is indicated in the figure caption, and at least 3 independent trials were performed for each experiment, control data repeated where necessary for comparison.

### **3.2.3 Fixation and fluorescent labeling**

For visualizing focal adhesions, cells seeded on patterned substrates were fixed 16 hours after plating with 4% formaldehyde (from 16% stock, Thermo Scientific), and stained with antibodies

against paxillin (Santa Cruz Biotechnology, Santa Cruz, CA), and Alexa Fluor 546 goat-anti-rabbit IgG secondary antibodies (Life Technologies).

For visualizing actin filaments, cells seeded on patterned substrates were fixed 7 hours after plating with 0.5% glutaraldehyde (Sigma) with 0.2% Triton-X 100 for 1 minute then 1% glutaraldehyde for 15 minutes. Samples were incubated with fresh 0.5 mg/mL NaBH<sub>4</sub> for 5 minutes and rinsed with PBS prior to staining with rhodamine-labeled phalloidin (Molecular Probes, Eugene, OR) for 30 minutes according to the manufacturer's instructions.

### **3.2.4 Microscopy and image analysis**

Phase contrast images were collected with a Nikon Eclipse Ti microscope using a 40x PlanFluor 0.75 N.A. dry objective. For time lapse videos, images were collected every 10 minutes for a period of 16 hours. For the analysis of pattern occupancy, images were collected after 16 hours of incubation. In all experiments, only single cells were counted for the analysis. For micromanipulation, a microneedle prepared with a vertical micropipette puller (Model 720, David Kopf Instruments, Tujunga, CA) was mounted on a Leitz micromanipulator to allow precise positioning of the tip. Phase contrast images were collected with a Zeiss Axiovert 200M using a 40x PlanNeofluar 0.75 N.A. dry objective. Images were collected every minute during microneedle manipulation. Fluorescence images were collected using a 100x PlanFluor 1.3 N.A. oil immersion lens. Focal adhesion size was quantified using ImageJ (National Institutes of Health, Bethesda, MD). Contrast was enhanced to reveal the very dim actin structures in thin protrusions in Figure 3.4A and C.

### **3.2.5 Scanning electron microscopy**

Cells on control substrates (with rigid underlying gels) were fixed 3 hours after plating, when cells start to occupy small islands, with 2% paraformaldehyde and 2% glutaraldehyde in phosphate buffered saline. Scanning electron microscopy was performed with help from Joe Suhan at the Electron Microscopy Facility at Carnegie Mellon University.

## 3.3 Results

### 3.3.1 NIH 3T3 cells modulate the size of focal adhesions based on the rigidity of underlying substrate

We have developed a substrate with a rigidity border across a small square region the area of a spread fibroblast (described in Chapter 2), using a previously developed method to create micropatterned composite materials<sup>21,22</sup>. In addition to testing the response to a rigidity border, the distance of 6.5  $\mu\text{m}$  between the islands allowed us to ask if and how cells sense substrate rigidity across a distance.

Results in Chapter 2 showed that NIH 3T3 cells respond to the rigidity of the underlying non-adhesive hydrogel, regardless of the constant rigidity of the adhesive SU-8 islands. Cells on control substrates readily crossed the rigidity border to occupy the full patterned area (Fig. 3.1A), while cells on testing substrates occupied only a small number of islands and were generally confined to the rigid large island area (Fig. 3.1B). The response to the composite material was further examined based on the size of focal adhesions, which is known to be a sensitive indicator of substrate rigidity and cell shape<sup>2,11</sup>. Focal adhesions, as shown by paxillin immunofluorescence, decreased from an average area of 0.79  $\mu\text{m}^2$  for cells confined to the large island (Fig. 3.1E and F), to 0.56  $\mu\text{m}^2$  for cells that spread across soft gel to adhere to one or more small islands (Fig. 3.1D and F). In contrast, cells that spread across the rigid gel of control substrates showed an increase in the size of focal adhesions (1.21  $\mu\text{m}^2$ , Fig. 3.1C and F), which reflected the dependence of focal adhesion size on cell spreading<sup>25,26</sup>. These results confirm that cells were able to sense the hydrogel rigidity and modulate adhesion size accordingly.

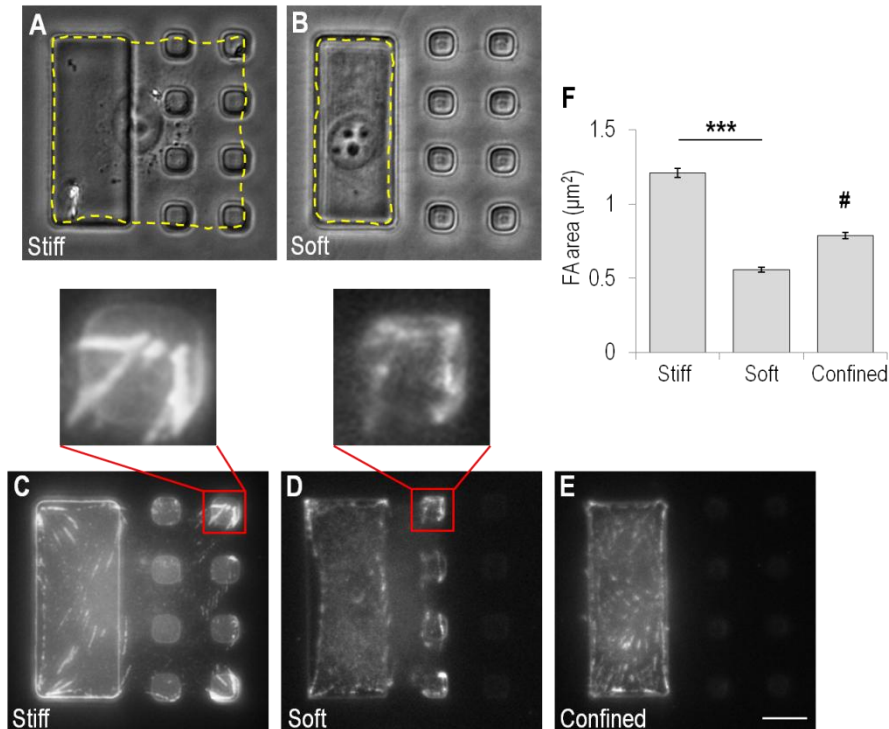


Figure 3.1. Focal adhesions respond to rigidity on composite substrate. NIH 3T3 cells spread over both large and small islands 16 hours after plating on control substrates (A), but remain on the large island (rigid domain) when plated on testing substrates (B). Cell outlines are indicated by yellow dashed lines. Immunofluorescence images of paxillin show large focal adhesions on both large and small islands for cells on control substrates (C), but only small focal adhesions in cells that spread onto some small islands on testing substrates (D). Cells confined to the large island also form small focal adhesions (E). Morphometry indicates that focal adhesions on control substrates (F, left bar; N=815 focal adhesions from 30 cells) are about twice the size of focal adhesions in cells that spread across soft gels on testing substrates (F, middle bar; N=696 focal adhesions from 19 cells). Cells that are confined to the large island show focal adhesions of intermediate size, regardless of the rigidity of the underlying gel (F, right bar; 412 focal adhesions from 18 cells). Scale bars, 10  $\mu\text{m}$ . Error bars represent S.E.M. \*\*\* $p < 0.001$ . # statistically significant from both stiff and soft conditions  $p < 0.001$ .

### 3.3.2 NIH 3T3 cells are able to detect substrate rigidity outside the cell border

The previous observations raise the possibility that cells were able to detect substrate rigidity outside their border before deciding if they should occupy the area. To understand how cells behave at the micropatterned rigidity border, we performed time lapse recording starting 30 minutes after plating to determine how cells spread from the large to small islands. The process

appeared to involve fine probing structures close to the detection limit of phase contrast optics (Fig. 3.2A and B, yellow arrowheads).

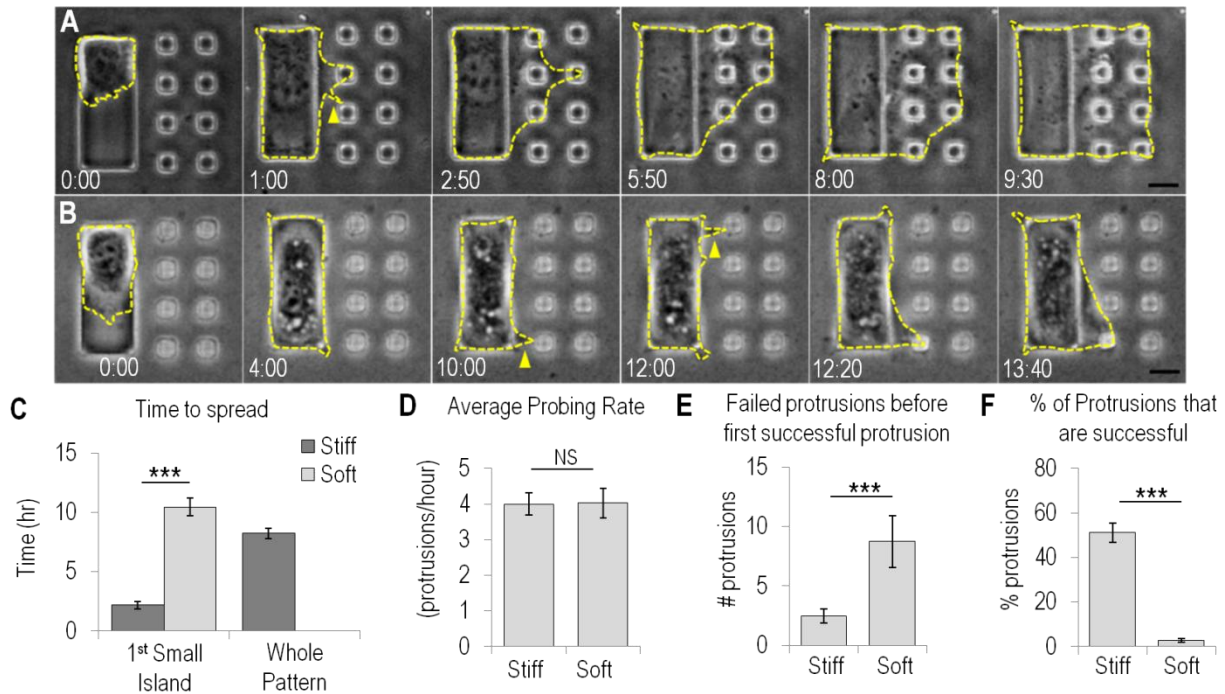


Figure 3.2. NIH 3T3 cells are able to detect substrate rigidity beyond the cell border. NIH 3T3 cells are observed with time-lapse phase contrast microscopy and outlines are indicated by yellow dashed lines (A and B). On control substrates, cells that initially attach to the large island are able to detect small islands across the non-adhesive hydrogel and spread over all the islands in less than 10 hours (A). On testing substrates, most cells that initially attach to the large island remain confined, although transient protrusions can be seen extending towards small islands (B, yellow arrows). A fraction of cells are able to occupy a small island after an extended period of incubation (B, lower right panel). Numbers at the bottom of each image indicate the lapse time in hours and minutes after initial cell attachment to a large island, which takes place ~30 minutes after plating. The average time required to occupy the first small island is much longer on testing substrates (C, left graph, light grey bar, N=18; out of 78 cells recorded only 18 occupied at least one small island) than on control substrates (C, left graph, dark grey bar, N=116). It takes on average 8 hours for cells on control substrates to occupy all of the small islands (C, right graph, N=49). Cells on testing substrates were never seen to occupy all the small islands. Cells on both stiff and soft substrates extend probing protrusions at the same rate (D, N=36, 73 cells). Cells on soft substrates extend more failed protrusions before successfully occupying one small island (E, N=35, 15 cells). The percentage of successful protrusions is much higher on stiff substrates than soft substrates (F, N=36, 68 cells). Scale bars, 10  $\mu$ m. Error bars represent S.E.M. \*\*\*  $p < 0.001$ .

Cells extended these thin probing extensions at a similar rate on both control and testing substrates (Fig. 3.2D); however, a much higher percentage of cells showed subsequent spreading

onto small islands on control substrates than on testing substrates (Fig. 3.2F). A spreading response involved the adhesion of a probing extension to a small island followed by the formation of lamellipodia to occupy the island area. Once adhered to the first small island on control substrates, most cells continued to spread onto the rest of the islands to occupy the full patterned area (Fig. 3.2A). It took on average 2 hours after initial plating for a cell to occupy the first island and by 8 hours, the majority of cells had spread over the remaining 7 islands (Fig. 3.2C).

On testing substrates, NIH 3T3 cells formed thin extensions similar to those seen on control substrates. Minute deflections of the small islands were occasionally visible, indicative of probing forces. However, most of the thin extensions failed to lead to spreading onto adjacent small islands (Fig. 3.2E and F). It took on average 10 hours for a fraction of cells on testing substrates to occupy one small island and no cell was found to occupy all of the small islands after 16 hours of plating (Fig. 3.2C). These observations suggest that cells use thin extensions to probe substrate rigidity outside their border. The mechanical signal then determines the stability of the extension, and the rate and efficiency of subsequent cell spreading. Soft substrates cause a low probability of spreading and a high probability of retraction.

To determine the role of Arp 2/3-mediated actin polymerization and lamellipodial protrusion in the response to rigid substrates<sup>27</sup>, we treated cells with 25  $\mu$ M Arp 2/3 inhibitor, CK666<sup>28</sup>. Treatment with CK666 decreased the percentage of successful spreading onto small islands (Fig. 3.3A and D) and increased the percentage of failed attempts (Fig. 3.3C), but increased the probing rate (Fig. 3.3B). Inhibition of the small GTPase Rac1 with 100  $\mu$ M inhibitor NSC23766, known to interfere with lamellipodia formation<sup>29</sup>, also decreased spreading on control substrates

(Fig. 3.3A). These results indicate that cell spreading across rigid substrates requires Arp 2/3- and Rac1-mediated actin polymerization and lamellipodia protrusion.

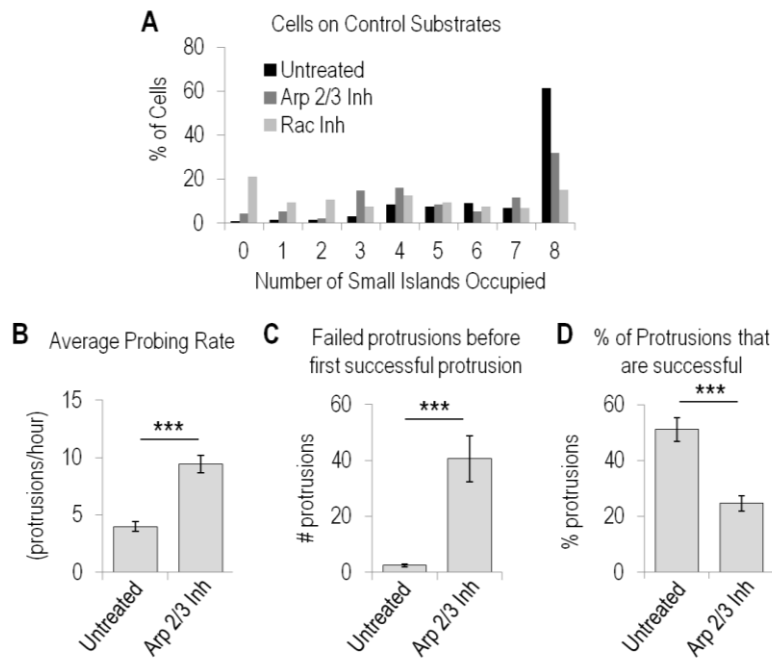


Figure 3.3. Cell spreading across control substrates involves Arp2/3 and Rac1 mediated lamellipodial protrusion. Histogram showing the distribution of the number of small islands occupied by NIH 3T3 cells treated with 100  $\mu$ M NSC23766 to inhibit Rac1 (A, light grey bars, N=160) or 25  $\mu$ M CK666 to inhibit Arp2/3 (A, dark grey bars, N=94) reduced the extent of spreading on control substrates. Inhibition of Arp 2/3 also increased both the rate of probing on control substrates relative to untreated cells (B, right bar, N=22) and the number of failed protrusions before the first successful protrusion (C, right bar, N=20), while reducing the percentage of successful protrusions on control substrates compared to untreated cells (D, right bar, N=22). Error bars represent S.E.M. \*\*\*  $p < 0.001$ .

### 3.3.3 Filopodia are involved in probing substrate rigidity

The above results suggest that thin extensions close to the detection limit of phase optics were involved in probing substrate rigidity in front of the cell. To capture these structures, cells on testing substrates were fixed and stained with fluorescent phalloidin 7 hours after plating, when cells were expected to probe actively across the rigidity border. Thin actin-containing filopodia protrusions were found to connect the cell body with adjacent small islands (Fig. 3.4A and B).

Similar structures were observed in cells that managed to occupy one small island and started to probe additional small island (Fig. 3.4C and D). Scanning electron microscopy of cells on control substrates also revealed fine protrusions extending from the cell body on the large island to adjacent small islands (Fig. 3.4E and F).

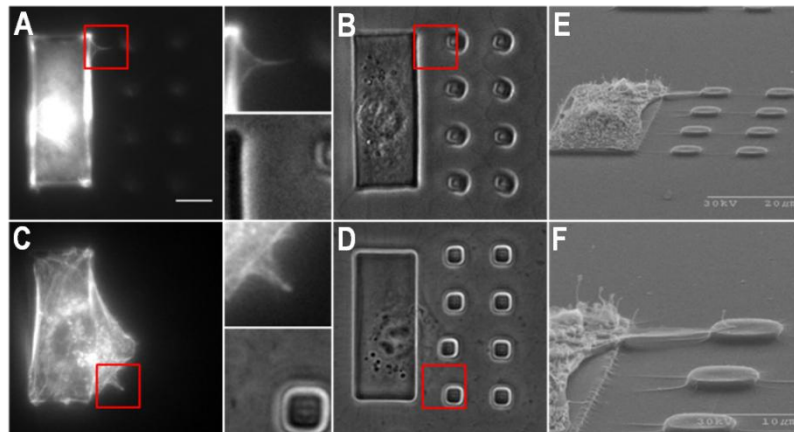


Figure 3.4. Actin-containing filopodia extensions bridge the cell body with substrate in front of the leading edge. Filopodia are often difficult to detect with phase contrast microscopy (B, inset), but become visible, upon staining with fluorescent phalloidin, as thin projections from the cell body (A, inset). Similar structures are found extending from cells that have already occupied one small island (C and D, inset). Scale bar, 10  $\mu\text{m}$ . Scanning electron microscope images show protrusions that extend from the cell body above the underlying hydrogel to land on an adjacent small island (E). Enlarged view shows a filopodia protrusion along the top edge of the cell (F).

Cdc42 and formins are known to regulate filopodia function<sup>30-32</sup>. Inhibition of Cdc42 or formins with 10  $\mu\text{M}$  inhibitor ML141 or SMIFH2 respectively caused a similar decrease in the rate of probing by thin extensions (Fig. 3.5A). Unexpectedly both agents caused a small increase in cell spreading onto adjacent small islands on testing substrates, allowing more cells to cross the rigidity border and at a higher rate than the spreading of untreated cells (Fig. 3.5B and C). These results suggest that probing of filopodia may be involved in generating a retraction signal against cell spreading on soft substrates.

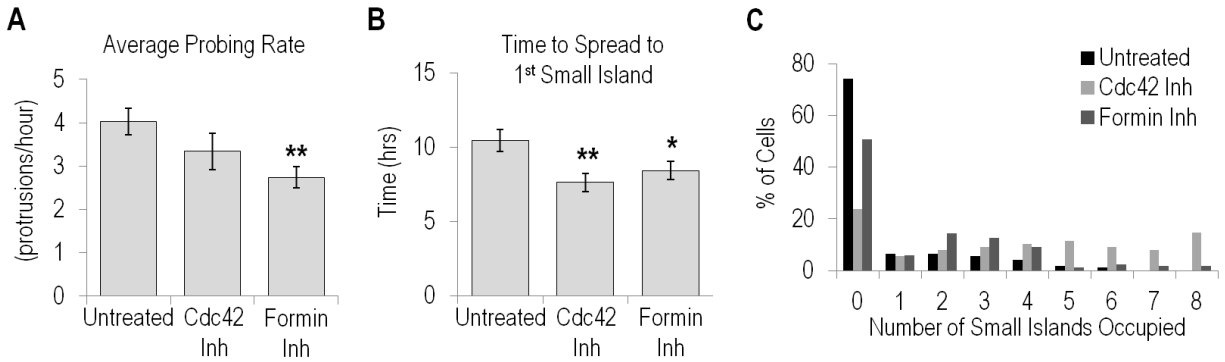


Figure 3.5. Interfering with filopodia formation can disrupt rigidity sensing. Inhibition of formins with 10  $\mu$ M SMIFH2 significantly reduces the probing rate, while Cdc42 inhibition with 10  $\mu$ M ML-141 causes a slight decrease in probing rate (C, middle and right bars, N=66, 64). Treated cells are able to occupy small islands at a slightly faster rate than untreated cells (B, middle and right bars, N=46, 35 respectively) and both treatments increase the percentage of fibroblasts that cross the rigidity border on testing substrates (A, middle and right bars, N=88, 173 respectively). Error bars represent S.E.M. \*  $p < 0.05$  \*\*  $p < 0.01$ .

### 3.3.4 Nascent protrusions detect substrate rigidity outside the cell border based on substrate strain

The results above suggest that thin extensions such as filopodia are responsible for probing substrate rigidity, which then activates a retraction response if the substrate is soft. Otherwise spreading represents the default response when the substrate is rigid, or when the sensing mechanism is defective. A plausible mechanism may involve the response to substrate movement caused by traction forces.

To test this hypothesis, we identified small islands on a rigid underlying gel that have recently been occupied by a cell extension, and used a microneedle to push the island toward the cell body to simulate the deformation of soft substrates caused by cellular probing forces (Fig. 3.6A and B). We found that nascent extensions, defined as filopodia or fine protrusions that became detectable in phase contrast optics for less than 10 minutes, readily retracted after the induced centripetal movement (91% retracted from the island; Fig. 3.6B). More mature protrusions,

which have typically expanded sufficiently to occupy a small island (Fig. 3.6A panel 1), showed a reduction in size but persisted without releasing from the island (87.5% remained associated with the island; Fig. 3.6A). These results suggest that while both nascent and mature protrusions respond to mechanical input, only nascent protrusions and the associated nascent adhesions are able to retract completely from soft substrates. The sensitivity to rigidity decreases once the lamellipodium spread over the adhered area.

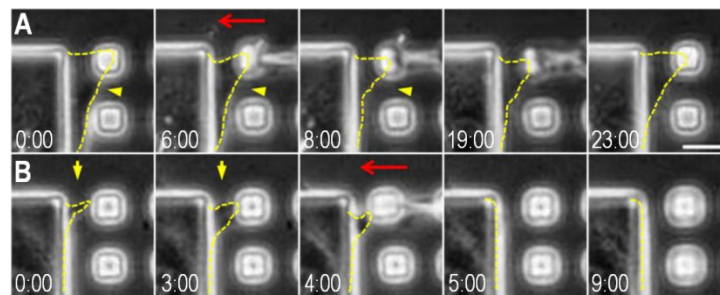


Figure 3.6. Deformation of the substrate by micromanipulation causes retraction of nascent but not mature protrusions. A microneedle was used to push a small island towards the cell body to simulate substrate deformation as a result of probing by traction forces (red arrows). Mature protrusions that adhere to the small island respond by decreasing their size without fully releasing from the island (A, yellow arrowheads). In contrast, nascent protrusions, which have become visible for less than 10 minutes, retract beyond detection in response to the same manipulation (B, yellow arrows). Cell protrusions are outlined by yellow dashed lines. Numbers at the bottom of each image indicate the lapse time in minutes and seconds. 0:00 is an arbitrary time that indicates the start of the time lapse imaging. Scale bar, 10  $\mu\text{m}$ .

### **3.3.5 Myosin II is required for both the probing forces and the subsequent retraction from soft substrates**

The previous results suggest that rigidity sensing involves pulling forces of filopodia or other thin extensions to probe the deformability of the substrate. We hypothesized that myosin II is responsible for generating these probing forces, such that cells should become insensitive to substrate rigidity and show the default behavior of spreading upon the inhibition of myosin II. Indeed, cells treated with 10  $\mu\text{M}$  blebbistatin readily crossed the rigidity border on testing

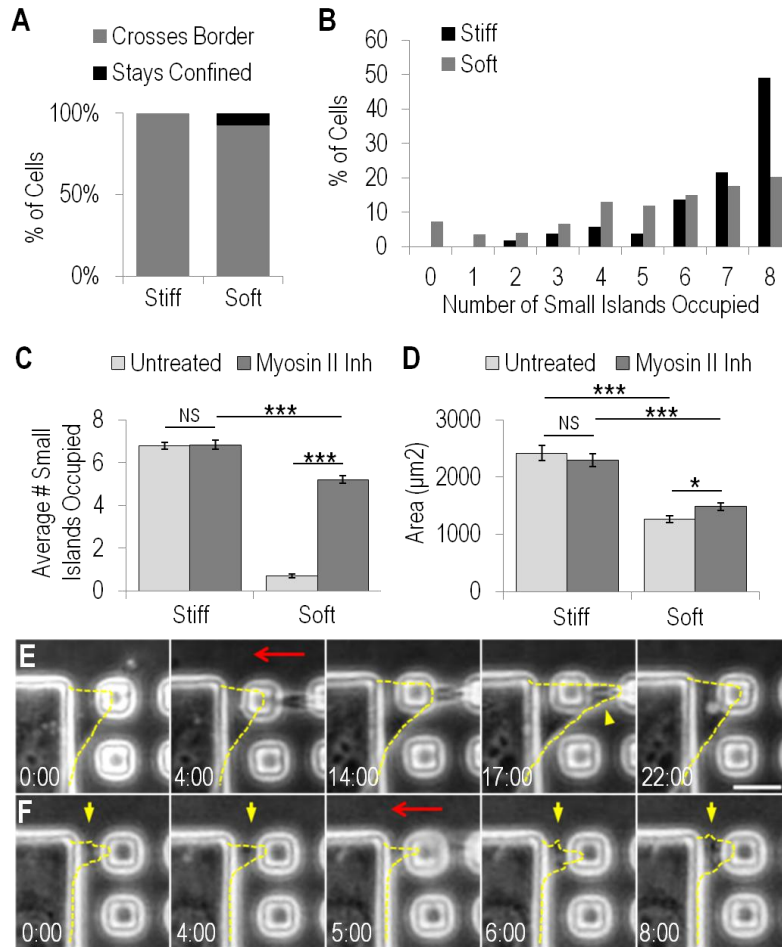


Figure 3.7. Myosin II is required for the cellular response to substrate rigidity. NIH 3T3 cells treated with 10  $\mu\text{M}$  blebbistatin are no longer confined to the large island on testing substrates with soft gels (A, right bar, N=192). Histogram showing the distribution of the number of small islands occupied show that treatment with 10  $\mu\text{M}$  blebbistatin causes a large increase in the fraction of cells that occupy most of the small islands on testing substrates, however, the extent of occupancy remains lower than that on control substrates (B, black bars, N=51). There is a significant increase in the number of small islands taken by treated cells (C, right graph dark grey bar, N=192). On rigid gels cells are able to occupy small islands to a similar extent regardless of blebbistatin treatment (C, left bars, N=51). On soft unpatterned polyacrylamide hydrogel substrates, blebbistatin treated NIH 3T3 cells spread to a slightly, but significantly, larger area than untreated cells (D, right bars, N=52, 52). There is no statistically significant difference in spreading area on stiff unpatterned polyacrylamide gels regardless of blebbistatin treatment (D, left bars N=51, 52). However, the spreading area of blebbistatin treated cells remains larger on stiff than on soft substrates (D, dark grey bars). These results are similar to the results on the composite substrates (C). Neither mature (E), nor nascent protrusions (F, yellow arrows) visibly respond to the deformation of the substrate (red arrows show the direction of microneedle manipulation). Some mature protrusions even continue to spread beneath the microneedle during the micromanipulation (E, yellow arrowhead). Protrusions are outlined by yellow dashed lines. Numbers at the bottom of each image indicate the lapse time in minutes and seconds. 0:00 is an arbitrary time that indicates the start of the time lapse imaging. Scale bar, 10  $\mu\text{m}$ . Error bars represent S.E.M. \*\*\*  $p < 0.001$ . \* $p < 0.05$ .

substrates (Fig. 3.7A and B) to occupy more small islands than untreated cells (Fig. 3.7C). In addition, as reported previously, blebbistatin treated cells adopted a more irregular shape regardless of the stiffness of the substrate<sup>19</sup>. There was still a small but significant difference in the average number of small islands occupied on testing substrates versus control substrates (Fig. 3.7C), which may be related to the difference in spreading area between stiff and soft homogenous hydrogels (Fig. 3.7D), and/or residual myosin II activities in blebbistatin treated cells. Nevertheless, these observations support the notion that, when a cell becomes unable to probe the substrate with contractile forces, it would interpret the substrates as being rigid.

If the sole function of myosin II in rigidity sensing is to provide contractile probing forces for deforming the substrate, then one may expect that artificial deformation of the substrate, as induced by a microneedle, described above, should cause cell protrusions to retract regardless of myosin II inhibition. However, neither nascent nor mature protrusions of blebbistatin treated cells retracted upon microneedle-induced centripetal movement of small islands (Fig. 3.7E and F). Some of these cells even spread beneath the microneedle during the pushing action (Fig. 3.7E yellow arrow head). These results may be explained if myosin II activity is required not only for probing but also for the subsequent retraction in response to substrate deformation. In addition, the results are consistent with the notion that spreading represents the default response to substrate adhesion in the absence of substrate deformation and associated reactions.

### 3.4 Discussion

We used the composite material designed for testing cellular responses at a simulated rigidity border to examine probing mechanism across the rigidity border. As described in Chapter 2, cells on testing substrates remained localized to the large island and did not spread across the soft underlying hydrogel to adjacent small islands while cells on control substrates easily spread to across most small islands. In addition, the results indicated that NIH 3T3 cells are able to sense substrate rigidity in front of their leading edge and regulate their response based on the strain of the underlying hydrogel.

Our observations with phalloidin staining and scanning electron microscopy suggested that actin-containing filopodia in front of the leading edge are responsible for rigidity sensing. This is complementary to other studies suggesting that filopodia play a role in probing the extracellular environment during axonal guidance and in the sensing of substrate topography, and that fluctuations in protrusive activities can bias directional cell migration<sup>33-35</sup>. Time-lapse recordings further indicated a probing process mediated by filopodia followed by the spreading of lamellipodia. While cells on both soft and rigid substrates exhibited a similar probing rate, there was a dramatic difference in the rate of subsequent spreading across soft or rigid substrates. On control substrates, it took ~3 hours for cells to spread onto the first island and another 5 hours onto the remaining 7 islands. In contrast, on testing substrates it took over 10 hours for a small fraction of cells to spread across soft hydrogels onto the first island. This difference was due to the differential stability of filopodia extensions following initial adhesion and probing. Extensions onto soft materials showed a high probability to release and retract, while extensions onto rigid materials were stable to allow continuous spreading. These results also suggest that fibroblasts are able to detect substrate rigidity at a distance in front of their leading edge through

nascent adhesions, which have been previously shown to generate strong traction stress likely for the purpose of probing substrates<sup>36</sup>. Supporting this hypothesis, we have observed minute deflections of small islands on soft gels just before extensions became visible in phase contrast optics. This finding is also supported by earlier observations that filopodia were able to exert forces on the surrounding substrate<sup>37,38</sup>.

One may consider two alternative mechanisms for rigidity sensing—through either the promotion of spreading on rigid substrates, or the promotion of retraction on soft substrates. Inhibition of Cdc42 or formins, two positive filopodia regulators, reduced the appearance of thin probing extensions while promoting cell spreading onto soft substrates. In addition, consistent with the previous suggestion that actomyosin dependent traction forces are crucial for rigidity sensing<sup>18,19</sup>, inhibition of myosin II also caused cells to spread onto soft substrates (Fig 3.7A). These results suggest that filopodia and associated traction forces are required for probing substrate rigidity and that spreading is the default response when the substrate fails to deform or when the downstream signal transduction mechanism is defective. One may then expect cell retraction when the substrate was pushed artificially toward the cell body to simulate the effect of traction forces, and that this retraction response be inhibited by blebbistatin. Both predictions were supported by experiments.

Using a similar composite substrate, we previously suggested that rigidity sensing is based on long-range strain of the substrate in response to cellular traction forces<sup>21</sup>. The present results indicate that this range is defined by the length of filopodia extensions, which may be as long as 20-30  $\mu\text{m}$ <sup>30,39,40</sup>, rather than the tip-to-tail length of the cell. A related question concerns rigidity sensitivity of mature focal adhesions, which was suggested by the retraction of cell lamellipodia

and shrinkage of mature focal adhesions when a spread region was pushed toward the cell body to reduce tension<sup>10</sup>. Based on their localization behind the leading edge, we suspect that mature focal adhesions play a secondary role in guiding cell migration, such as during durotaxis. They may nevertheless facilitate the responses to dynamic changes in substrate rigidity, as demonstrated upon softening of the anterior substrate using a UV-sensitive hydrogel substrate<sup>41</sup>.

Figure 3.8 depicts a plausible rigidity sensing mechanism, where myosin II driven pulling forces are exerted at nascent adhesions at the tip of filopodia to induce substrate deformation. Resistance of rigid substrates causes tension to build up at nascent adhesions, which promotes maturation of focal adhesions and allows the default response of active extension/spreading of the cell possibly by maintaining the small GTPase Rac<sup>42,43</sup> and Arp 2/3 mediated actin polymerization<sup>27,44</sup>. On soft materials, the strain of the substrate inhibits the buildup of tension at nascent adhesions and keeps them from maturation into focal adhesions, which then promotes the retraction of filopodia through myosin II-dependent contractile forces. In the absence of these mechanically active filopodia, or in the absence of proper downstream responses to substrate deformation, cells exhibit the default response of spreading.

Sensing mediated by filopodia in front of the leading edge provides an efficient mechanism for durotaxis and possibly other responses to physical properties of the substrate, by allowing cells to determine physical characteristics before moving over an area and to avoid the formation of mature focal adhesions on soft substrates to prevent back-tracking. Although the present study was conducted with cells in 2D culture, the mechanism may also allow cells to maintain a similar sensitivity in physiologically relevant 3D environments, where they are unable to form broad

lamellipodia or large focal adhesions but maintain the ability to form filopodia and other types of extensions.

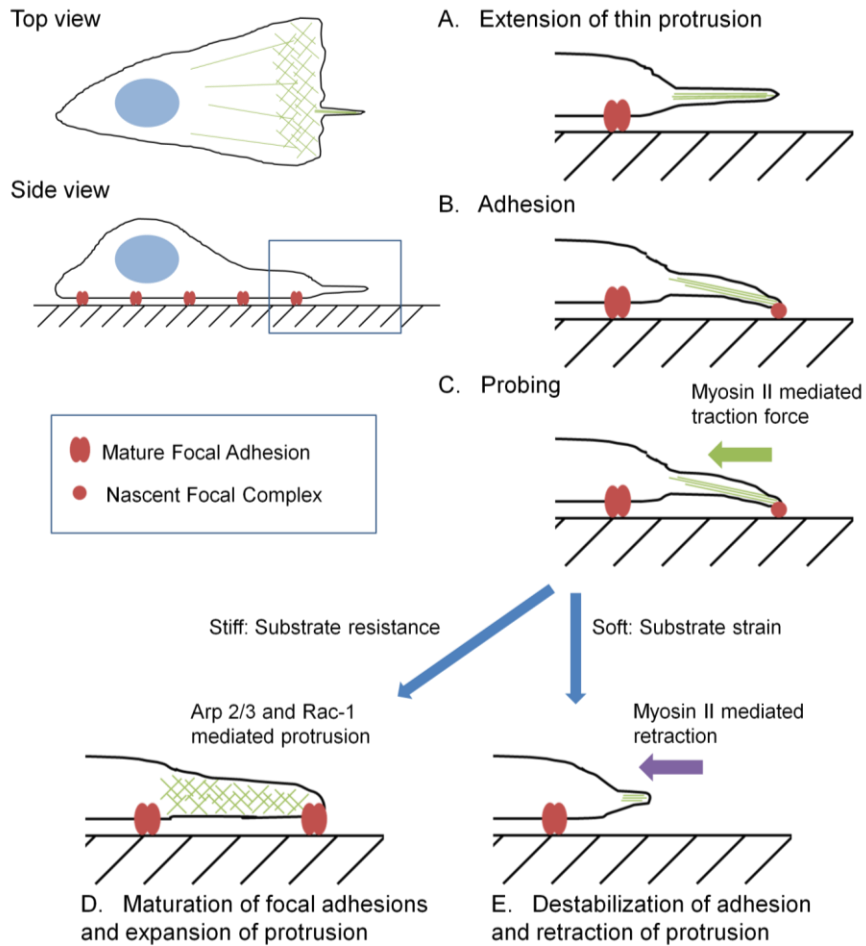


Figure 3.8. Schematic of rigidity sensing in front of the leading edge. Actin-containing filopodia extend in front of the leading edge (A), and establish nascent adhesions at a distance in front of the leading edge (B). Myosin II-mediated traction forces drive the filopodia probing process by pulling on the nascent adhesions (C). The resulting strain then determines the cellular response. Resistance from rigid substrates causes nascent adhesions to mature into focal adhesions and allows protrusions to expand via Arp 2/3 and Rac1 mediated actin polymerization (D). Large strain from soft substrates causes nascent adhesions to disassemble and protrusions to retract via a myosin II dependent process (E).

### 3.5 References

1. Wang, H., Dembo, M. & Wang, Y. Substrate flexibility regulates growth and apoptosis of normal but not transformed cells. *Am. J. Physiol. Cell Physiol.* **279**, C1345–C1350 (2000).
2. Discher, D. E., Janmey, P. & Wang, Y.-L. Tissue cells feel and respond to the stiffness of their substrate. *Science* **310**, 1139–43 (2005).
3. Engler, A. J., Sen, S., Sweeney, H. L. & Discher, D. E. Matrix elasticity directs stem cell lineage specification. *Cell* **126**, 677–89 (2006).
4. Butcher, D. T., Alliston, T. & Weaver, V. M. A tense situation: forcing tumour progression. *Nat. Rev. Cancer* **9**, 108–22 (2009).
5. Paszek, M. J. *et al.* Tensional homeostasis and the malignant phenotype. *Cancer Cell* **8**, 241–54 (2005).
6. Tilghman, R. W. *et al.* Matrix rigidity regulates cancer cell growth and cellular phenotype. *PLoS One* **5**, e12905 (2010).
7. Ulrich, T. a, de Juan Pardo, E. M. & Kumar, S. The mechanical rigidity of the extracellular matrix regulates the structure, motility, and proliferation of glioma cells. *Cancer Res.* **69**, 4167–74 (2009).
8. Levy-Mishali, M., Zoldan, J. & Levenberg, S. Effect of scaffold stiffness on myoblast differentiation. *Tissue Eng. Part A* **15**, 935–44 (2009).
9. Mason, B. N., Califano, J. P. & Reinhart-king, C. A. in *Eng. Biomater. Regen. Med.* (Bhatia, S. K.) 19–38 (Springer New York, 2012). doi:10.1007/978-1-4614-1080-5
10. Lo, C. M., Wang, H., Dembo, M. & Wang, Y.-L. Cell movement is guided by the rigidity of the substrate. *Biophys. J.* **79**, 144–52 (2000).
11. Pelham, R. J. & Wang, Y. Cell locomotion and focal adhesions are regulated by substrate flexibility. *Cell* **94**, 13661–13665 (1997).
12. Tan, J. L. *et al.* Cells lying on a bed of microneedles : An approach to isolate mechanical force. *Proc. Natl. Acad. Sci.* **100**, 1484–1489 (2002).
13. Jiang, G., Huang, A. H., Cai, Y., Tanase, M. & Sheetz, M. P. Rigidity sensing at the leading edge through alphavbeta3 integrins and RPTPalpha. *Biophys. J.* **90**, 1804–9 (2006).
14. Plotnikov, S. V, Pasapera, A. M., Sabass, B. & Waterman, C. M. Force Fluctuations within Focal Adhesions Mediate ECM-Rigidity Sensing to Guide Directed Cell Migration. *Cell* **151**, 1513–27 (2012).
15. Gray, D. S., Tien, J. & Chen, C. S. Repositioning of cells by mechanotaxis on surfaces with micropatterned Young ' s modulus. *J. Biomed. Mater. Res.* 605–614 (2003).
16. Nemir, S., Hayenga, H. N. & West, J. L. PEGDA hydrogels with patterned elasticity: Novel tools for the study of cell response to substrate rigidity. *Biotechnol. Bioeng.* **105**, 636–44 (2010).
17. Kawano, T. & Kidoaki, S. Elasticity boundary conditions required for cell mechanotaxis on microelastically-patterned gels. *Biomaterials* **32**, 2725–33 (2011).
18. Trichet, L. *et al.* Evidence of a large-scale mechanosensing mechanism for cellular adaptation to substrate stiffness. *Proc. Natl. Acad. Sci.* **109**, 6933–8 (2012).
19. Raab, M. *et al.* Crawling from soft to stiff matrix polarizes the cytoskeleton and phosphoregulates myosin-II heavy chain. *J. Cell Biol.* **199**, 669–83 (2012).
20. Breckenridge, M. T., Desai, R. a., Yang, M. T., Fu, J. & Chen, C. S. Substrates with Engineered Step Changes in Rigidity Induce Traction Force Polarity and Durotaxis. *Cell.*

- Mol. Bioeng.* **7**, 26–34 (2013).
21. Hoffercker, I. T., Guo, W. & Wang, Y. Assessing the spatial resolution of cellular rigidity sensing using a micropatterned hydrogel-photoresist composite. *Lab Chip* **11**, 3538–44 (2011).
  22. Wong, S., Guo, W., Hoffercker, I. T. & Wang, Y. in *Methods Cell Biol.* (2014).
  23. Stroka, K. M. & Aranda-Espinoza, H. Neutrophils display biphasic relationship between migration and substrate stiffness. *Cell Motil. Cytoskeleton* **66**, 328–41 (2009).
  24. Flanagan, L. A., Ju, Y., Marg, B., Osterfield, M. & Paul, A. Neurite branching on deformable substrates. *Neuroreport* **13**, 2411–2415 (2002).
  25. Rape, A. D., Guo, W.-H. & Wang, Y.-L. The regulation of traction force in relation to cell shape and focal adhesions. *Biomaterials* **32**, 2043–51 (2011).
  26. Chen, C. S., Alonso, J. L., Ostuni, E., Whitesides, G. M. & Ingber, D. E. Cell shape provides global control of focal adhesion assembly. *Biochem. Biophys. Res. Commun.* **307**, 355–361 (2003).
  27. Suraneni, P. *et al.* The Arp2/3 complex is required for lamellipodia extension and directional fibroblast cell migration. *J. Cell Biol.* **197**, 239–51 (2012).
  28. Nolen, B. J. *et al.* Characterization of two classes of small molecule inhibitors of Arp2/3 complex. *Nature* **460**, 1031–4 (2009).
  29. Steffen, A. *et al.* Rac function is crucial for cell migration but is not required for spreading and focal adhesion formation. *J. Cell Sci.* **126**, 4572–88 (2013).
  30. Nobes, C. D. & Hall, a. Rho, rac, and cdc42 GTPases regulate the assembly of multimolecular focal complexes associated with actin stress fibers, lamellipodia, and filopodia. *Cell* **81**, 53–62 (1995).
  31. Jaiswal, R. *et al.* The formin daam1 and fascin directly collaborate to promote filopodia formation. *Curr. Biol.* **23**, 1373–1379 (2013).
  32. Mellor, H. The role of formins in filopodia formation. *Biochim. Biophys. Acta* **1803**, 191–200 (2010).
  33. Dalby, M. J. J., Gadegaard, N., Riehle, M. O., Wilkinson, C. D. W. & Curtis, A. S. G. Investigating filopodia sensing using arrays of defined nano-pits down to 35 nm diameter in size. *Int. J. Biochem. Cell Biol.* **36**, 2005–2015 (2004).
  34. Davenport, R. W., Dou, P., Rehder, V. & Kater, S. B. A sensory role for neuronal growth cone filopodia. *Nature* **361**, 721–724 (1993).
  35. Caballero, D., Voituriez, R. & Riveline, D. Protrusion fluctuations direct cell motion. *Biophys. J.* **107**, 34–42 (2014).
  36. Beningo, K. A., Dembo, M., Kaverina, I., Small, J. V. & Wang, Y. Nascent focal adhesions are responsible for the generation of strong propulsive forces in migrating fibroblasts. *J. Cell Biol.* **153**, 881–8 (2001).
  37. Albuschies, J. & Vogel, V. The role of filopodia in the recognition of nanotopographies. *Sci. Rep.* **3**, (2013).
  38. Chan, C. E. & Odde, D. J. Traction Dynamics of Filopodia on Compliant Substrates. *Science* **322**, 1687–1691 (2008).
  39. Lehnert, D. *et al.* Cell behaviour on micropatterned substrata: limits of extracellular matrix geometry for spreading and adhesion. *J. Cell Sci.* **117**, 41–52 (2004).
  40. Partridge, M. A. & Marcantonio, E. E. Initiation of Attachment and Generation of Mature Focal Adhesions by Integrin-containing Filopodia in Cell Spreading □. *Mol. Biol. Cell* **17**, 4237–4248 (2006).

41. Frey, M. T. & Wang, Y. A photo-modulatable material for probing cellular responses to substrate rigidity. *Soft Matter* **5**, 1918–1924 (2009).
42. Ridley, a J. & Hall, a. The small GTP-binding protein rho regulates the assembly of focal adhesions and actin stress fibers in response to growth factors. *Cell* **70**, 389–99 (1992).
43. Waterman-Storer, C. M., Worthylake, R. a, Liu, B. P., Burridge, K. & Salmon, E. D. Microtubule growth activates Rac1 to promote lamellipodial protrusion in fibroblasts. *Nat. Cell Biol.* **1**, 45–50 (1999).
44. Wu, C. *et al.* Arp2/3 Is Critical for Lamellipodia and Response to Extracellular Matrix Cues but Is Dispensable for Chemotaxis. *Cell* **148**, 973–87 (2012).

## Chapter 4

# FAK Plays an Essential Role in Rigidity Sensing through its Regulation of Rho Activities

Cells migrate preferentially toward stiff substrates in a process termed durotaxis. To facilitate the study of the mechanism of rigidity sensing, we have previously developed a micropatterned composite material that traps cells at a rigidity border, thereby allowing highly efficient identification of conditions that impair durotaxis and cause cells to cross from a rigid onto a soft domain. Consistent with previous results using a conventional approach, we found that focal adhesion kinase null (FAK  $-/-$ ) cells were defective in rigidity sensing while re-expression of focal adhesion kinase (FAK) rescued the response. A similar defect was observed after treating NIH 3T3 cells with the microtubule disrupter nocodazole, or with a Rho activator, supporting the notion that hyperactivity of Rho, which represents a common feature of these cells, may be responsible for the defect in rigidity sensing. Inhibiting Rho activity indeed rescued rigidity sensing in FAK  $-/-$  cells, while inhibiting Rho downstream effector mDia1, but not Rho activated kinase (ROCK), also rescued the defect. Cells expressing F397-FAK, a mutation blocking autophosphorylation without increasing Rho activities, exhibited a normal rigidity response. Our results indicate that enhanced activities of Rho, and downstream effector mDia1, is sufficient to impair rigidity sensing and that FAK mediates rigidity sensing by constraining Rho activities on soft substrates.

## 4.1 Introduction

The ability of a cell to sense substrate rigidity and migrate preferentially towards stiff areas is referred to as durotaxis<sup>1</sup>. Since its initial discovery more than a decade ago, durotaxis has become an essential component of consideration in regenerative medicine, such as the optimization of scaffold design<sup>2</sup>. It is also suspected to play a role in cancer pathology, including metastasis and tumor formation<sup>3,4</sup>.

Studies on the sensing and signaling mechanisms underlying durotaxis have implicated a variety of molecules including focal adhesion kinase (FAK)<sup>5</sup> and myosin II<sup>6</sup>. FAK is a cytoplasmic protein kinase implicated in mediating many adhesion-activated processes<sup>7</sup>. In response to integrin mediated cell adhesion, FAK activity is upregulated via the phosphorylation at multiple tyrosine sites<sup>8</sup>. Specifically, phosphorylation of FAK at tyrosine 397 in response to integrin clustering is believed to initiate multiple signaling cascades by creating a motif recognized by SH2 domain containing proteins<sup>7-11</sup>.

FAK has been shown to regulate focal adhesion disassembly<sup>12,13</sup>, including that induced by microtubules<sup>14</sup>, and at the tail of migrating cells<sup>15</sup>, which may explain migration deficiencies of FAK *-/-* cells through reduced focal adhesion turnover<sup>16</sup>. FAK has also been implicated in regulating proliferation<sup>17</sup> and microtubule stabilization in response to adhesion<sup>18</sup>. It has been shown that FAK induces down-regulation of the small GTPase Rho, and that FAK *-/-* cells have increased Rho activity<sup>13,17</sup>, such that the regulation of Rho activity may represent as a common driving factor in many of FAK-mediated processes.

Most studies on rigidity sensing use a series of hydrogels or micropillar arrays of varying stiffness. However, it is difficult for experiments using separate substrates to address spatial-

temporal responses to changes in substrate rigidity, while substrates with a single rigidity border also prove inefficient for capturing the event. We utilize the previously developed a composite substrate, described in Chapter 2, that traps cells at a simulated rigidity border, to allow the probing of responses to changes in substrate rigidity<sup>19</sup>. In the present study, we first applied this material to reproduce the defective rigidity sensing of FAK  $-/-$  cells, then proceed to show that elevated Rho activities in these cells are responsible for the defect. In addition, the effector mDia1 downstream of Rho, but not the Rho dependent kinase (ROCK), is likely involved in mediating rigidity sensing.

## 4.2 Experimental Methods

### 4.2.1 Preparation of substrates

Composite substrates with micropatterned islands of SU-8 photoresist grafted on the surface of polyacrylamide hydrogels were prepared as described previously<sup>20,21</sup>. Briefly, fresh polyacrylamide solutions: 8% acrylamide (Bio-Rad) and 0.2% bis-acrylamide (Bio-Rad), and 5% acrylamide and 0.04% bis-acrylamide<sup>22,23</sup> were prepared and degassed. Polymerization initiators ammonium persulfate (Sigma) and N,N,N',N' tetramethylethylenediamine (Bio-Rad) were added at 0.6% and 0.4% respectively, and a 20  $\mu$ L drop of this solution was pipetted onto a Bind-Silane activated coverslip (GE Healthcare), to allow bonding of the polyacrylamide gel to the glass surface during polymerization. A 25 mm circular coverslip, spin-coated with 50% w/v sucrose solution at 5,000 rpm for 20 seconds, was inverted onto the acrylamide drop. After 1 hour of polymerization, the sucrose solution was dissolved to allow gentle removal of the circular coverslip. The gel was equilibrated in deionized water for 30 minutes then dehydrated overnight. Arrays of rigid islands were grafted onto dried polyacrylamide gels using a negative photoresist SU-8 2000 and standard photolithography techniques (Microchem). After development coverslips were rinsed twice with 95% ethanol, then baked at 95°C for 4 hours to ensure removal of any residual developer. Before use, the substrate was immersed in phosphate buffered saline for 1 hour to rehydrate the hydrogel and incubated with oxidized gelatin for 15 minutes to facilitate cell adhesion to the SU-8 islands.

Unpatterned polyacrylamide hydrogels for cell spreading and traction force microscopy were prepared as described previously<sup>24</sup>. Briefly, a circular coverglass was incubated for 45 minutes with a 0.1% (w/v) gelatin solution that had been activated with 3.5 mg/mL sodium periodate

(Sigma), then dried using N<sub>2</sub> gas. A freshly prepared solution of 5% acrylamide and 0.06% or 0.1% bis-acrylamide (Bio-Rad) was degassed; 0.2 μm fluorescent beads (Molecular Probes) were added at a 1:2000 dilution if the substrate was to be used for traction force microscopy. After addition of 6 μL and 4 μL the initiators 10% ammonium persulfate solution (Sigma) and N,N,N',N'-tetramethylethane-1,2-diamine (EMD Millipore, Billerica, MA), a 30 μL drop was pipetted onto a large coverslip pre-treated with Bind-Silane (GE Healthcare). The gelatin coated coverglass was immediately placed protein-side down onto the acrylamide drop. After complete acrylamide polymerization, the top coverslip was carefully removed. Polyacrylamide hydrogel substrates were mounted into chamber dishes, sterilized under ultraviolet light for 30 min, and incubated in cell culture media for 1 hour at 37°C before use. The final gels had an estimated Young's modulus of approximately 1.8 kPa and 3.5 kPa<sup>25,26</sup>.

#### **4.2.2 Cell culture and pharmacological treatments**

Mouse embryonic fibroblasts expressing wild-type or Y397F-FAK under the control of tetracycline were maintained in Advanced Dulbecco's modified Eagle's medium (Advanced DMEM; Life Technologies) supplemented with 10% fetal bovine serum (Thermo Scientific), 2mM L-glutamine, 50 μg/mL streptomycin, 50 U/mL penicillin (Life Technologies) and 1 μg/mL tetracycline. Fresh tetracycline was added every other day to maintain the inhibition of FAK expression. To induce the expression of wild-type or Y397F-FAK, cells were replated in media lacking tetracycline for at least 48 hours to reach maximal expression as shown previously<sup>27</sup>.

NIH 3T3 cells (ATCC) were maintained in Dulbecco's modified Eagle's medium (DMEM; Life Technologies) supplemented with 10% adult donor bovine serum (Thermo Scientific), 2 mM L-glutamine, 50  $\mu\text{g}/\text{mL}$  streptomycin, and 50 U/mL penicillin (Life Technologies).

To inhibit FAK activity, cells were treated with 10  $\mu\text{M}$  PF 573-228 approximately 30 minutes after plating for 16 hours before quantitative analysis of pattern occupancy. To assess the importance of Rho, cells were treated with 1.0  $\mu\text{g}/\text{mL}$  CN03 to upregulate Rho activity (Cytoskeleton, Denver, CO), 10  $\mu\text{M}$  nocodazole to depolymerize microtubules and increase Rho activity, or 2.0  $\mu\text{g}/\text{mL}$  CT04 to inhibit Rho activity (Cytoskeleton) for either 30 minutes before starting time lapse imaging or 16 hours before quantitative analysis of pattern occupancy. Rho activation studies were performed in parallel on the composite substrate and for traction force generation to ensure that the activator was inducing a defect in pattern occupancy even when no traction stress increase was observed. Cells were treated with 10  $\mu\text{M}$  SMIFH2 to inhibit formins including mDia1 (EMD Millipore), or 10  $\mu\text{M}$  Y27632 to inhibit ROCK (Tocris) for either 30 minutes before starting time lapse imaging or 16 hours before quantitative analysis of pattern occupancy. The number of cells analyzed for each graph is indicated in the figure caption, and at least 3 independent trials were performed for each experiment, control data repeated where necessary for comparison.

### **4.2.3 Traction force microscopy**

Phase contrast images of single cells spread on a uniformly-coated polyacrylamide gels of varying stiffness were collected with a Nikon Eclipse Ti microscope using a 40X N.A. 0.75 PlanFluor dry objective and an Andor iXon CCD camera and custom software. Fluorescence images of the embedded beads near the surface of the hydrogel were taken before and after cells

were removed with 0.05% Trypsin-EDTA (Life Technologies). Cell outlines were manually drawn, and bead displacement fields were computed using custom software. Traction stress was computed using LIBTRC software package (Prof. Micah Dembo, Boston University).

#### **4.2.4 Microscopy and image analysis**

Phase contrast images were collected with a Nikon Eclipse Ti microscope using a 40x PlanFluor 0.75 N.A. dry objective. For time lapse videos, images were collected every 10 minutes for a period of 16 hours. For the analysis of pattern occupancy, images were collected after 16 hours of incubation. In all experiments, only single cells were counted for the analysis. For micromanipulation, a microneedle prepared with a vertical micropipette puller (Model 720, David Kopf Instruments) was mounted on a Leitz micromanipulator to allow precise positioning of the tip. Phase contrast images were collected with a Zeiss Axiovert 200M using a 40x PlanNeofluar 0.75 N.A. dry objective. Images were collected every minute during microneedle manipulation. Fluorescence images were collected using a Nikon 100x PlanFluor 1.3 N.A. oil immersion lens. Focal adhesion size was quantified using ImageJ (National Institutes of Health).

## 4.3 Results

### 4.3.1 Defect of FAK $-/-$ cells in durotaxis as measured with a cell-on-a-chip composite substrate

We have previously developed a cell-on-a-chip approach for detecting and measuring durotaxis using a soft-stiff composite material<sup>19</sup>. A micropatterned array of SU-8 islands grafted onto a soft gel creates a rigidity border where cells must decide whether or not to spread from a large rigid island onto a soft domain of small moveable islands. A similar array of islands grafted onto a stiff hydrogel served as a control substrate. This approach allows easy detection and quantitative assessment of defects in durotaxis, based on the percentage histogram of cells that were able to occupy various numbers of small islands.

In an earlier study using adjoining polyacrylamide gels of different stiffness, FAK  $-/-$  cells were found to be able to move from rigid onto soft surface. Re-expression of FAK rescued the normal behavior of avoiding softer substrates<sup>5</sup>. The defect in durotaxis was readily demonstrated using the present approach (Fig. 4.1A and C). We found that 55% of rescued cells were confined entirely to the rigid large island (Fig. 4.1F black bars) and none of rescued cells were able to cover the soft domain. On average rescued cells covered approximately one small island, while in contrast, FAK  $-/-$  cells occupied more than 3 small islands on average (Fig. 4.1E), Approximately 10% of FAK  $-/-$  cells covered the entire patterned area (Fig. 4.1F darkest grey bars) while 74% of cells occupied at least one small island (Fig. 4.1G). Inhibiting FAK activity in NIH 3T3 fibroblasts with small molecule inhibitor PF 573,228 produced results very similar to the FAK  $-/-$  cells (Fig. 4.1D). FAK inhibited cells also occupied on average over 3 small islands

(Fig. 4.1E), and 73% were able to spread across the rigidity border (Fig. 4.1F medium grey bars and G).

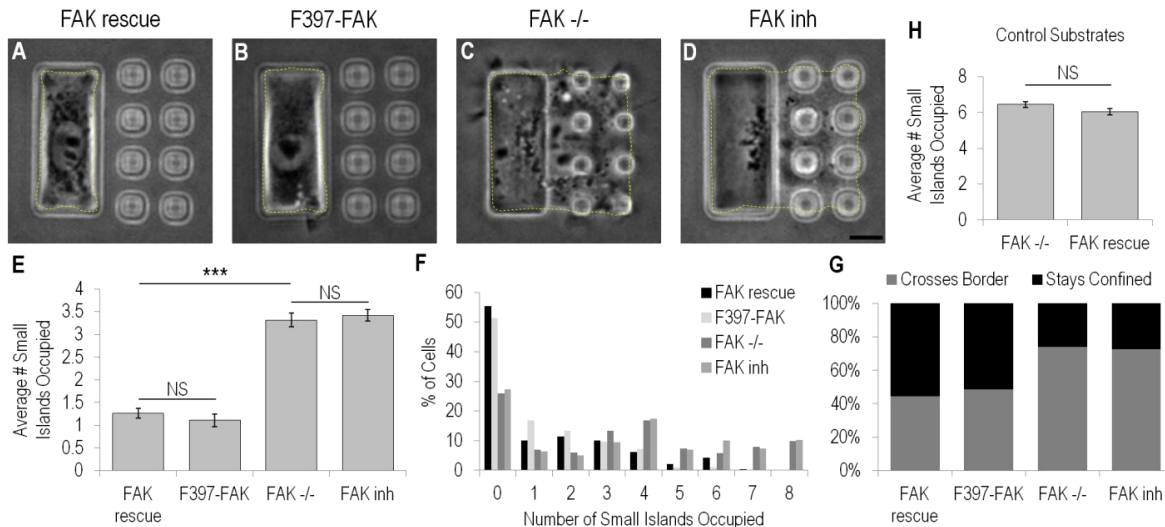


Figure 4.1. Cellular response to a conventional rigidity border can be captured on the composite substrate. Representative images of cells re-expressing WT-FAK (A) or F397-FAK (B), FAK  $-/-$  cells (C), and 3T3 fibroblasts treated with 10  $\mu$ M FAK inhibitor PF 573,228 (D). FAK  $-/-$  and cells treated with FAK inhibitor occupy an increased number of small islands and cross the border more often compared to cells re-expressing WT-FAK or F397-FAK (E-G, N=287, 113, 315, 520). No difference in spreading was observed between FAK  $-/-$  and FAK rescued cells on control substrates with a stiff underlying hydrogel (H, N=155, 174). Scale bar, 10  $\mu$ m. Error bars represent S.E.M. \*\*\* $p < 0.001$ .

Re-expression of F397-FAK rescued rigidity sensitivity similar to re-expression of WT-FAK in FAK rescued cells (Fig. 4.1B). Cells expressing F397-FAK were mostly confined to the large island (51%, Fig. 4.1F lightest grey bars and G) and occupied on average approximately one small island (Fig. 4.1E). No difference was observed between FAK  $-/-$  and FAK rescued cells on control substrates made with SU-8 islands on stiff polyacrylamide, indicating that the difference on testing substrates cannot be attributed to the geometric pattern of the islands (Fig. 4.1H).

### 4.3.2 Impaired response of FAK $-/-$ cells to substrate strain

We showed previously that mechanical probing via fine extensions in front of the leading edge played an important role in rigidity sensing. The resulting deformation of the substrate

determined whether the cell spread onto or retracted from the probed area<sup>19</sup>. Probing activities were examined starting 30 minutes after plating, example images of probing protrusions are shown in Figure 4.2A-D. Analysis showed FAK <sup>-/-</sup> cells were much more successful in spreading over the soft domain than FAK rescued cells, occupying the first small island 5.3 hours after plating compared 7.2 hours for FAK rescued cells (Fig. 4.2E). However, the difference cannot be easily explained by the slight but significant decrease in the extension of probing protrusions (Fig. 4.2F), but may be attributed to the decreased retraction response of FAK <sup>-/-</sup> cells upon contacting a small island on soft substrates (Fig. 4.2G). FAK<sup>-/-</sup> cells were also seen to reoccupy islands upon initial retraction, consistent with the reported increase in lamellipodial dynamics following the loss of FAK<sup>28</sup>.

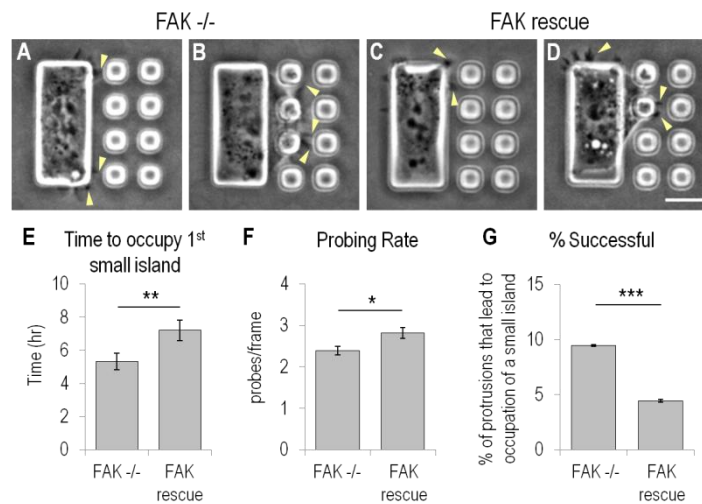


Figure 4.2. FAK <sup>-/-</sup> cells have an increased probability of spreading after probing on testing substrates. FAK <sup>-/-</sup> cells extend multiple probing protrusions per frame while confined to the large island (A) and as the cell spreads across adjacent small islands (B). FAK rescued cells also extend multiple protrusions out from the cell body when on the large island (C) or spread across small islands (D). FAK <sup>-/-</sup> cells occupy the first small island faster than FAK rescued cells (E, N=64, 41). Although FAK rescued cells extended probing protrusions at a slightly higher rate than FAK <sup>-/-</sup> cells (F, N=102, 70) FAK<sup>-/-</sup> cells have a higher percentage of successful protrusions (G). Scale bar, 10  $\mu$ m. Error bars represent S.E.M. \*p<0.05, \*\*p<0.01, \*\*\*p<0.001.

To confirm that FAK <sup>-/-</sup> cells failed to respond to substrate deformation, we tested the response of cells to substrate deformation induced artificially by pushing small islands on stiff substrates

with a microneedle upon the adhesion of protrusions. FAK<sup>-/-</sup> cells failed to retract from deformed substrates, 14 out of 17 protrusions tested remained associated with the small island (Fig. 4.3). These observations suggest that FAK<sup>-/-</sup> cells fail to avoid soft substrates because the protrusions are unable to properly retract in response to substrate strain.

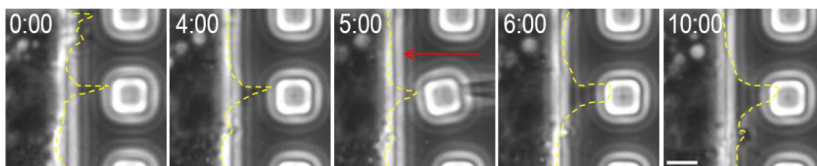


Figure 4.3. FAK<sup>-/-</sup> cells are unable to retract protrusions in response to deformation of the substrate by micromanipulation. A microneedle was used to push a small island towards the cell body to simulate substrate deformation as a result of probing by traction forces (red arrow). Nascent protrusions, which have become visible for less than 10 minutes, do not visibly respond to the deformation of the substrate (red arrows show the direction of microneedle manipulation). Protrusions are outlined by yellow dashed lines. Numbers at the bottom of each image indicate the lapse time in minutes and seconds. 0:00 is an arbitrary time that indicates the start of the time lapse imaging. Scale bar, 10  $\mu\text{m}$ .

### 4.3.3 Involvement of Rho activity in rigidity sensing defect

FAK is known to suppress Rho activities to promote focal adhesion turnover<sup>13,17</sup>. FAK<sup>-/-</sup> cells show elevated Rho GTPase activities, which may be responsible for unregulated spreading onto soft substrates through the activation of mDia1 and the resulting unregulated actin assembly. Treating NIH 3T3 fibroblasts with CN03, a Rho activator, caused cells to cross the rigidity border, similar to the treatment with FAK inhibitor (Fig. 4.4A-C). A similar defect was found upon the treatment of cells with nocodazole to disassemble microtubules (Fig. 4.4A-C), which are known to interact with focal adhesions through FAK and the downstream effector mDia1. Disassembly of microtubules is also known to stimulate Rho activities<sup>29</sup>, possibly during the response to stiff substrates<sup>30</sup>. Interestingly, the histogram of occupancy of small islands looked strikingly similar for FAK<sup>-/-</sup> cells and cells treated with CN03, nocodazole, or FAK inhibitor (Fig. 4.4B).

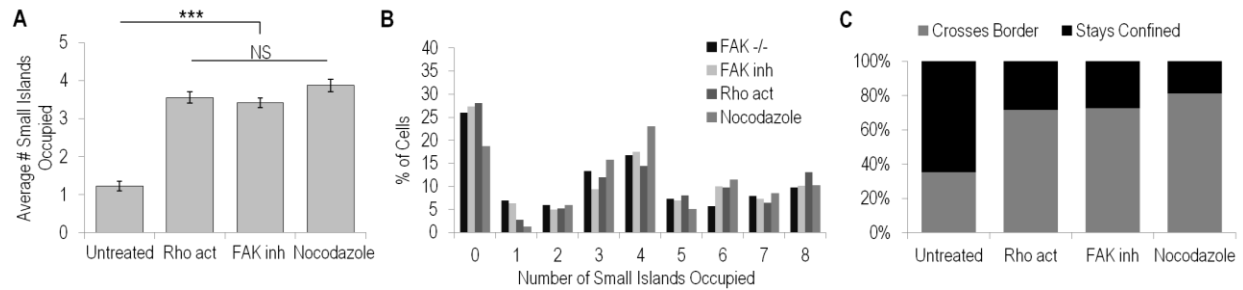


Figure 4.4. Increased Rho activity is sufficient to produce a rigidity sensing defect. Increasing Rho activity directly with 1.0  $\mu\text{g}/\text{mL}$  Rho activator CN03, or indirectly via depolymerization of microtubules after 10  $\mu\text{M}$  nocodazole treatment caused cells to occupy an increased number of small islands similar to what was seen with FAK inhibition (A, N=209, 359, 520, 235). Treated cells were able to occupy or all small islands in the patterned area (B) and the percentage of cells that crossed the rigidity border increased compared to untreated cells (C). Error bars represent S.E.M. \*\*\* $p < 0.001$ .

To determine if Rho activation is necessary for impaired rigidity sensing of FAK  $-/-$  cells, we asked if inhibiting Rho activity in FAK $-/-$  cells would rescue the defect. Upon the treatment with CT04, a small molecule inhibitor specific to RhoA, FAK  $-/-$  cells showed a reduced extent of spreading onto soft substrates (Fig. 4.5A light grey bars, and B). The percentage of confined cells also increased from 26% to 52% (Fig. 4.5C), and 70% of cells occupied 1 small island or less. Treatment with Rho inhibitor had no effect on the spreading over control substrates (Fig. 4.5D), indicating that inhibition of Rho does not affect cell spreading in general but impairs only spreading over soft surfaces. Neither did the Rho inhibitor affect the rigidity sensing of control cells (Fig. 4.5A dark grey bars, and E).

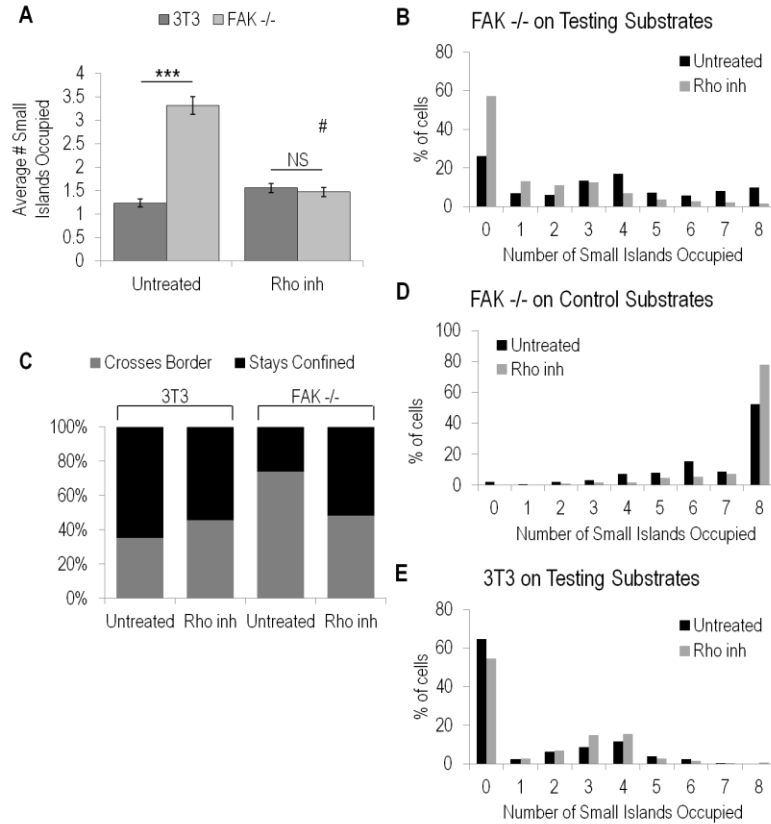


Figure 4.5. Inhibiting Rho activity in FAK  $-/-$  cells is sufficient to rescue rigidity sensing. Treatment of FAK  $-/-$  cells with 2.0  $\mu\text{g}/\text{mL}$  Rho inhibitor CT04 reduced the average number of small islands occupied (A light grey bars,  $N=315, 210$ ) but did not affect control 3T3 cells (A dark grey bars,  $N=209, 257$ ). Rho inhibition reduced the percentage of FAK  $-/-$  cells occupying multiple adjacent small islands (B). Rho inhibition of FAK  $-/-$  cells reduced the ability of cells to cross the rigidity border to similar levels as control cells (C). Rho inhibition did not impair spreading on control substrates (D). Control cells treated with Rho inhibitor showed little change in behavior (E). Error bars represent S.E.M. \*\*\* $p < 0.001$ . # is significantly different from untreated condition  $p < 0.001$ .

#### 4.3.4 Role of contractility in the defect of rigidity sensing of FAK $-/-$ cells

Given the involvement of contractility and traction forces in rigidity sensing and in the retraction from a soft substrate<sup>19,31,32</sup>, we asked if modulation of traction forces played a role in the impaired rigidity sensing of FAK $-/-$  or Rho activated cells<sup>5</sup>. Traction stress for control cells increased ( $270.4 \pm 19.4$  Pa versus  $348.8 \pm 20.7$  Pa) with an increase of gel stiffness from approximately 1.8 to 3.5 kPa. In contrast, cells treated with FAK inhibitor showed no significant

difference in traction stress ( $399.2 \pm 53.3$  Pa versus  $392.2 \pm 26.8$  Pa) (Fig. 4.6A), which seems consistent with previous observations for FAK  $-/-$  cells<sup>5</sup>. Similarly, traction stress of cells on either gel stiffness treated with nocodazole showed a striking increase ( $718.4 \pm 144.8$  Pa and  $675.1 \pm 58.6$  Pa) but also failed to respond to substrate rigidity. Thus, the higher traction stress of FAK  $-/-$  cells and cells treated with nocodazole may be related to the activation of Rho, however, these cells lost their response to substrate rigidity.

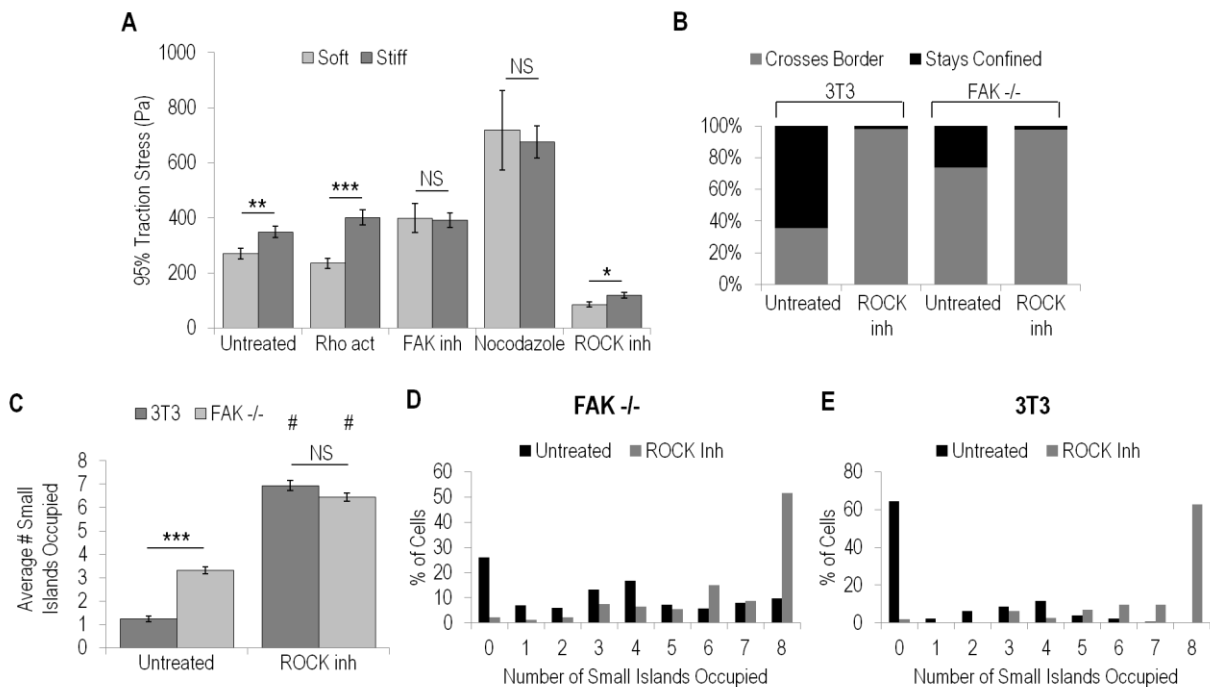


Figure 4.6. Traction stress regulation cannot fully account for rigidity sensing defect. Traction stress measurements show that untreated cells and cells treated with the Rho activator showed an increase in traction with increased gel stiffness (A, N=28, 30, 20, 20). In comparison, FAK  $-/-$  and nocodazole treated cells had similar levels regardless of gel stiffness, although at different values (A, N=20, 19, 9, 13), while inhibition of ROCK with 10  $\mu$ M Y27632 severely reduced traction output (A, N=20, 20). Treatment with Y27632 caused both control and FAK  $-/-$  cells to readily cross the rigidity border (B, N=209, 113, 315, 93) and occupy an increased number of small islands (C). Histograms of the distribution of small islands occupied show that a large number of cells are able to occupy the full patterned area (D and E). Error bars represent S.E.M. \* $p < 0.05$ , \*\* $p < 0.01$ , \*\*\* $p < 0.001$ . # is significantly different from untreated condition  $p < 0.001$ .

Interestingly, control cells treated with Rho activator CN03, in spite of their defect in rigidity response, maintained the response of traction stress to substrate rigidity ( $235.1 \pm 18.5$  Pa versus

401.6±27.9 Pa) (Fig. 4.6A), suggesting that differences in traction forces are not sufficient to drive rigidity sensing and that there is a mechanism to maintain low contractility on soft substrates that is insensitive to CN03. Conversely, inhibition of traction forces with ROCK inhibitor Y27632 suppressed traction stress output without rescuing the defect in rigidity sensing of FAK *-/-* cells (Fig. 4.6A far right graph, and B-D), similar to control cells treated with ROCK inhibitor (Fig. 4.6E). Together, these results suggest that while traction forces respond to substrate rigidity, the response is unable to explain rigidity-dependent spreading behavior or durotaxis.

#### **4.3.5 A role for Rho effector mDia1 in rigidity sensing**

We next investigate the possibility that spreading of FAK *-/-* cells over soft substrates was caused by an upregulation of mDia1, an effector of Rho that can mediate the assembly of actin filaments particularly in filopodia<sup>33,34</sup>. Treating FAK *-/-* cells with SMIFH2 to inhibit mDia1 reduced the number of cells that crossed into soft substrates (Fig. 4.7A and C), as well as the average number of small islands occupied to a level similar to control cells treated with SMIFH2 (Fig. 4.6B and D). Similar treatment did not impair the spreading of 3T3 or FAK *-/-* cells on control substrates (Fig. 4.7E). These results suggest that the regulation of mDia1 via FAK and Rho signaling is involved in probing substrate rigidity and modulating the cellular response to the resulting substrate strain.

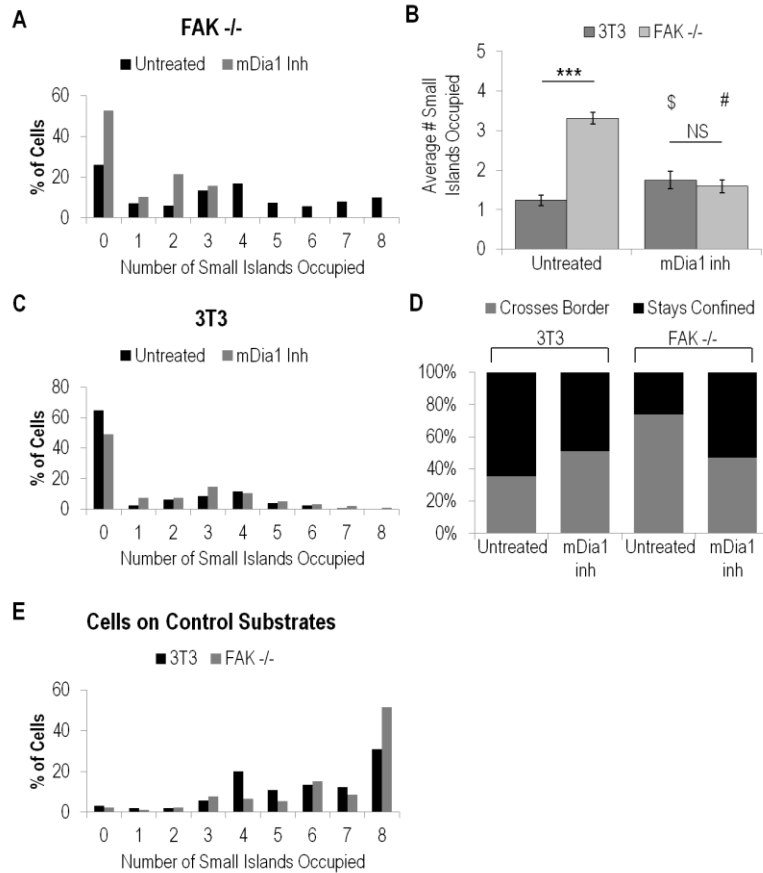


Figure 4.7. Rho downstream effector mDia1 not ROCK is involved in the FAK  $-/-$  rigidity sensing defect. Inhibiting formin mDia1 with 10  $\mu$ M SMIFH2 reduced the number of small islands occupied in FAK  $-/-$  cells (A, N=107) down to levels similar to control cells treated with SMIFH2 (B). There is a slight but significant increase in the number of small islands occupied by control 3T3 cells treated with SMIFH2 (C, N=96). SMIFH2 treatment also reduced the number of FAK  $-/-$  cells able to cross the rigidity border (D). Cells treated with SMIFH2 could still easily spread across control substrates (E, N=156, 93). Error bars represent S.E.M. \*\*\* $p < 0.001$ . # is significantly different from untreated condition  $p < 0.001$ . \$ is significantly different from untreated condition  $p < 0.05$ .

## 4.4 Discussion

Much attention has been focused on cellular behavior in response to mechanical properties of the extracellular environment including during durotaxis, the preferential migration of cells towards stiffer substrates. These studies are often hampered by the indirect inference that comes from the comparison of cells on separate substrates or the time-consuming search for cells that transiently cross a rigidity border. The present approach sought to address these limitations by using a cell-on-a-chip approach to trap cells at a simulated rigidity border for investigating probing and spreading dynamics. Although these cells were not migrating by a notable distance, we demonstrated that the approach can capture durotaxis behavior as reported previously with conventional approaches, thereby providing an efficient, and high-throughput method for investigating the underlying mechanisms. The average number and histogram of island occupancy on the soft domain, along with the percentage of cells that cross the simulated rigidity border, serve as key parameters for identifying and quantifying the defects in rigidity sensing

We found that FAK  $-/-$  cells ignored the rigidity border and crossed readily from stiff to soft domain, while cells re-expressing wild type FAK or NIH 3T3 cells remained on the stiff domain. In addition, experiments with FAK inhibition PF 573,233, which interacts with the ATP binding domain of FAK<sup>35</sup>, showed that tyrosine kinase activity of FAK is essential for rigidity sensing. However, although (auto)phosphorylation of FAK at Y397 is critical for the binding of various SH2-containing proteins<sup>7,36</sup>, phosphorylation at Y397 proved dispensable for the response to substrate rigidity as indicated by the restoration of rigidity sensing by the expression of Y397F-FAK in FAK  $-/-$  cells, suggesting the involvement of other proteins or sites of phosphorylation. Our results further implicates the requirement of sites regulating Rho activities, since pharmacological stimulation of Rho activities was sufficient to induce defects in rigidity sensing

of wild type cells. In addition, elevated Rho activity was reported in FAK<sup>-/-</sup> cells but not in cells re-expressing Y397F-FAK<sup>17</sup>. Other conditions that raise Rho activities, including the disassembly of microtubules upon nocodazole treatment, also induce similar defects in rigidity sensing as indicated by the histogram of spreading onto the soft domain (Fig. 4B).

From the results in Chapter 3, we expect that abnormal spreading onto soft substrates should involve a defect in the retraction of probing protrusions, which seems incompatible with the elevation in Rho activities and the resulting enhancement of traction forces in FAK<sup>-/-</sup> cells. In addition, defects in rigidity sensing were observed when control cells were treated with either a Rho activator CN03, or with Y27632 that causes inhibition of ROCK and traction forces<sup>37,38</sup>. Our measurements showed no simple relationship between rigidity sensing and either the magnitude of traction stress or the difference in traction stress on stiff versus soft substrates. Defects in rigidity sensing occurred under conditions of elevated (FAK knockout and treatment with CN03 or nocodazole) or suppressed (treatment with Y27632) traction forces, and under conditions that eliminate (FAK knockout and treatment with nocodazole) or maintain (treatment with CN03) the differential in traction stress on stiff versus soft substrates. In addition, treatment of FAK<sup>-/-</sup> cells with Y27632 to reverse the stimulation of ROCK due to upregulated Rho activity failed to rescue rigidity sensing and instead caused the cell to spread even more extensively across onto soft substrates.

Thus, given the convincing evidence for the requirement of Rho/ROCK mediated contractility in cellular responses to substrate rigidity<sup>39-42</sup>, the most plausible explanation of the present results is that additional pathways downstream of FAK and Rho may be involved in rigidity sensing. FAK<sup>-/-</sup> cells show impaired disassembly of focal adhesions, for example after induced substrate

strain<sup>5</sup>, which results in an increase in the size and stability of focal adhesions<sup>12,16</sup>. The formin/mDia1 pathway downstream of Rho may fulfill the role of rigidity sensing in conjunction with ROCK, by promoting actin assembly to promote the stability of filopodia and nascent focal adhesions. Supporting this idea, we found that the inhibition of mDia1 via SMIFH2 was able to partially reverse the defect in rigidity sensing of FAK <sup>-/-</sup> cells (Fig. 4.7). In addition, activation of mDia1 has been shown to be necessary and sufficient for external force-induced focal contact assembly<sup>43</sup>, and for bypassing the integrin-FAK/Rho signaling pathway for microtubule stabilization<sup>18</sup>. Loss of FAK, and the resulting elevation of Rho activities, may therefore short-circuit proper feedback mechanism for rigidity sensing and prevent retraction on soft substrates.

The present study may be relevant to the understanding of cancer metastasis, since many tumor cells have been shown to display elevated Rho activities<sup>3,44,45</sup>, which may in turn lead to aberrant rigidity sensing and durotaxis to impair the maintenance of transformed cells within home tissues. While FAK or ROCK has been suggested as possible therapeutic targets for controlling cancer proliferation and metastasis<sup>46,47</sup>, our results suggest that selective suppression of FAK or ROCK inhibition could introduce unexpected effects possibly to aggravate the defect in rigidity sensing. Effective therapies of cancer metastasis likely require a comprehensive understanding of the entire control circuit of rigidity sensing, much above the understanding of the functions of single proteins.

## 4.5 References

1. Lo, C. M., Wang, H., Dembo, M. & Wang, Y.-L. Cell movement is guided by the rigidity of the substrate. *Biophys. J.* **79**, 144–52 (2000).
2. Levy-Mishali, M., Zoldan, J. & Levenberg, S. Effect of scaffold stiffness on myoblast differentiation. *Tissue Eng. Part A* **15**, 935–44 (2009).
3. Paszek, M. J. *et al.* Tensional homeostasis and the malignant phenotype. *Cancer Cell* **8**, 241–54 (2005).
4. Tilghman, R. W. *et al.* Matrix rigidity regulates cancer cell growth and cellular phenotype. *PLoS One* **5**, e12905 (2010).
5. Wang, H., Dembo, M., Hanks, S. K. & Wang, Y. Focal adhesion kinase is involved in mechanosensing during fibroblast migration. *Proc. Natl. Acad. Sci.* **98**, 11295–300 (2001).
6. Raab, M. *et al.* Crawling from soft to stiff matrix polarizes the cytoskeleton and phosphoregulates myosin-II heavy chain. *J. Cell Biol.* **199**, 669–83 (2012).
7. Mitra, S. K., Hanson, D. a & Schlaepfer, D. D. Focal adhesion kinase: in command and control of cell motility. *Nat. Rev. Mol. Cell Biol.* **6**, 56–68 (2005).
8. Schaller, M. D. Biochemical signals and biological responses elicited by the focal adhesion kinase. *Biochim. Biophys. Acta* **1540**, 1–21 (2001).
9. Schlaepfer, D. D., Hauck, C. R. & Sieg, D. J. Signaling through focal adhesion kinase. *Prog Biophys Mol Biol* **71**, 435–478 (1999).
10. Cary, L. a, Chang, J. F. & Guan, J. L. Stimulation of cell migration by overexpression of focal adhesion kinase and its association with Src and Fyn. *J. Cell Sci.* **109** ( Pt 7, 1787–94 (1996).
11. Abbi, S. & Guan, J. L. Focal adhesion kinase : Protein interactions and cellular functions. *Histol Histopathol* **17**, 1163–1171 (2002).
12. Webb, D. J. *et al.* FAK–Src signalling through paxillin, ERK and MLCK regulates adhesion disassembly. *Nat. Cell Biol.* **6**, 154–161 (2004).
13. Ren, X. D. *et al.* Focal adhesion kinase suppresses Rho activity to promote focal adhesion turnover. *J. Cell Sci.* **113** ( Pt 2, 3673–8 (2000).
14. Ezratty, E. J., Partridge, M. a & Gundersen, G. G. Microtubule-induced focal adhesion disassembly is mediated by dynamin and focal adhesion kinase. *Nat. Cell Biol.* **7**, 581–90 (2005).
15. Iwanicki, M. P. *et al.* FAK, PDZ-RhoGEF and ROCKII cooperate to regulate adhesion movement and trailing-edge retraction in fibroblasts. *J. Cell Sci.* **121**, 895–905 (2008).
16. Ilić, D. *et al.* Reduced cell motility and enhanced focal adhesion contact formation in cells from FAK-deficient mice. *Nature* **377**, 539–44 (1995).
17. Pirone, D. M. *et al.* An inhibitory role for FAK in regulating proliferation: a link between limited adhesion and RhoA-ROCK signaling. *J. Cell Biol.* **174**, 277–88 (2006).
18. Palazzo, A. F., Eng, C. H., Schlaepfer, D. D., Marcantonio, E. E. & Gundersen, G. G. Localized stabilization of microtubules by integrin- and FAK-facilitated Rho signaling. *Science* **303**, 836–9 (2004).
19. Wong, S., Guo, W.-H. & Wang, Y.-L. Fibroblasts probe substrate rigidity with filopodia extensions before occupying an area. *Proc. Natl. Acad. Sci.* **111**, 1–6 (2014).
20. Hoffecker, I. T., Guo, W. & Wang, Y. Assessing the spatial resolution of cellular rigidity sensing using a micropatterned hydrogel-photoresist composite. *Lab Chip* **11**, 3538–44 (2011).

21. Wong, S., Guo, W., Hoffecker, I. T. & Wang, Y. in *Methods Cell Biol.* (2014).
22. Stroka, K. M. & Aranda-Espinoza, H. Neutrophils display biphasic relationship between migration and substrate stiffness. *Cell Motil. Cytoskeleton* **66**, 328–41 (2009).
23. Flanagan, L. A., Ju, Y., Marg, B., Osterfield, M. & Paul, A. Neurite branching on deformable substrates. *Neuroreport* **13**, 2411–2415 (2002).
24. Rape, A. D., Guo, W.-H. & Wang, Y.-L. The regulation of traction force in relation to cell shape and focal adhesions. *Biomaterials* **32**, 2043–51 (2011).
25. Chowdhury, F. *et al.* Material properties of the cell dictate stress-induced spreading and differentiation in embryonic stem cells. *Nat. Mater.* **9**, 82–8 (2010).
26. Tse, J. R. & Engler, A. J. Preparation of hydrogel substrates with tunable mechanical properties. *Curr. Protoc. Cell Biol.* **Chapter 10**, Unit 10.16 (2010).
27. Owen, J. D., Ruest, P. J., Fry, D. W. & Hanks, S. K. Induced focal adhesion kinase (FAK) expression in FAK-null cells enhances cell spreading and migration requiring both auto- and activation loop phosphorylation sites and inhibits adhesion-dependent tyrosine phosphorylation of Pyk2. *Mol. Cell. Biol.* **19**, 4806–4818 (1999).
28. Owen, K. a. *et al.* Regulation of lamellipodial persistence, adhesion turnover, and motility in macrophages by focal adhesion kinase. *J. Cell Biol.* **179**, 1275–1287 (2007).
29. Liu, B. P., Chrzanoska-Wodnicka, M. & Burridge, K. Microtubule depolymerization induces stress fibers, focal adhesions, and DNA synthesis via the GTP-binding protein Rho. *Cell Adhes. Commun.* **5**, 249–55 (1998).
30. Heck, J. N. *et al.* Microtubules regulate GEF-H1 in response to extracellular matrix stiffness. *Mol. Biol. Cell* **23**, 2583–2592 (2012).
31. Wolfenson, H. *et al.* Tropomyosin controls sarcomere-like contractions for rigidity sensing and suppressing growth on soft matrices. *Nat. Cell Biol.* **18**, 33–42 (2015).
32. Vicente-Manzanares, M. Cell migration: cooperation between myosin II isoforms in durotaxis. *Curr. Biol.* **23**, R28–9 (2013).
33. Mellor, H. The role of formins in filopodia formation. *Biochim. Biophys. Acta* **1803**, 191–200 (2010).
34. Sarmiento, C. *et al.* WASP family members and formin proteins coordinate regulation of cell protrusions in carcinoma cells. *J. Cell Biol.* **180**, 1245–1260 (2008).
35. Slack-Davis, J. K. *et al.* Cellular characterization of a novel focal adhesion kinase inhibitor. *J. Biol. Chem.* **282**, 14845–52 (2007).
36. Hamadi, A. *et al.* Regulation of focal adhesion dynamics and disassembly by phosphorylation of FAK at tyrosine 397. *J. Cell Sci.* **118**, 4415–25 (2005).
37. Sinnott-Smith, J., Lunn, J. a, Leopoldt, D. & Rozengurt, E. Y-27632, an inhibitor of Rho-associated kinases, prevents tyrosine phosphorylation of focal adhesion kinase and paxillin induced by bombesin: dissociation from tyrosine phosphorylation of p130(CAS). *Exp. Cell Res.* **266**, 292–302 (2001).
38. Beningo, K. a, Hamao, K., Dembo, M., Wang, Y.-L. & Hosoya, H. Traction forces of fibroblasts are regulated by the Rho-dependent kinase but not by the myosin light chain kinase. *Arch. Biochem. Biophys.* **456**, 224–31 (2006).
39. McBeath, R., Pirone, D. M., Nelson, C. M., Bhadriraju, K. & Chen, C. S. Cell shape, cytoskeletal tension, and RhoA regulate stem cell lineage commitment. *Dev. Cell* **6**, 483–95 (2004).
40. Plotnikov, S. V, Pasapera, A. M., Sabass, B. & Waterman, C. M. Force Fluctuations within Focal Adhesions Mediate ECM-Rigidity Sensing to Guide Directed Cell Migration.

- Cell* **151**, 1513–27 (2012).
41. Hoj, J. P. *et al.* Cellular contractility changes are sufficient to drive epithelial scattering. *Exp. Cell Res.* **326**, 187–200 (2014).
  42. McGrail, D. J., Kieu, Q. M. N. & Dawson, M. R. The malignancy of metastatic ovarian cancer cells is increased on soft matrices through a mechanosensitive Rho-ROCK pathway. *J. Cell Sci.* **127**, 2621–6 (2014).
  43. Rivelino, D. *et al.* Focal contacts as mechanosensors: externally applied local mechanical force induces growth of focal contacts by an mDia1-dependent and ROCK-independent mechanism. *J. Cell Biol.* **153**, 1175–86 (2001).
  44. Khalil, B. D. & El-Sibai, M. Rho GTPases in primary brain tumor malignancy and invasion. *J. Neurooncol.* **108**, 333–9 (2012).
  45. Fritz, G., Just, I. & Kaina, B. Rho GTPases are over-expressed in human tumors. *Int. J. Cancer* **81**, 682–687 (1999).
  46. McLean, G. W., Avizientyle, E. & Frame, M. C. Focal adhesion kinase as a potential target in oncology. *Expert Opin. Pharmacother.* **4**, 227–234 (2005).
  47. Rath, N. & Olson, M. F. Rho-associated kinases in tumorigenesis: re-considering ROCK inhibition for cancer therapy. *EMBO Rep.* **13**, 900–8 (2012).

## Chapter 5

# Migration State Regulates Traction Force through Mechanical Crosstalk between Newly Formed and Existing Adhesions

Adherent cells are keenly sensitive to external and internal physical states, such as substrate rigidity and topography, and cell shape and spreading area. Many of these responses are believed to involve coupled input and output of mechanical signals for probing and sensing, which then regulate downstream functions such as cell growth and differentiation. We demonstrated previously that compared to migrating cells, stationary cells generate stronger, less dynamic, and more peripherally localized traction forces. We find here that this response is not due to cell size or aspect ratio but is controlled by migration state. Using cells migrating along a strip of checkerboard micropattern, we show that the appearance of frontal traction forces and focal adhesions promotes the down-regulation of pre-existing traction forces and focal adhesions that lag behind. Our results suggest that migration state of a cell can influence the output/input of cellular mechanical activities, and that continuous protrusion and formation of focal adhesion directly in front of existing adhesions prevent traction force build up in migrating cells.

## 5.1 Introduction

Adherent cells are known to be sensitive to not only chemical signals but also mechanical parameters of their environment. Differentiation can be influenced by alteration of the mechanical or physical parameters of the cell environment<sup>1-4</sup>. A variety of conditions, including culture on stiff substrates or micropatterning to increase cell spread area, aspect ratio, or concavity, have all been shown to favor osteogenic differentiation, while opposite conditions favor neurogenic or adipogenic differentiation. Conditions that favor osteogenic differentiation are also associated with elevated traction force generation and conditions that favor adipogenic or neurogenic differentiation are associated with decreased traction force generation<sup>5</sup>.

Myosin II dependent traction forces are commonly thought to be generated for driving cell migration<sup>6,7</sup>, however, recent studies have indicated that traction forces may be important for probing the external or internal physical state to regulate cellular functions<sup>8-15</sup>, where the readout may involve responses to the deformation of the substrate and/or to intracellular tension caused by actomyosin contractility<sup>11,16,17</sup>. Supporting this idea, previous studies have shown that cellular contractility and traction force output are involved in directing stem cell differentiation<sup>1</sup>. In addition, defective regulation of traction forces and cellular contractility has been implicated in the metastatic potential of cancer cells. Increases in traction forces correlate with increased metastatic potential in many cancer models<sup>18</sup>, while Ras-oncogene transformed fibroblasts display disorganized traction force generation<sup>19</sup>. Measurement of traction forces and traction force distribution may thus serve as a method for identifying conditions that affect cell growth and function.

Recent studies have shown that NIH 3T3 cells exert approximately two-fold stronger traction stresses when confined to 50x50  $\mu\text{m}$  islands, where strong traction forces were localized in peripheral regions of limited dynamics, compared with cells migrating on unpatterned substrates or along lines<sup>20</sup>. Since a similar increase in traction forces took place when cell migration stopped at the end of a patterned line, the increase upon confinement was not an artifact of micropatterning. In addition, traction force generation correlated negatively with migration speed.

Traction forces are generated by actomyosin contractility transmitted to the underlying substrate via integrin engagement at focal adhesions<sup>21-23</sup>. A comparison of focal adhesion dynamics revealed that stationary cells exhibited much larger focal adhesions that persisted for extended periods of time particularly at the corners, compared to focal adhesions in migrating cells<sup>20,24</sup>. In this study, we show that the dependence of traction forces on migration state is unrelated to common parameters such as cell size or spreading area. Using a novel checkerboard pattern, we show that the appearance of new focal adhesions and traction forces directly in front of existing adhesions may serve to down-regulate pre-existing traction force. The response may be explained by mechanical cross-talk between newly formed and pre-existing focal adhesions.

## 5.2 Experimental Methods

### 5.2.1 Substrate preparation

Micropatterned polyacrylamide hydrogels were prepared as described previously<sup>13</sup>. Briefly, a PDMS stamp was incubated for 45 minutes with a 0.1% (w/v) gelatin solution that had been activated with 3.5 mg/mL sodium periodate (Sigma). The stamp was dried under a stream of N<sub>2</sub> gas then lightly pressed onto a small glass coverslip.

To prepare polyacrylamide substrates, a freshly prepared solution of 5% acrylamide and 0.1% bis-acrylamide (Bio-Rad) was degassed and 0.2 μm fluorescent beads (Molecular Probes) were added at a 1:2000 dilution if the substrate was to be used for traction force microscopy. After addition of 6 μL of 1% (w/v) ammonium persulfate (Sigma) and 4 μL of N,N,N',N'-tetramethylethane-1,2-diamine (EMD Millipore), a 30 μL drop was pipetted onto a large coverslip pre-treated with Bind-Silane to allow bonding of polyacrylamide (GE Healthcare). The small stamped coverslip was immediately placed pattern-side down onto the acrylamide drop. After the completion of polymerization, the top coverslip was carefully removed with a razor blade and a pair of tweezers. Micropatterned polyacrylamide hydrogel substrates were then mounted into chamber dishes, sterilized under ultraviolet light for 30 minutes, and incubated in cell culture media for 1 hour at 37°C before use. The final gel had an estimated Young's modulus of 3.5 kPa<sup>25</sup>.

A teardrop-shaped island pattern served as a control to provide the same adhesive area as the average spreading area on unpatterned surfaces, while forcing a shape similar to that of typical migrating cells. Checkerboard patterns were designed as shown in Figure 5.3A, with alternating 4x16 μm adhesive and non-adhesive areas flanked by a 2 μm-wide adhesive border.

### **5.2.2 Cell culture**

NIH 3T3 cells (ATCC) were cultured in Dulbecco's modified Eagle's medium (Life Technologies) supplemented with 10% donor adult bovine serum (Thermo Scientific), 2 mM L-glutamine, 50 µg/mL streptomycin, and 50 U/mL penicillin (Life Technologies), and were maintained under 5% CO<sub>2</sub> at 37°C.

### **5.2.3 Traction force microscopy**

Phase contrast images of single cells on a uniformly-coated polyacrylamide gel or spread across a micropatterned island were collected with a Nikon Eclipse Ti microscope using a 40X 0.75 N.A. PlanFluor dry objective (Nikon) and an Andor iXon CCD camera and custom software. Fluorescence images of the embedded beads near the surface of the hydrogel were taken before and after cells were removed with 0.05% Trypsin-EDTA (Life Technologies). For time-lapse recordings, paired phase-contrast images of the cell and fluorescence images of the underlying beads were collected every 10 minutes for 4 hours. For high resolution tracking of substrate strain, phase contrast images of the cell and corresponding fluorescence images of underlying beads were collected using a 100X 1.3 N.A. Plan Fluor oil immersion objective (Nikon) at a frequency of 4 minutes for up to 2 hours. Cell outlines were manually drawn, and bead displacement fields were computed using custom software. Color heat maps of traction force-induced strains were generated using MATLAB (MathWorks, Natick, MA). Plots of substrate displacement were generated in regions visually identified as generating strong substrate displacements. The displacements were normalized to a range of 0-1 then averaged within local regions to generate the plots shown in Figure 5.4E and F. Traction stress and strain energy were computed using LIBTRC software package provided by Prof. Micah Dembo, Boston University.

Mechanical output under different conditions was compared based on 95% traction stress, which was concentrated at cell periphery, while the stress detected under the remainder of the cell represented predominantly noise.

## 5.3 Results

### 5.3.1 The difference in traction force between stationary and migrating cells cannot be explained by cell spreading area or aspect ratio

Previous work showed that NIH 3T3 cells exerted a 95% traction stress of  $356 \pm 25.6$  Pa and  $370 \pm 22.4$  Pa respectively when spread on an unpatterned surface and migrating along micropatterned strips. In contrast, on surfaces micropatterned as  $50 \times 50$   $\mu\text{m}$  square islands to inhibit cell migration, NIH 3T3 cells exerted a 95% traction stress of  $718 \pm 124$  Pa<sup>20</sup>. Since traction stress is known to be sensitive to spreading size and aspect ratio<sup>13</sup>, we compared cell area and aspect ratio of stationary and migrating cells. Interestingly, unconfined cells often spread over a larger area and showed a higher aspect ratio than cells confined to  $50 \times 50$   $\mu\text{m}$  islands (Fig. 5.1A and B), contrary to what one may expect based on the two-fold higher traction stress of confined cells than unconfined cells.

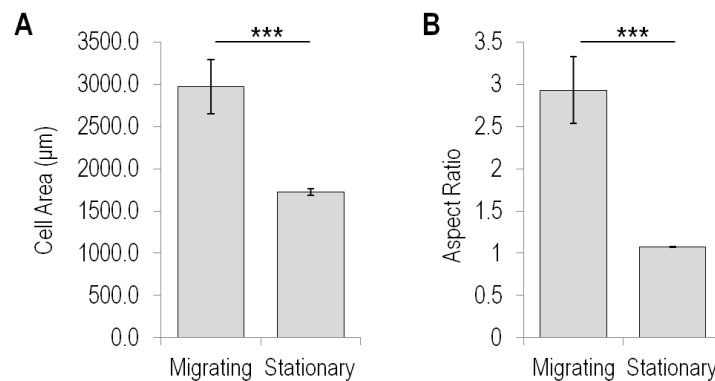


Figure 5.1. Spreading area and aspect ratio cannot account for traction force difference between migrating and stationary cells. Higher average cell spreading area (A, N=17, 15) and aspect ratio (B, N=22, 47) in migrating than in stationary cells. \*\*\* $p < 0.001$ . Error bars represent S.E.M.

Calculation of total strain energy further indicated that while cell area and total strain energy were positively correlated on unpatterned surfaces, consistent with what has been previously reported<sup>26</sup>, cells on micropatterned islands generated a wide range of strain energy at a constant

spreading area (Fig. 5.2A), with a significantly higher average strain energy than that for unconfined cells of a similar size (Fig. 5.2B). This suggests that migration state can regulate traction force generation independently of cell shape or spreading area.

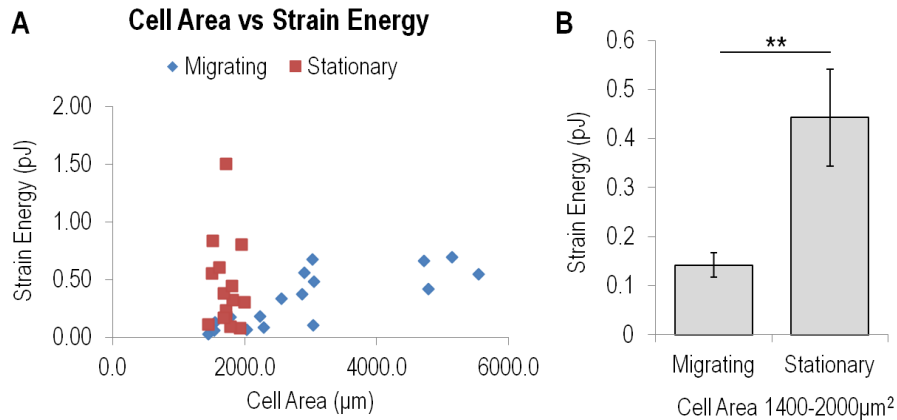


Figure 5.2. Strain energy generation differs between migrating and stationary cells. Total strain energy as a function of spreading area for migrating and stationary cells (A, N=17, 15). Average total strain energy for migrating and stationary cells with an area of 1400-2000  $\mu\text{m}^2$  (B, N= 12, 15). \*\* $p < 0.01$ . Error bars represent S.E.M.

### 5.3.2 Mechanical output at existing focal adhesions is regulated by the formation of new focal adhesions

We postulated that the difference in mechanical output between stationary and migrating cells may be due to the continuous protrusion and focal adhesion formation in front of pre-existing, mature focal adhesions in migrating cells, which may then cause a reduction in traction forces at mature adhesions. To test this hypothesis, we designed a checkerboard micropattern where the leading edge may extend away from existing focal adhesions for a distance of up to 16  $\mu\text{m}$  without forming new focal adhesions directly in front of existing adhesions (Fig. 5.3A). Cell shape and spreading were not significantly influenced by the checkerboard patterning (Fig. 5.3B and C).

Traction force microscopy indicated that cells on the checkerboard exerted 21% higher traction stress than cells migrating on lines or unpatterned substrates (Figure 5.3D). Cells migrated at a similar speed along checkerboard and continuous strips (Fig. 5.3E), ruling out the possibility that the difference in traction stress was due to differences in migration speed, which was shown previously to influence traction force output<sup>20</sup>.

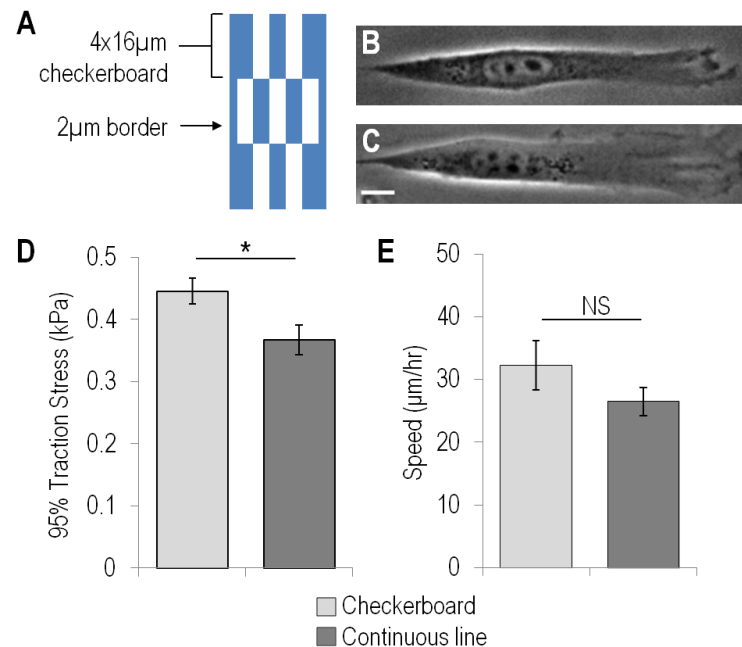


Figure 5.3. NIH 3T3 cells migrating along a checkerboard pattern generate a stronger traction stress than cells migrating along a continuous strips. The checkerboard pattern consists of alternating 4x16 μm rectangular adhesive areas flanked by continuous adhesive lines 2 μm in width (A, adhesive areas in blue). Representative images of cells migrating along continuous lines (B) or checkerboard patterned lines (C) show indistinguishable shape and size. Cells exert higher 95% traction stress on checkerboard patterns than cells on continuous strips (D, N=28, 20). Migration speed is also similar on checkerboard and continuous strips (E, N=16, 22). Scale bar 10 μm. Error bars represent S.E.M. \*p<.05.

To understand how the inability to form new adhesions on non-adhesive areas affect existing focal adhesions behind, time lapse recording at a high magnification was used to map substrate displacement relative to the leading edge. NIH 3T3 cells migrating on continuous strips showed maximal substrate displacements on average 7.9 μm behind the leading edge, which moved forward as the leading edge advanced. On checkerboard patterns, this distance was increased to

an average of  $13.6 \mu\text{m}$  (Fig. 5.4C). Displacements also reached a higher maximum on checkerboard substrates,  $4.02 \pm 0.98 \mu\text{m}$  versus  $2.32 \pm 0.029 \mu\text{m}$  on continuous strips, and persisted

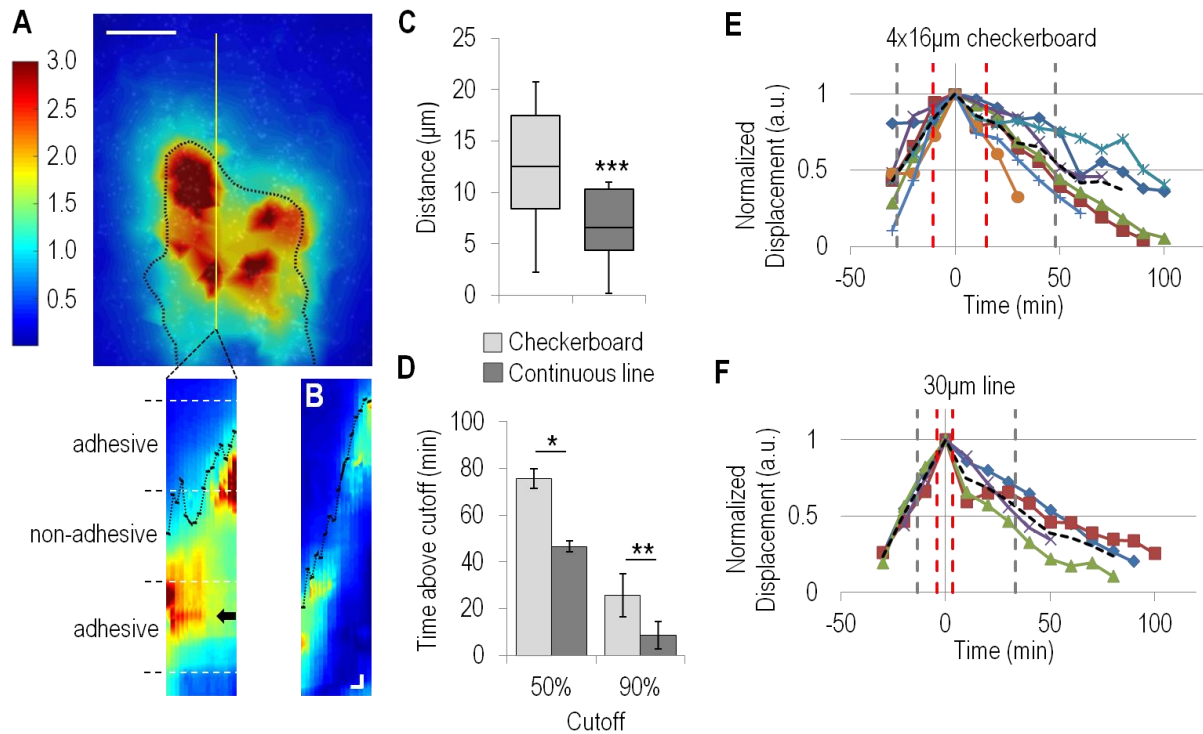


Figure 5.4. Formation of new adhesions at the front promotes the decrease of traction forces behind. Heat maps depict substrate displacements caused by cells migrating along a strip with checkerboard pattern (A). Dotted black line represents cell outline. Yellow line indicates the region of interest for generating kymographs as the cell migrates across alternating adhesive and non-adhesive regions (lower left panel). Black arrow on the kymograph indicates where substrate displacement persists while the leading edge migrates across a non-adhesive region (A, lower panel). For cells migrating along continuous adhesive strips  $30 \mu\text{m}$  in width, substrate displacement is more transient as indicated by the shorter duration of displacement on the kymograph (B, plotted using the same color scale as A). Duration of kymograph, 1 hour. The point of maximum substrate displacement is also further behind the leading edge on checkerboard than on continuous strips (C,  $N=131, 72$ ). In addition, the duration when the displacement stays above 50% or 90% of the maximum is longer for cells migrating along checkerboard strips than along continuous strips (D,  $N=14, 15$ ). Kinetics of substrate displacement at fixed sites with strong displacement show consistently a longer duration for cells migrating along checkerboard (E) than those on continuous strips (F). Red dotted lines denote the time when the displacement stays above 90% of the maximum, while black dotted lines denote the time when the displacement stays above 50% of the maximum. Scale bar,  $10 \mu\text{m}$ . Kymograph scale: vertical  $2 \mu\text{m}$ , horizontal 10 minutes. Error bars represent S.E.M. \* $p < .05$ , \*\* $p < .01$ , \*\*\* $p < .001$ .

longer when the leading edge migrated across a non-adhesive region than along continuous strips (Fig. 5.4A and B). The slower decay of substrate displacement was also evident from the

kinetics; cells on the checkerboard pattern maintained higher substrate strain, measured as a percentage of the maximum strain, for a longer duration compared to cells on continuous lines taking 25.7 minutes vs. 7.3 minutes respectively, to fall below 90% of the maximum (Fig. 5.4D-F). Taken together these observations support the notion that mechanical crosstalk between new and pre-existing focal adhesions limits the development of traction forces in migrating cells.

## 5.4 Discussion

Using micropatterning of elastic polyacrylamide hydrogels to simultaneously control cell migration and measure traction force generation, we found that the previously observed dependence of traction forces on migration state cannot be explained by differences in cell spread area or aspect ratio, as cells confined to 50x50  $\mu\text{m}$  squares exhibited stronger traction forces and strain energies at smaller spreading areas and aspect ratios. These observations support the idea that migration state may serve as an even stronger regulatory parameter for the output of traction forces.

To explain the stronger traction stress underneath nascent focal adhesions than mature focal adhesions<sup>21,27</sup>, previous speculations have leaned toward an age-based mechanism, where focal adhesions lose their mechanical activities as they “mature” over time<sup>28</sup>. Our observations instead suggest a position-based mechanism, where traction forces build up within a narrow active zone near the leading edge, then drop as soon as new nascent focal adhesions form at the leading edge in front. This process is inhibited in stationary cells, as a result traction forces reach a high level because focal adhesions remain trapped within the active zone. Cell migration causes focal adhesions to traverse through the active zone, such that traction forces are allowed to build up for only a finite period of time. This explains why peak traction force increases with decreasing speed, due to the increased time that focal adhesions stay in the active zone.

What might be responsible for the creation of an active zone for traction force to build up? Since focal adhesions are responsive to mechanical forces<sup>29</sup>, one appealing possibility is that traction forces generated by nascent focal adhesions at the leading edge may affect mature focal adhesions that fall behind. Such rearward forces exerted on the substrate at the very front would

generate forward-pointing counter forces to pull the rest of the cell forward. These counter forces generated at the leading edge may cancel out rear-pointing contractile forces on the focal adhesions further back in the lamellipodia.

The above explanation is supported by results from high resolution imaging of substrate displacement in cells migrating along continuous or checkerboard strips. On continuous strips, the point of maximal substrate displacement moved forward in a wave-like fashion with the advancing leading edge, reflecting a continual transfer of traction force to newer adhesions during migration. In contrast, in cells migrating along checkerboard strips, inhibition of focal adhesion formation on non-adhesive areas caused regions of maximal displacement directly behind to stay put, which was accompanied by an increase in substrate displacement. Maximal substrate displacement also persisted for a longer duration while becoming further separated from the leading edge. This enhancement of traction forces may in turn cause altered mechanotransduction signaling.

In summary, we provide evidence for a mechanism by which migration state and speed may modulate traction force output. This may in turn regulate intracellular chemical activities through mechanosensitive pathways. As cell size and shape have been shown to play a pivotal role in regulating stem cell differentiation and gene expression<sup>4,5,30,31</sup>, we suspect that the state of migration may play a similarly important role. For example, during tissue formation, it may make sense to suppress differentiation and expression of certain genes while a cell is migrating, which is lifted only when the cell has arrived at the destination and is ready to perform physiological functions. Likewise, defects in migration sensing may cause cancer cells to lose control over their growth activities, gene expression, and differentiation state.

## 5.5 References

1. Engler, A. J., Sen, S., Sweeney, H. L. & Discher, D. E. Matrix elasticity directs stem cell lineage specification. *Cell* **126**, 677–89 (2006).
2. Zouani, O. F. *et al.* Altered nanofeature size dictates stem cell differentiation. *J. Cell Sci.* **125**, 1217–1224 (2012).
3. Dalby, M. J. *et al.* The control of human mesenchymal cell differentiation using nanoscale symmetry and disorder. *Nat. Mater.* **6**, 407–413 (2007).
4. Kilian, K. a, Bugarija, B., Lahn, B. T. & Mrksich, M. Geometric cues for directing the differentiation of mesenchymal stem cells. *Proc. Natl. Acad. Sci.* **107**, 4872–7 (2010).
5. McBeath, R., Pirone, D. M., Nelson, C. M., Bhadriraju, K. & Chen, C. S. Cell shape, cytoskeletal tension, and RhoA regulate stem cell lineage commitment. *Dev. Cell* **6**, 483–95 (2004).
6. Dembo, M. & Wang, Y.-L. Stresses at the cell-to-substrate interface during locomotion of fibroblasts. *Biophys. J.* **76**, 2307–2316 (1999).
7. Morin, T. R., Ghassem-Zadeh, S. a. & Lee, J. Traction force microscopy in rapidly moving cells reveals separate roles for ROCK and MLCK in the mechanics of retraction. *Exp. Cell Res.* **326**, 280–294 (2014).
8. Prager-Khoutorsky, M. *et al.* Fibroblast polarization is a matrix-rigidity-dependent process controlled by focal adhesion mechanosensing. *Nat. Cell Biol.* **13**, 1457–65 (2011).
9. Discher, D. E., Janmey, P. & Wang, Y.-L. Tissue cells feel and respond to the stiffness of their substrate. *Science* **310**, 1139–43 (2005).
10. Lo, C. M., Wang, H., Dembo, M. & Wang, Y.-L. Cell movement is guided by the rigidity of the substrate. *Biophys. J.* **79**, 144–52 (2000).
11. Trichet, L. *et al.* Evidence of a large-scale mechanosensing mechanism for cellular adaptation to substrate stiffness. *Proc. Natl. Acad. Sci.* **109**, 6933–8 (2012).
12. Wang, N., Ostuni, E., Whitesides, G. M. & Ingber, D. E. Micropatterning tractional forces in living cells. *Cell Motil. Cytoskeleton* **52**, 97–106 (2002).
13. Rape, A. D., Guo, W.-H. & Wang, Y.-L. The regulation of traction force in relation to cell shape and focal adhesions. *Biomaterials* **32**, 2043–51 (2011).
14. Chang, S. S., Guo, W., Kim, Y. & Wang, Y. Guidance of cell migration by substrate dimension. *Biophys. J.* **104**, 313–21 (2013).
15. Baker, B. M. & Chen, C. S. Deconstructing the third dimension: how 3D culture microenvironments alter cellular cues. *J. Cell Sci.* **125**, 3015–24 (2012).
16. Vogel, V. & Sheetz, M. Local force and geometry sensing regulate cell functions. *Nat. Rev. Mol. Cell Biol.* **7**, 265–75 (2006).
17. Rape, A. D., Guo, W. & Wang, Y. in *Mechanobiol. Cell-Cell Cell-Matrix Interact.* (Wagoner Johnson, A. & Harley, B. A. C.) 1–10 (Springer US, 2011). doi:10.1007/978-1-4419-8083-0
18. Indra, I. *et al.* An in vitro correlation of mechanical forces and metastatic capacity. *Phys. Biol.* **8**, 015015 (2011).
19. Munevar, S., Wang, Y.-L. & Dembo, M. Traction Force Microscopy of Migrating Normal and H-ras Transformed 3T3 Fibroblasts. *Biophys. J.* **80**, 1744–1757 (2001).
20. Chang, S. S. Mechanosensing of Substrate Dimension and Migration State in Adherent Cells. (2015).
21. Beningo, K. A., Dembo, M., Kaverina, I., Small, J. V. & Wang, Y. Nascent focal

- adhesions are responsible for the generation of strong propulsive forces in migrating fibroblasts. *J. Cell Biol.* **153**, 881–8 (2001).
22. Geiger, B., Spatz, J. P. & Bershadsky, A. D. Environmental sensing through focal adhesions. *Nat. Rev. Mol. Cell Biol.* **10**, 21–33 (2009).
  23. Vicente-Manzanares, M., Ma, X., Adelstein, R. S. R. S. & Horwitz, a. R. A. R. Non-muscle myosin II takes centre stage in cell adhesion and migration. *Nat. Rev. Mol. Cell Biol.* **10**, 778–790 (2009).
  24. Parker, K. K. *et al.* Directional control of lamellipodia extension by constraining cell shape and orienting cell tractional forces. *FASEB J.* **16**, 1195–204 (2002).
  25. Tse, J. R. & Engler, A. J. Preparation of hydrogel substrates with tunable mechanical properties. *Curr. Protoc. Cell Biol.* **Chapter 10**, Unit 10.16 (2010).
  26. Oakes, P. W., Banerjee, S., Marchetti, M. C. & Gardel, M. L. Geometry Regulates Traction Stresses in Adherent Cells. *Biophys. J.* **107**, 825–833 (2014).
  27. Stricker, J., Aratyn-Schaus, Y., Oakes, P. W. & Gardel, M. L. Spatiotemporal constraints on the force-dependent growth of focal adhesions. *Biophys. J.* **100**, 2883–2893 (2011).
  28. Zaidel-Bar, R., Cohen, M., Addadi, L. & Geiger, B. Hierarchical assembly of cell-matrix adhesion complexes. *Biochem. Soc. Trans.* **32**, 416–420 (2004).
  29. Galbraith, C. G., Yamada, K. M. & Sheetz, M. P. The relationship between force and focal complex development. *J. Cell Biol.* **159**, 695–705 (2002).
  30. Leight, J. L., Wozniak, M. a, Chen, S., Lynch, M. L. & Chen, C. S. Matrix rigidity regulates a switch between TGF- $\beta$ 1-induced apoptosis and epithelial-mesenchymal transition. *Mol. Biol. Cell* **23**, 781–91 (2012).
  31. Cao, B., Peng, R., Li, Z. & Ding, J. Effects of spreading areas and aspect ratios of single cells on dedifferentiation of chondrocytes. *Biomaterials* **35**, 6871–6881 (2014).

## Chapter 6

# Conclusions and Future Directions

## **6.1 Conclusions**

### **6.1.1 Creation and testing of a model system for studying durotaxis**

A major challenge in the study of durotaxis is difficulties in locating a sufficient number of cells interacting with a rigidity border. Such inefficiency in current experimental systems has limited the potential for effective testing of molecular pathways involved in durotaxis. In Chapter 2, I present an optimized method for fabricating a composite substrate to investigate durotaxis. The composite system is designed with areas of micropatterned rigidity to trap single cells at or near a rigidity border. This cell-on-a-chip approach can be used for high throughput analysis of conditions that affect rigidity sensing and durotaxis. These composite substrates allow a unique approach for the dissection of molecular mechanisms underlying cellular sensing and response at a rigidity border.

### **6.1.2 Cells use filopodia protrusions to test substrate rigidity in front of the leading edge**

In Chapter 3, I show that fibroblasts extend filopodia protrusions to test substrate rigidity in front of the leading edge before the extension of lamellipodia to occupy the area. This mechanism allows cells to migrate efficiently by avoiding the backtracking from mechanically unfavorable areas. The use of filopodia in probing mechanical properties of the extracellular environment is consistent with earlier reports of filopodia exerting forces on the substrate to deflect embedded fluorescent beads<sup>1</sup>. This type of a mechanism may be universally applicable as cells in 3D can easily form filopodia or other fine extensions during migration even though they are unable to form broad lamellipodia<sup>2</sup>. Through use of these composite substrates I am able to easily investigate mechanisms of rigidity sensing that may otherwise be difficult to detect. I found that

probing force generated by myosin II contractility is an essential component of the rigidity sensing mechanism, consistent with many other reports showing myosin II contractility is necessary for the response to substrate rigidity. Interestingly, I also found that myosin II is required for the retraction of protrusions in response to substrate strain. This unique perspective is afforded through advantages of the composite substrate and reveals that the role of myosin II in rigidity sensing is multifaceted.

### **6.1.3 FAK $-/-$ cells show impaired probing of substrate rigidity due to elevated Rho activity**

In Chapter 4, I extend the use of composite substrates for screening conditions that may affect rigidity sensing and durotaxis. I am able to capture responses consistent with previously observed behaviors of FAK  $-/-$  cells and cells re-expressing WT-FAK or F397-FAK, a non-phosphorylatable mutant. The ease with which cellular responses to a rigidity border can be captured on the composite substrate points to its future use as a straightforward and robust screening platform. My results suggest that the kinase activity of FAK is a crucial component of the rigidity sensing pathway, while phosphorylation at tyrosine 397 does not appear to play a role. The signaling process likely involves the modulation of Rho activity, consistent with reports showing that FAK can down-regulate Rho activity<sup>3</sup> and that FAK  $-/-$  cells have elevated levels of Rho activity<sup>4</sup>. The modulation of Rho activity appears to drive rigidity sensing as conditions that favor elevated Rho activity induce a rigidity sensing defect. Furthermore, I show that Rho downstream effector mDia1 may play a different but still important a role in rigidity sensing as its well-studied counterpart ROCK. These results provide insight into how FAK mediates rigidity sensing, and how Rho plays a central role in the associated signaling mechanism.

#### **6.1.4 Traction force generation involves mechanical crosstalk between newly formed and existing adhesions**

In Chapter 5, I provide a plausible explanation of why active traction forces appear only transiently at nascent focal adhesions at the leading edge, which maintains frontal location of probing forces during cell migration. Using a checkerboard pattern designed to limit adhesion formation along parts of the leading edge, I show that the cell displaces the substrate to a greater extent, and for a longer period of time when new adhesions are unable to form directly in front of existing adhesions. In addition, maximal substrate displacements remain stationary during cell migration, unlike the wave-like progression seen in cells migrating along continuous strips, which leads to an increased distance between the leading edge and the point of maximal substrate displacement. This result suggests that it is mechanical crosstalk between newly formed and pre-existing focal adhesions, rather than “aging” of focal adhesions, that causes the dissipation of traction forces at mature focal adhesions. Additionally, as reports have suggested local mechanical interactions between adjacent adhesions for rigidity sensing<sup>5,6</sup>, disruption of the sequence of events, as in non-migrating cells, may alter the generation of traction forces and affect downstream mechanosensing outputs. While previous Chapters have shown the mechanical sensitivity of nascent adhesions at the tip of filopodia, which grow into mature adhesions on stiff substrates, this Chapter shows an opposite kind of mechanical sensitivity where adhesions disassemble upon the formation of nascent adhesions in front of the existing ones.

### **6.1.5 Significance and biological importance**

This thesis illustrates how cells apply probing forces followed by the “readout” of their consequences, such as displacement of the substrate, for the purpose of sensing mechanical properties of the environment. The readout then triggers downstream chemical effects likely through force-induced molecular conformational changes, to regulate events such as cell behavior or gene expression<sup>7-9</sup>. Through a feedback mechanism, the readout also regulates the generation of probing forces as a function of the environment. Disrupting either the probing forces or the readout can have profound effects on cell phenotype and behavior<sup>10</sup>. Our understanding of the makeup of this probing mechanism and the transduction of downstream signals is still far from complete. It is particularly important to understand the rigidity sensing mechanism, given the fundamental role of rigidity in guiding an ever increasing list of cellular processes.

## **6.2 Future Directions**

### **6.2.1 The effect of strain rate on protrusion stability and rigidity sensing**

In Chapter 3, I show that nascent protrusions are sensitive to substrate strain, which can promote retraction of the protrusion and prevent cell lamellipodial spreading over the area. It has been suggested that stepwise myosin contractility drives sensing of rigidity, where stepped contractions proceed until a specific force threshold is reached, at which time there is reinforcement of focal adhesions and the actin cytoskeleton<sup>5</sup>. This implies that cells are highly susceptible to the rate of substrate deformation when responding to substrate rigidity. To modulate the amount of strain perceived by the cell, a microneedle can be used to push one of the small islands of the composite substrate, occupied by a nascent protrusion, toward the cell body at a controlled rate. Slow deformations may be insufficient to cause protrusion retraction, while there may be a strain rate threshold that regulates the switch between adhesion strengthening or protrusion retraction. Studies using controlled substrate strain may also be able to address whether the loss of rigidity sensing in cells with increased Rho activity is due to a change in the force threshold at which adhesion strengthening occurs or if another mechanism may be involved.

### **6.2.2 The involvement of Rho effector mDia1 in rigidity sensing**

In Chapter 4 I showed that rigidity sensing in front of the leading edge likely depends on the Rho/mDia1 pathway instead of the classic Rho/ROCK contractility based pathway. Additionally, it was previously reported that Rho effector mDia1 was necessary for externally applied force induced focal adhesion maturation, while ROCK was dispensable<sup>11</sup>. mDia1 has been shown to be mechanosensitive where the application of pulling forces increased the mDia1-mediated

elongation rates of actin filaments<sup>12</sup>. This supports the idea that mDia1 may be involved in the response to substrate rigidity by influencing focal adhesion formation and maturation, possibly through interactions with the actin cytoskeleton. Perhaps, when mDia1 activity is upregulated a lower force is necessary to stabilize nascent focal adhesions. Over stabilization and/or increased maturation could lead to the observed rigidity sensing defect of spreading over soft substrates in cells with elevated Rho activity. mDia1 is also known to interact with microtubules, which have been found to both interact with FAK and to affect Rho activity. In addition, a recent study implicated microtubule destabilization as the mechanism for regulating Rho in response to substrate stiffness<sup>13</sup>. It is possible that mDia1 may also influence rigidity sensing through interactions with microtubules. Future work should investigate the mechanism and role of mDia1 in rigidity sensing.

### **6.2.3 Biological significance of traction force difference between migrating and stationary cells**

Generation of myosin II dependent traction forces has been shown to be important in probing the external or internal state of the cell and for regulating various cellular functions. We saw in Chapter 5, that traction force output differs between migrating and stationary cells independently of previously reported parameters such as cell area and aspect ratio and was instead dependent on continual adhesion turnover during active protrusion of the lamellipodia. Since we know that the generation of traction forces, and the associated increase in cytoskeletal contractility can influence differentiation and regulation of gene expression<sup>14-16</sup>, we suspect that traction force differences between migrating and stationary cells could similarly translate into differences in downstream regulation. Future work could further investigate the downstream effects of differential traction regulation due to migration state to determine if this process could influence

cell behavior *in vivo*. Regulation of traction forces based on migration state could be an important factor in physiological processes, such as during development where it may make sense to suppress differentiation while a cell is migrating, and allow the cell to undergo differentiation to perform its physiological functions once the cell has reached its destination.

## 6.3 References

1. Chan, C. E. & Odde, D. J. Traction Dynamics of Filopodia on Compliant Substrates. *Science* **322**, 1687–1691 (2008).
2. Petrie, R. J. & Yamada, K. M. At the leading edge of three-dimensional cell migration. *J. Cell Sci.* **125**, 5917–5926 (2012).
3. Ren, X. D. *et al.* Focal adhesion kinase suppresses Rho activity to promote focal adhesion turnover. *J. Cell Sci.* **113** ( Pt 2, 3673–8 (2000).
4. Pirone, D. M. *et al.* An inhibitory role for FAK in regulating proliferation: a link between limited adhesion and RhoA-ROCK signaling. *J. Cell Biol.* **174**, 277–88 (2006).
5. Wolfenson, H. *et al.* Tropomyosin controls sarcomere-like contractions for rigidity sensing and suppressing growth on soft matrices. *Nat. Cell Biol.* **18**, 33–42 (2015).
6. Ghassemi, S. *et al.* Cells test substrate rigidity by local contractions on submicrometer pillars. *Proc. Natl. Acad. Sci.* **109**, 5328–5333 (2012).
7. Bershadsky, A. D., Balaban, N. Q. & Geiger, B. Adhesion-dependent cell mechanosensitivity. *Annu. Rev. Cell Dev. Biol.* **19**, 677–95 (2003).
8. Grashoff, C. *et al.* Measuring mechanical tension across vinculin reveals regulation of focal adhesion dynamics. *Nature* **466**, 263–6 (2010).
9. Schoen, I., Pruitt, B. L. & Vogel, V. The Yin-Yang of Rigidity Sensing: How Forces and Mechanical Properties Regulate the Cellular Response to Materials. *Annu. Rev. Mater. Res.* **43**, 589–618 (2013).
10. Wang, H., Dembo, M. & Wang, Y. Substrate flexibility regulates growth and apoptosis of normal but not transformed cells. *Am. J. Physiol. Cell Physiol.* **279**, C1345–C1350 (2000).
11. Rivelino, D. *et al.* Focal contacts as mechanosensors: externally applied local mechanical force induces growth of focal contacts by an mDia1-dependent and ROCK-independent mechanism. *J. Cell Biol.* **153**, 1175–86 (2001).
12. Jégou, A., Carlier, M.-F. & Romet-Lemonne, G. Formin mDia1 senses and generates mechanical forces on actin filaments. *Nat. Commun.* **4**, 1883 (2013).
13. Heck, J. N. *et al.* Microtubules regulate GEF-H1 in response to extracellular matrix stiffness. *Mol. Biol. Cell* **23**, 2583–2592 (2012).
14. Engler, A. J., Sen, S., Sweeney, H. L. & Discher, D. E. Matrix elasticity directs stem cell lineage specification. *Cell* **126**, 677–89 (2006).
15. Leight, J. L., Wozniak, M. a, Chen, S., Lynch, M. L. & Chen, C. S. Matrix rigidity regulates a switch between TGF- $\beta$ 1-induced apoptosis and epithelial-mesenchymal transition. *Mol. Biol. Cell* **23**, 781–91 (2012).
16. Lv, H. *et al.* Mechanism of regulation of stem cell differentiation by matrix stiffness. *Stem Cell Res. Ther.* **6**, 103 (2015).